TYCO LABORATORIES, INC.
BEAR HILL, WALTHAM 54, MASS.
(617) 899-1650

Development of Cathodic Electrocatalysts for Use in Low Temperature H_2/O_2 Fuel Cells with an Alkaline Electrolyte

Contract No. NASW-1233

Q-5

Fifth Quarterly Report
Covering July 1, 1966
Through September 30, 1966

for

National Aeronautics and Space Administration
Headquarters, Washington, D. C.

DEVELOPMENT OF CATHODIC ELECTROCATALYSTS FOR USE IN LOW TEMPERATURE H_2/O_2 FUEL CELLS WITH AN ALKALINE ELECTROLYTE

Contract No. NASW-1233

Q-5

Fifth Quarterly Report
Covering July 1, 1966
Through September 30, 1966

by
J. Giner
J. Parry
L. Swette
R. Cattabriga

for
National Aeronautics and Space Administration
Headquarters, Washington, D. C.

DEVELOPMENT OF CATHODIC ELECTROCATALYSTS FOR USE IN LOW TEMPERATURE H_2/O_2 FUEL CELLS WITH AN ALKALINE ELECTROLYTE

CONTRACT OBJECTIVES

The research under contract NASW-1233 is directed towards the development of an improved oxygen electrode for use in alkaline H_2/O_2 fuel cells. The work is being carried out for the National Aeronautics and Space Administration, with Mr. E. Cohn as technical monitor. Principal investigators are Dr. J. Giner, and Dr. J. Parry.

CONTENTS

CONTENTS (Cont.)

SUMMARY AND CONCLUSIONS

The experimental studies of solid intermetallic electrodes of the Ti_3Au type were continued. The aim was to explore the high activity observed for Ti_3Au itself. Additional materials examined were TiAu, Zr_2Pd, $TiRh_3$, $Ti(Rh_{1.5}Au_{1.5})$, and Zr_3Au. Ti_3Au corrodes significantly when in powder form. TiAu is corrosion resistant but its activity is somewhat lower. Its half-wave potential ($E_{1/2}$) is 800 mv vs. RHE, (compare this to 840 mv for Ti_3Au). Zr_2Pd does not corrode over the whole potential range studied. However, its activity is less than that of pure palladium. $TiRh_3$ and $Ti(Rh_{1.5}Au_{1.5})$ both show activity in the range of 400 - 600 mv vs. RHE. $TiRh_3$ is corrosion resistant, but its activity is quite low with $E_{1/2}$ = 460 mv. Zr_3Au corrodes significantly at all potentials.

The influence of absorbed oxygen films on the activity of noble metals towards oxygen reduction is being studied with a series of gold alloys (the surface of gold being oxygen-free at oxygen reduction potentials). The system gold-palladium has been examined; gold-platinum and gold-silver alloys are being studied and an interpretation of the results will be given when these series are complete.

A 1.7% Mg alloy of Ag did not show an increase in intrinsic activity over that of pure Ag. Larger currents obtained with the Mg alloy are directly attributable to its higher surface roughness.

A number of dispersed materials have been studied after being formed into Teflon-bonded electrodes. The activity of Teflon-bonded electrodes depends on their structure which in turn depends on the physical and chemical nature of the catalyst. In order to obtain valid comparisons between different dispersed materials, it is necessary to establish an optimum electrode structure for each catalyst. Studies with Pt-black, carbon, graphite, and nickel carbide have shown that the optimum Teflon content depends on the measured bulk density of the catalyst and that optimum conditions for sintering are 275°C for 15 minutes.

A number of interstitial compounds of the transition metals, including nickel carbide and nickel nitride, have been prepared and tested for oxygen activity. Both nickel carbide and nitride show catalytic activity greater by an order of magnitude than that of nickel. The best performance found so far was with a nickel-cobalt carbide which yielded 200 ma/cm^2 at 0.74 v vs. RHE.

A comprehensive series of interstitial compounds is being prepared by the Bureau of Mines (Pittsburgh Coal Research Center); these will be tested as they become available. The following materials prepared under this program showed no significant activity towards oxygen reduction: ϵ - iron carbonitride, $Fe(OH)_3 + Ag_2O$, and $\epsilon - Fe_2C + Fe_3O_4$.

GENERAL INTRODUCTION

A survey of catalyst materials for the cathodic reduction of oxygen in basic electrolytes at low temperatures encompassed a number of elements, including all transition metals with the exception of technetium, a large series of intermetallic compounds and alloys of transition metals, and interstitial carbon and nitrogen compounds of Group VIII and of the refractory metals. Our previous results are summarized briefly below in order to place our current work in its proper perspective.

Electrodes forming oxides below the oxygen potential can be classified into three groups: The first group includes metals on which oxygen reduction begins only when bare metal surface becomes available, that is after substantial reduction of an oxide or chemisorbed oxygen layer. The reduction of oxygen proceeds directly to water on the bare surface with very little hydrogen peroxide accumulation. Examples of metals of this type include those of the Pt group and silver. Within this group Pt has the highest activity at low temperatures, with the possible exception of osmium which shows a small, kinetically controlled limiting current for O_2-reduction at higher potentials than on Pt. The metals Zr, Ta, Hf, and Nb can be included in this group insofar as an oxide layer is present at all potentials and no appreciable O_2-reduction occurs.

The next group contains elements such as Ti, Ni, Fe, and graphite. Oxygen is reduced on these materials on oxide-covered surfaces with varying degrees of reversibility. For example, reduction of oxygen on passivated Ti requires an overvoltage of about 1 v, while on graphite (which is completely covered by oxygen) oxygen can be reduced to hydrogen peroxide with a high degree of reversibility.

The third group includes elements such as Mn and Co on which redox reactions of the type

$$Mn^{4+}/Mn^{3+} \text{ or } Co^{3+}/Co^{2+}$$

have a specific effect on oxygen reduction. In these cases, a maximum activity is found in the range of potentials where these reactions occur. A maximum can be observed directly on pure Mn but is masked on pure cobalt by a corrosion current. It is, however, observed on Ni-Co alloys where the corrosion current is very small. The activity of the $NiCo_2$ alloy may be additionally due to a synergistic effect related to the spinel Co_2NiO_4.

Gold is a special case since it is the only metal essentially free of oxide or chemisorbed oxygen below 1.23 v, that is below the reversible O_2-potential. Reduction of oxygen to hydrogen peroxide is virtually reversible on gold, while the further reduction of HO_2^- to water (or OH^-) is slow.

Our experiments with many intermetallic compounds show that enhancement of the catalytic properties by formation of a new phase is generally small. The catalytic properties of the components of an alloy appear to be more important than the electronic or crystallographic structure of any phase that may be formed. However, compounds or alloys may show substantially higher activity and stability than the components. This result is generally related to the effect of the electronic or crystallographic structure of the compound on the properties of the surface oxide formed during oxygen reduction on all nonnoble metals.

A substantial effect of chemical compound formation is also apparent in corrosion.

Of the specific systems studied, the intermetallic compounds of platinum and nickel and the interstitial compounds of the transition elements with carbon and nitrogen are of particular interest.

From our study of intermetallic compounds of Pt with nonnoble metals we may conclude that:

(a) Appreciable dilution by a nonnoble metal (e.g. Pt_2Ta) causes no decrease of the platinum activity for comparable surface roughness factors.

(b) Considerable surface increase can be obtained in some intermetallic compounds, probably by leaching of the nonnoble metal component. This effect may be useful in obtaining platinum particles with a high and stable surface for practical electrodes.

(c) Although addition of cobalt to nickel imparts a considerable increase in activity, $PtCo_3$ does not show a corresponding improvement. This may be due to the high intrinsic activity of Pt. This conforms to the general pattern observed, namely that no intermetallic compound tested to date shows more activity than platinum.

Nickel alloys with Co and Mn show improvement in performance over nickel. The corrosion resistance of a metal which corrodes in alkali is improved on the other hand, by addition of Ni. This general trend was noticed for all nickel alloys; the best example was NiAl which behaved exactly as nickel.

Ti_3Au is a particularly interesting intermetallic compound. Its initial performance is higher than titanium or gold (but somewhat lower than platinum). With time, this performance increased to a level higher than platinum, but it was accompanied by a pronounced increase in double layer capacity, implying roughening of the surface. This was confirmed by electron microscopy. Analysis of the surface with an electron microprobe showed the surface exposed to the electrolyte to be more rich in titanium than the bulk of the sample.

Of the "interstitials" of the refractory metals, borides and silicides generally exhibited high corrosion currents which eliminated them as possible oxygen electrodes in caustic electrolytes.

The nitrides and carbides are another matter, especially in the cases of VC, VN, NbC, and TiN all of which are more resistant than their parent metals. The carbides (and the nitrides to a lesser extent) are all more active for O_2-reduction than the parent metals; some activity is found even when the metal itself is inert, for instance with Hf, Ta, and Cr.

Another example of interest is Ti and TiN. The decrease of corrosion current and of overvoltage for O_2-reduction (about 500 mv) observed with TiN is hard to explain as a pure surface area effect and must be due to the favorable effect of an oxynitride of titanium covering the TiN surface.

The interstitial compounds of Fe, Ni, and Co are also of considerable interest. Ni_3C and Ni_3N, tested as Teflon-bonded electrodes, showed considerably greater activity than nickel. A solid, rotated iron electrode with a carbide surface (presumably Fe_2C) also showed more activity for O_2-reduction than did a pure iron electrode.

In the past the technique mostly used in screening catalysts was the rotating disc electrode, which allows the measurement of the intrinsic catalytic properties of a material free from structural factors. Measurements with Teflon-bonded, porous electrodes were limited to a few cases. These measurements have been extended during this report period, since many of the materials we now wish to screen are available only as dispersed powders. These include the carbides, nitrides and carbonitrides of Fe, Ni, and Co and mixtures of these and other catalysts. Most of these catalysts are being prepared by the Bureau of Mines (Pittsburgh Coal Research Center). In addition, highly dispersed noble metals, Ti_3Au, and related materials are being tested as hydrophobic, porous electrodes.

The structural factors influencing the performance of Teflon-bonded electrodes were examined, since proper evaluation of a dispersed catalyst requires optimization of the Teflon-bonded structure used for its study.

The tests with the rotating disc electrode are being continued along with the above studies. Intermetallic compounds of the Ti-Au system and other compounds of the groups IVB and IB of the periodic table have been evaluated. This study aims to explain, in order to exploit it, the high performance observed with the Ti_3Au-compound. In addition, a series of Pt/Os, Pd/Au, Pt/Au, Ag/Au, Pt/Pd, and Ag-based alloys are being investigated.

This report is divided into two parts: One deals with solid electrodes; the other, with porous electrodes.

PART ONE

SOLID ELECTRODES

I. INTRODUCTION

A. Intermetallic Compounds of Group IVB and IB

The following systems were investigated during this reporting period: TiAu, Zr_2Pd, $TiRh_3$, $Ti(Rh_{1.5}Au_{1.5})$ and Zr_3Au. (Zr_2Pd and $TiRh_3$ are included in this classification for purposes of comparison.) The objective of this work was twofold: to investigate materials related to the $AuTi_3$-compound in order to understand its working mechanism and to compare the activity of such isoelectronic structures as $Ti(Rh_{1.5}Au_{1.5})$ and $TiPt_3$. Rh and Au are not miscible in the desired ratio for a direct comparision with Pt, but an intermetallic compound with Ti permits comparison with $TiPt_3$.

B. Precious Metal Alloys with Au

The systems under investigation are Pd:Au, Pt:Au, and Ag:Au; the purpose of the study is to investigate the influence of gold (which does not form an adsorbed layer of oxygen at potentials < 1300 mv vs. RHE) on the extent of adsorbed oxygen coverage and activity towards the oxygen reduction reaction. These alloys are also of interest in that they exhibit a regular gradation of electronic structure (d-band vacancies) and lattice dimensions with composition. Fishman and Rissman[1] have shown some experimental evidence of a discontinuity in the activity vs. composition curve for Au:Pd, with maximum activity at ~ 35% Au. This they relate to the filling of the d-band of palladium. Bockris, Damjanovic and Rao[2] have shown that the amount of adsorbed oxygen may be related to alloy composition and d-band vacancies.

Another point of view with the Au-containing alloys is that Pt, Pd, and Ag are inhibited by the presence of oxides or chemisorbed oxygen at potentials of < 900 mv where the adsorbed oxygen layer begins to be

reduced. Gold, however, does not form an oxide layer in the potential region of interest (< 1200 mv) but also does not readily effect the complete reduction of oxygen beyond the peroxide intermediate. Alloying Au to Pt, Pd, or Ag may result in a retardation of the oxide formation or a decrease of its inhibiting action on these metals.

C. Silver-Magnesium Alloys

Beer and Sandler[3] have examined as catalysts for the oxygen-reduction reaction silver with different surface pretreatments and silver-based alloys. Improved performance was found for a 1.7% Mg:Ag alloy; this was considered to be related to its enhanced secondary electron emission. This work did not include a determination of the real surface area of these materials. A comparison of the real surface areas of Ag and the alloy was carried out in this laboratory in conjunction with activity tests on these materials.

II. PREPARATION OF CATALYSTS AND EXPERIMENTAL METHODS

A. Intermetallic Compounds of Groups IVB and IB

The following materials have been prepared as solid ingots by arc melting in an inert atmosphere: Zr_3Ar, $TiRh_3$, $Ti(Rh_{1.5}Au_{1.5})$, Zr_2Pd, and TiAu. These materials were classified according to the Fourth Quarterly Report of this contract, as B. 4. — Alloys and Intermetallic Compounds of the Transition Metals: Ti, Zr, and Hf alloys.

B. Au Alloys of Pd, Pt, and Ag

Au alloys of Pd, Pt, and Ag have been obtained from Williams Metals Co., Buffalo, New York, as cylindrical rods 1/4" x 1/4" diameter at 10% increments in composition.

C. Silver-Magnesium Alloys

The silver-magnesium alloy was obtained as foil from Handy and Harman Co., New York, and silver foil was purchased from Williams Metals. The foils were polished to a bright finish with alumina.

D. Experimental Methods

All these materials except the Ag and Ag:Mg samples were tested as ingots in the rotating electrode cell described in[4]. The Ag and Ag:Mg foils were cut into 1 cm x 1 cm squares, welded to an Ag-wire, and sealed in glass.

The electrochemical examination of these alloy systems requires experimental techniques capable of far greater precision than those previously employed in routine screening of catalysts; activity levels now need to be determined to better than a few millivolts. The approach to the problem was to consider in detail the initial part of the polarization curve ($i < 500\ \mu a/cm^2$) where the reaction rate is entirely activation controlled and not influenced by diffusion processes. Due to the higher sensitivity required in the current scale, possible limitations to the precision of the determination of the current had to be reduced further. The following improvements were found desirable in order to be able to increase the sensitivity:

1. The voltage signal source was isolated from the x-y recorder (a relatively low impedance instrument) by means of a high impedance input 1:1 amplifier. This eliminated both a small leakage current through the reference electrode circuit and a common ground leak between the two input signals to the recorder. Both of these contribute to small linear distortion to the recorded trace which becomes significant when working at high current sensitivities.

2. Occasional electrolyte leakage between the electrode and its mounting was eliminated; this can result in significant areas of the electrode being coupled in parallel with the working surface through a electrical resistance/high diffusional resistance path. When leakage occurs, it is impossible to interpret the results with any degree of precision. Since these alloys are not brittle, the Stern-Makrides[5] form of rotating electrode was the most effective means (more so than Kel-F wax) of mounting the electrode without leakage.

The use of the Stern-Makrides electrodes with the base and the wall surfaces of the cylinder governed by different hydrodynamic conditions (and therefore controlled by different diffusion rates) makes quantitative interpretation of the curves in the limiting current region difficult. But since we are concerned with electrodes of identical configuration and are primarily interested in the activation controlled region of the curve, this does not seriously affect the comparative studies of these alloys.

The standard method of earlier experiments, using Koldmount resin — necessitated by the brittle nature of most of the intermediate alloys tested previously — was not considered suitable for the cylindrical form of these electrodes. The Koldmount could introduce a level of impurities that would be sufficient to influence the higher precision required for these measurements.

3. Effect of Impurities

The often observed effect of impurities in electrochemical measurements is very pronounced when working with alkaline electrolytes

such as KOH, due in part both to the relatively high level of impurities present in the commercial reagent and to active impurities leaching from the glassware. This effect is clearly illustrated by the observed time effect on charging curves or fast potential sweeps made on Pt and on H_2-oxidation or evolution on Pt, when working with KOH electrolyte.

In a coarse screening of catalysts for O_2-reduction, the effect of impurities is tolerable. (It is minimized by the relatively high potentials of O_2-reduction and by the cleaning effect of oxide formation and reduction.)

The effect of impurities becomes more critical when we wish to distinguish changes of a few millivolts to 100 mv. This may occur, for instance, in a series of alloys of two components in varying proportion, when oxides are not allowed to form. For our measurements we have partially solved the problem by (a) reducing the alkali concentration to 2N instead of the 35% solution used in low temperature fuel cells, (b) by decreasing the temperature to 25°C instead of the 80°C used previously, and (c) by investigating time effects and obtaining i(E)-curves at several sweep rates.

The effects of containers other than glass (Teflon, quartz, Pt, etc.) and of different batches of commercial KOH are being investigated. Depending on the results it may be necessary to expend some effort to prepare more pure electrolytes.

The experimental work is at a stage where slow sweep results exactly reproduce points determined manually, indicating that instrumental distortion important at high sensitivity of the current scale has been eliminated from the recorder trace.

III. RESULTS

A. Groups IVB - IB Intermetallic Compounds

Zr_2Pd This material is corrosion resistant over the whole potential range studied; its activity for oxygen reduction $E_{1/2}$ = 730 mv is lower than that of pure palladium $E_{1/2}$ = 835 mv (Fig. 1).

$Ti(Rh_{1.5}Au_{1.5})$ The activity of $Ti(Rh_{1.5}Au_{1.5})$ with $E_{1/2}$ = 570 mv (Fig. 2) is very much lower than the platinum analogue $TiPt_3$ which with an $E_{1/2}$ = 825 mv is only slightly less active than Pt, $E_{1/2}$ = 840 mv.

$TiRh_3$ Although corrosion resistant, as shown in Fig. 3, this alloy shows very low activity with $E_{1/2}$ = 460 mv.

Zr_3Au This material corrodes significantly at all potentials with a large corrosion peak in the 300-500 mv range (Fig. 4).

TiAu The corrosion rate was significantly reduced compared with Ti_3Au (Fig. 5), particularly at potentials below + 700 mv. In addition, the double-layer capacity of the electrode did not change significantly throughout the experiment, indicating no surface roughening. This is in contrast to Ti_3Au for which the double layer capacity increased by an order of magnitude. The appearance of the electrode was unchanged at the end of the experiment. The activity for O_2 reduction remains encouraging, with $E_{1/2}$ = 800 mv compared with 840 - 880 mv for Ti_3Au; corresponding E_1 values are 860 mv for TiAu and 900 mv for Ti_3Au.

B. Gold-Containing Alloys

The most recent family of curves for Au and Au:Pd is shown in Figs. 6 to 21. These curves are being treated as provisional results due to the anodic current observed above 100 mv, which is higher for curves made in the presence of oxygen. This effect may be related to an impurity being accumulated in the electrolyte.

In the absence of impurities, the high sweep rates define the potentials of formation and reduction of the surface oxygen layer; the intermediate sweep rates present information on the influence of adsorbed impurities. The low sweep rates give the information on the steady state process, a real measure of the activity.

For these activity measurements the potentials scanned are limited to +400 mv to +1000 mv to prevent H_2 absorption in the palladium at the lower potentials and etching of the surface at very high potentials. The fast sweeps, intended to study the formation and reduction of adsorbed oxygen films, necessarily extend over a larger potential range +400 mv to +1600 mv. The fast sweeps have been determined first and the samples repolished prior to activity measurements. To confirm that the surface layers are of identical composition as the bulk of the alloy, electron microprobe analysis will be carried out.

The data collected so far are insufficient to attempt any detailed analysis. The activity is seen to increase as the palladium content of the alloy is increased; this is much more apparent at the higher temperature. The Au:Pd 90:10 alloy is apparently out of order in the activity progression. The experiment will be repeated in order to ascertain whether it is a real effect or an artifact due to electrolyte leakage, as is suspected.

The difference in the potential at which the adsorbed oxygen layer forms on the two metals is readily appreciated from the fast sweep results, Figs. 22 to 32. On pure gold no adsorbed layer forms until a potential of +1300 mv is reached; in the presence of even 10% Pd, the adsorbed layer begins to form at 900 mv. The effect is even more marked in the reduction of the adsorbed oxygen; the peaks corresponding to Pd and Au are completely resolved, suggesting that the components behave in very much the same way as they do in the pure state. The first reduction peak disappears for Au:Pd 40:60 alloy; the remaining peak moves to lower potentials as the Pd content is further increased. An anodic peak due to oxidation of hydrogen occluded at the lower potentials is apparent in the palladium

rich alloys. Since this occlusion results in lattice distension with considerable hysteresis, the requirement to reverse the potential sweep at 400 mv during activity measurements, in order to avoid changes in the nature of the surface, becomes obvious. All the fast sweep curves presented in this report were the fourth cycle of the potential sweep; the first three were used to define the position of the trace on the oscilloscope. It is assumed that the surface is not significantly changed by the initial three sweeps.

C. Silver-Magnesium Alloys

The current potential curves for these materials are shown in Figs. 33 and 34. A comparative figure for the real surface areas of the Ag and Ag:Mg foils was obtained from the ratio of their double-layer capacities. The capacities were measured with a 50 mv triangular sweep at 400 and 700 mv at the beginning and at the end of each activity determination. The ratio of the real surface areas ranged from 3.2 to 6, the Ag:Mg alloy having the higher surface area. A series of experiments at different sweep rates showed that the surface was substantially free of adsorbed impurities.

A comparison of the potentials at a current density of 200 $\mu a/cm^2$ (corrected for the difference in surface roughness) where there are no mass transfer limitations shows no greater intrinsic activity for the Ag:Mg alloy. Refer to Table III.

This finding is more consistent with the thinking that catalytic activity is unrelated to secondary electron emission properties. Secondary electron emission is related to the work function, which determines the potentials of zero charge of the electrode-electrolyte interphase. As has been shown, the point of zero charge has little relevance to overvoltage[6, 7].

It has to be kept in mind, however, that small additions of Mg or MgO to highly dispersed Ag can contribute to higher stability of the surface and therefore to practical electrodes of enhanced activity.

IV. SUMMARY OF RESULTS ON SOLID ELECTRODES

TABLE I

Intermetallic Compounds on IB and IV Metals (75°C)

	$E_{1/2}$ mv	E_1 mv	Corrosion	Fig. No.
Intermetallic of IB and IVB Metals (75°C)				
TiAu	800	860	very small	5
Zr_2Pd	730	830	resistance	1
$Ti(Rh_{1.5}Au_{1.5})$	570	790	very small	2
$TiRh_3$	460	670	very small	3
Zr_3Au	no activity		rapid	4

TABLE II

Precious Metal Alloys with Gold*

			25°C			75°C	
	Sweep Rate		50	200	400	50	mv/min
Au	E_{200} (mv)	=	877	880	884	865	
Au:Pd 90:10	E_{200} (mv)	=	904	897	892	869	
Au:Pd 80:20	E_{200} (mv)	=	872	885	887	896	
Au:Pd 70:30	E_{200} (mv)	=	899	890	891	903	

* Due to the greater precision arrived at in these measurements. The data are expressed in terms of potential E_{200} vs. RHE at which a current density of 200 $\mu a/cm^2$ is observed

TABLE III

Comparison of Silver and Silver-Magnesium Alloys

		E vs. RHE	
		Ag	Ag:Mg
25°C	i = 200 $\mu a/cm^2$	863	858 mv
75°C	i = 200 $\mu a/cm^2$	900	880 mv

PART TWO

DISPERSED CATALYST AND POROUS ELECTRODES

I. INTRODUCTION

A. Effect of Manufacturing Techniques on Performance of Porous Electrodes

The preparation of high surface area electrodes demonstrating optimum activity for a particular catalyst is not a straightforward process. It is, however, a very important part of the investigation, since materials showing activity in ingot form must be made into high surface area electrodes for further testing; furthermore, some materials are obtainable only in a highly dispersed form.

The problem of making electrodes of this kind has two main aspects:

(1) The preparation of a highly dispersed powder with the essential catalytic activity of the solid electrode

(2) The fabrication of an electrode with good mass transport characteristics

The second aspect is intimately related to such physical properties of the powder as particle size, surface area, porosity, and bulk density. Therefore, relying on a standard preparation of the electrode to test all catalysts could result in a useful catalyst being overlooked. The preferred approach is to regard the incorporation of each catalyst in an electrode structure as an individual problem, though it is to be hoped that experience and established procedures will reduce the number of parameters to be changed in this process. This has been the objective in the work reported here.

Our interest has been restricted to the Teflon-bonded screen electrode structure, the basis of several successful commercial electrodes. The present work seeks to define and control the variables associated with

the fabrication process and to relate them as far as is possible to the physical characteristics of the catalyst. The variables are considered to be:

(1) The catalyst to Teflon ratio

(2) The catalyst loading

(3) The catalyst-Teflon mixture distribution technique (spraying, spreading, brushing, rolling)

In addition, in the case of catalysts of high thermal instability, methods of preparing electrodes have to be developed which do not require sintering at high temperature (275°C). A possible binder is Elvax* which has shown promise for short term tests.

B. Interstitial Compounds of Ni, Co, and Fe

The main interest during this report period has been preparing nickel carbide, nickel nitride, cobalt carbide, and cobalt nitride. These nickel compounds showed an activity an order of magnitude greater than did nickel in previously reported tests. It was intended, for confirmation of these observations, to study the activity in more detail and to look for comparable effects with the cobalt and nickel/cobalt compounds.

Details of the preparations attempted are given below. Future work will be based on a comprehensive selection of carbides and nitrides being prepared by the Bureau of Mines for testing at Tyco.

C. Ti_3Au Powder Electrodes

In screening materials for O_2-reduction activity by the solid-ingot rotating electrode technique, it was found that Ti_3Au reduced oxygen as well as or better than did platinum under similar conditions. This exceptional performance was accompanied, however, by an eightfold increase in roughness over a period of 24 hours and by evidence of corrosion currents. Metallographic data corroborated the evidence of surface roughening indicated by double layer capacity measurements.

---

* DuPont polyvinyl resin

Initially, it was thought that a high surface area of gold was being created through leaching of titanium, but this was contradicted by microprobe analysis of the surface which indicated that it was titanium-rich relative to the original composition. Subsequently, it was postulated that nonstoichiometric conductive titanium oxide was being redeposited and that there was a net loss of gold.

A literature survey of the titanium oxygen system with emphasis on the preparation of nonstoichiometric oxides and their resistivity, catalytic activity, and electrochemical behavior showed some interesting properties. For instance, the conductivity of TiO_2 increases very rapidly when it assumes an oxygen deficient structure $10^{-10}\ \Omega^{-1}cm^{-1}$ for TiO_2, $10^{-1}\Omega^{-1}cm^{-1}$ for $TiO_{1.9995}$, and $10^{2}\Omega^{-1}cm^{-1}$ for $TiO_{1.75}$[8].

Douglass, St. Pierre and Spieser[9] report that attempts to nitride TiO_2 with NH_3 in Ar at 900 - 1070°C resulted in the reduction of the oxide to form successively $TiO_{1.96}$, Ti_9O_{17}, Ti_8O_{15}, Ti_7O_{13}, Ti_2O_3, and TiO with the eventual formation of some TiN. This is in contrast to the reports of Gilles, Lejus, and Colonguy[10] where no oxynitride was detectable by X-ray analysis. Hollander and Castro[11] have prepared nonstoichiometric oxides of titanium by the reduction of single crystals of TiO_2 (rutile) by H_2 in Ar at 600 - 1000°C. In this case, the conductivity was measured as a function of crystal orientation and was found to be markedly anisotropic; the maximum ratio for the conductivities along the a and c planes ρ_a/ρ_c was reported as 10,000:1. This fact is used to explain previous discrepancies in measured conductivities that were reported in the literature. Dorin and Tartakovskaya[12] have reported the preparation of the nonstoichiometric oxide by heating TiO_2 with Ti in an inert atmosphere at 700 - 1100°C. Boltaks, Vesenin, and Salunina[13] have used H_2 and CO in the presence of C as reducing agents and report material of higher conductivity from the H_2 reduction. They stress that the material prepared from CO and carbon contained no residual carbon or carbide.

Measurements of conductivity as a function of composition have been made by Greener[14], Ariya and Bogdanova[15] (also as a function of temperature), Morin[16], Sawai, Terada, Okamura and Ueno[17], and Boltaks et al.[13]. The conductivity of TiO_x is greatly increased by the incorporation of WO_3 in the oxide lattice, Grunewald[18].

The catalytic activity of TiO_x (anatase structure) towards the oxidation of CO has been related to the defect structure by Long and Tiechner[19] and to conductivity for oxidation processes by Mysanikov[20]. When titanium metal is oxidized in 1N NaOH + 0. 1N H_2O_2, Mazza, Mussoni, and Trasatti[21] describe the black (oxide) coating as 200 - 300 mv more noble than titanium with respect to the oxygen and peroxide reactions; the black is identified as an oxygen deficient oxide. They conclude, in general, that the black favorably influences electrodic behavior. In a further paper Mazza[22] attributes the formation of the black in the presence of H_2O_2 to the dissolution of a subvalent ion which subsequently forms the nonstoichiometric oxide. Dean and Hornstein[23] have related the oxygen content of TiO_x to its rest potential in solution, while a survey of the anodic behavior of TiO, Ti_2O_3, and titanium nitrides and carbides has been made by Smirnov, Ivanovskii, and Krasnov[24].

A considerable amount of information is available on the corrosion of Ti under widely varying conditions. This is best summarized in the potential-pH diagram for the Ti - H_2O system by Schmets and Pourbaix[25]. A phase diagram for the Ti - TiO_2 system has been constructed by DeVries and Roy[26].

With regard to Ti_3Au, it is interesting to note that Philipsborn and Laves[21] have described an induced $\beta \rightarrow \alpha$ phase transition (Cr_3Si or β W type to Cu_3Au type) on remelting in the presence of small amounts of oxygen, nitrogen, or carbon; the transformation is described as irreversible.

II. EXPERIMENTAL

The preparation of materials and electrodes is described in the text when discussing the results of the specific group of catalysts. Two coarse techniques were developed during this period to determine the electrical resistance of catalyst powder and its bulk density.

The resistance measurements were carried out by compressing between two pieces of platinum foil a sample of powder contained by an O-ring 1/2" OD and 5/16" ID. The extent of compression was defined by a torque wrench (P. A. Sturtevant Co., Model F-25-1) at 15-inch pounds.

Bulk density was determined by weighing quantities of catalyst in graduated tubes after vibration and after centrifuging.

The materials prepared by the Bureau of Mines required special handling since they were pyrophoric; they were shipped under CO_2 and have been subsequently handled in a glove box in an argon atmosphere. During all the handling procedures a freshly prepared sample of Raney nickel was exposed to the atmosphere in the glove box; the procedures were considered satisfactory if this material was still pyrophoric on subsequent exposure to air. The samples were initially divided into eight samples of about 3g each, and at this time the resistivity of the powders was measured.

The electrodes have been tested as 1 cm^2 samples in a floating electrode cell described previously[4]. It has been shown that the results obtained by this method are reproducible and are meaningful in the prediction of real system performance[28].

III. RESULTS

A. Effect of Manufacturing Techniques on Performance of Porous Electrodes

1. Platinum Electrodes

Platinum electrodes have been prepared by spraying, brushing, spreading, and rolling methods. All preparations to date have been made with approximately 30% Teflon, considered from previous work to be optimum, and a Pt loading of about 10 mg/cm^2. Deviations from the 10 mg/cm^2 loading are due to uncertainties in the expected loss of material for each fabrication method. All electrodes are cut from larger pieces to 1 cm^2 for testing.

2. Catalyst Distribution Methods

a. Spraying Technique

Electrodes numbered 1, 2a, TR-1, TR-2, TR-3A, TR-3B, TR-4A, TR-4B, TR-6, TR-7, TR-8 (Figs. 35-42), were sprayed with an air gun to determine the relation between loading and spraying techniques. Electrodes 1 and 2a were prepared on 100 cm^2 of screen, and 50% excess platinum was used for a projected 10 mg/cm^2 loading after losses. These electrodes were sintered at 260°C and had 10 mg/cm^2 Pt. Electrodes TR-1, TR-2, TR-3 and TR-4 were prepared on 36 cm^2 of screen, and 20% excess platinum was used for a projected 10 mg/cm^2. These electrodes had approximately 3-7 mg/cm^2 of platinum. Electrodes TR-3A and TR-4A were sintered at 260°C and showed extremely low performance; subsequently, electrodes TR-3B and TR-4B, sintered at 310°C, showed improved performance. Electrodes TR-6, TR-7 and TR-8 were also sprayed on 36 cm^2 screens with 20% excess platinum but with the following changes in technique: Cab-o-SiL was added to the platinum-Teflon mix on a 1:1 volume ratio. Since this extended the liquid volume and produced a thicker spraying mix, continuous drying was employed. These electrodes had a good uniform physical appearance and loadings (8 - 10 mg/cm^2) were closer to the

projected loading. However, the Cab-o-SiL may have had an adverse effect on the wetting characteristics of the electrodes. The electrodes were sintered at 285°C, since 260°C seems to be on the borderline of the critical minimum sintering temperature. The influence of sintering temperature is considered in more detail below.

b. Spreading Technique

It has been found that spraying produces the most uniform distribution of catalyst but does not work well with a small quantity of material. The spreading process (spreading a thick paste with a spatula) lends itself better to small quantities but usually does not yield uniform electrodes. Electrode TR-5 (Fig. 44) was made in this manner on 8 cm^2 of screen starting with no excess material; 13% of the material was lost.

c. Brushing Technique

Electrode TR-9 (Fig. 45) was made by applying a paste with a small brush to 12 cm^2 of screen mounted on a portable jig for weighing "in situ." An excess of 100% was used in order to work with a paste of the same consistency throughout application. This method has not been investigated sufficiently to permit a critical analysis at this time. The performance of the electrode was exceptionally high, surpassing all previous runs to date.

d. Rolling Technique

Electrode TR-10 (Fig. 46) was made by forming the platinum-Teflon into a rubbery dough and rolling it between Teflon sheets over the defined area of screen. This electrode was not made specifically for this program and consequently did not have a 10 mg/cm^2 loading. It has been found that the rolling method produces uniform electrodes with no loss of material, but they show comparatively low performance. No duplication of runs has been made. The results are summarized in Fig. 47. The variation in performance was assumed to be mainly related to sintering temperature. This was examined as described below.

B. Effect of Sintering Temperatures

A number of electrodes cut from a single sheet of electrode material prepared by the spray method have been sintered at 250°C, 275°C, 300°C, and 325°C for five-minute and fifteen-minute intervals. The sintering temperatures in these experiments have been accurately defined. In previous work the thermocouple controlling the sintering furnace was influenced by radiant heat. Since the electrodes were effectively shielded from the radiant heat by aluminum foil, the true sintering temperature was some 26° lower than that registered on the controller/indicator.

The results are presented in Figs. 48-53. The two electrodes sintered at 250°C were not hydrophobic and were not tested. On the basis of these results summarized in Table IV, the sintering technique has been improved and made more reliable, and the optimum sintering conditions (for platinum) have been defined as 275°C for 15 minutes. Results obtained under these conditions compare favorably with the best previously reported for electrodes prepared in the same way. The change in real surface area during this sintering process at 275°C has been measured by a BET technique. The figures before and after sintering were 22.6 m^2/g and 15.6 m^2/g respectively; the platinum black from which the electrodes were prepared had a surface area of 29.0 m^2/g. Similar measurements will be made as a matter of routine in the investigation of the highly dispersed catalysts.

C. Carbon and Graphite Electrodes

The performance of carbon and graphite powders were initially of interest as a basis for comparison of metal carbides. They also present a good opportunity for studying techniques of preparing high surface area electrodes, because of the wide range of samples available with such different physical properties as bulk density and surface area. They have consequently been used to examine the influence of PTFE/catalyst ratio on performance. The bulk densities of the catalysts have been measured to discover if a better correlation can be made in terms

TABLE IV

Effect of Sintering Time and Temperature

		E = 950 mv	E = 900 mv
250°C	---------- not tested ----------		
275°C	5 min	i = 4	5 ma/cm^2
	15 min	28	242 "
300°C	5 min	5	10 "
	15 min	18	130 "
325°C	5 min	20	214 "
	15 min	25	230 "

of a volume rather than a weight ratio. The following samples have been examined: graphite with 22.5%, 25%, 27.5%, 30%, 35%, 40% PTFE content and acetylene black with 45%, 50%, 55%, 60%, 70% PTFE content. A summary of performance is given in Table V; the complete range of performance curves is given in Figs. 54-64. The optimum PTFE contents were deduced to be 27.5% for graphite and 50% for acetylene black, although the curves showed fairly flat maxima so that these figures are not too critical. Two other samples of carbon, shown in Figs. 65 and 66, were also examined.

The bulk densities have been measured after vibration and after centrifuging. Each method is reproducible to about 5%, but as can be seen from Table VI, the agreement between the two methods is not good. This is not an unusual occurrence in the determination of bulk densities, since the particle shape factor has a different effect in the various methods of measurement[29]. The data available to correlate bulk density and PTFE content are shown in Fig. 67. It is apparent that the correlation is a useful guide and that the centrifuging method gives the more consistent data.

TABLE V

Performance as a Function of PTFE Content

Graphite	20	22.5	25	27.5	30	35	40	% PTFE
Current at 800 mv	----	9	7	22.2	5	61	4	ma/cm^2
Current at 600 mv	----	44.5	78	95.5	68	26.6	22	ma/cm^2
Acetylene Black	45	50	55	60	70			% PTFE
Current at 800 mv	2.4	7	5	4	3			ma/cm^2
Current at 600 mv	21.4	94.5	45	48	42			ma/cm^2

TABLE VI

Bulk Density Measurements

Material	Bulk Density (gm/cc) Vibration	Centrifuge	% PTFE
Acetylene black	0.125	0.130	50
Graphite	0.350	0.425	27.5
Engelhard Pt black	0.540	0.435	30
Carbon #7706	0.940	0.735	20
Carbon #8946	0.830	0.580	20
Ni_3C	0.689	0.927	10
$Ni_3C + Co_2C$	0.814	0.780	10

D. Interstitial Compounds of Group VIII

1. Materials Prepared by Tyco Laboratories

#38 Ni_3N

Preparation and selection of nitriding temperatures based on the work of Rienacker & Mohl[30]

Starting Material: nickel formate and ferric formate (1% by weight)
Heated 3 hours in H_2 at 225°C to decompose the formate and then 20 hours in N_2 at 300°C

X-ray: Ni + Ni_3N + minor phases, Fe, etc.

Surface Area: 9.26 m^2/g

Comments

This was an attempt to reproduce a previously successful preparation (57% Ni_3N). In this case, because the X-ray intensities indicated a very low nitride content, the material was not electrochemically tested.

#39 Ni_3C

Preparative method based on a paper by Liecester and Redman[31]

Starting Material: nickel acetate
decomposed at 300°C in N_2 for 3 hours

X-ray: Ni_3C + Ni

Surface Area: 19.3 m^2/g

Electrochemical Test: Fig. 68

Comments

The performance was ~ 50 mv lower at 200 ma/cm^2 than electrode 20a reported previously[4]. The observed current maximum at 600 mv is discussed later.

#40 Co_2N Preparation based on that reported by Juza and Sachs[32]

Starting Material: $Co(NO_3)_2$ to give Co_3O_4
Reduced in H_2 at 350°C for 3 hours; then heated in NH_3 at 380°C for 3 hours, cooled in NH_3, ground in mortar, and heated for a further 3 hours in NH_3 at 380°C

X-ray: The diffraction pattern could not be interpreted and could not even be identified.

Comments

The electrochemical test showed a behavior characteristic of cobalt metal with a rest potential at about 150 mv vs. RHE and small cathodic currents < 4 ma/cm^2 on the completely oxidized surface.

#41 $Ni_3C + Co_2C$ Preparative conditions as #39 for Ni_3C

Attempted preparation of mixed carbide by decomposition of the acetates; starting material 80% nickel acetate, 20% cobalt acetate, ground together.

Decomposed in N_2 at 300°C for 6 hours

X-ray: Ni_3C + Ni; the presence of Co_2C as such cannot be confirmed by X-ray analysis in the presence of Ni_3C because the diffraction patterns are identical.

Electrochemical Test: Fig. 69

Comments

Initial performance in the region of activation control is better than Ni_3C, but the polarization increases more rapidly at higher current densities.

#42 $Ni_3C + Co_2C$ — As #41, with the acetates dissolved in water and then evaporated prior to decomposition to obtain more intimate mixing

Electrochemical Test: Fig. 70

Comments

As with #41, high potentials are also observed at very low current densities, but performance is otherwise poor.

#43 Co_2N — Repeat of Preparation #40, identical X-ray pattern and electrochemical characteristics.

#44 $Ni_3C + Co_2C$ — Repeat of #42

Electrochemical Test: Fig. 71

Comments

This electrode was prepared with a lower PTFE content. The performance is the best observed for this series and represents an improvement on the best results reported for Ni_3C.

#45 Ni_3C — Prepared by the decomposition of nickel acetate in N_2 at 275°C for 12 hours
Not yet tested.

#46 Ni_3C — Prepared by the decomposition of nickel acetate in N_2 at 300°C for 12 hours
Not yet tested.

#47 Ni_3C — Prepared by the decomposition of nickel acetate in N_2 at 300°C for 6 hours

#48 $Ni_3C - Co_2C$ — Repeat of #42

Electrochemical Test: Fig. 72

2. Materials Prepared by the Bureau of Mines

The following materials constitute the first samples* of a series prepared by the Bureau of Mines, Pittsburgh Coal Research Center, as part of a coordinated project with Tyco.

2-C, ϵ - Fe_2C + Fe_3O_4;

4-C, χ -Fe_2C + Fe_3O_4;

6-C, χ -Fe_2C + θ-Fe_3C;

2-N, γ' -Fe_4N + ϵ - Fe_3N;

5-N, ϵ - Fe_3N γ' -Fe_4N;

6-N, ϵ - Fe_3N + ζ -Fe_2N (γ' -Fe_4N)

1-CN, ϵ - FeX (carbon and/or nitrogen);

8-N, γ-Fe_4N;

9-N, ζ -Fe_2N;

1-CP, $Fe(OH)_3$ + Ag_2O (Fe/Ag = 3/1)

II-CP $Fe(OH)_3$ + Ag_2O (Fe/Ag = 1/1);

III-CP $Fe(OH)_3$ + Hg_2O (Fe/Ag = 1/3).

The resistance of a sample of each material was measured under an argon atmosphere. Subsequently, a small sample was exposed to air and the resistance measured again. If the resistance showed a significant increase or if the material was obviously pyrophoric, then controlled deactivation techniques were attempted. So far, these have involved covering the sample with water and allowing the sample to dry out slowly in air. The following results have been obtained for the first six of the samples examined.

Sample	Resistance (Unexposed)	Resistance (Exposed)	Resistance (Deactivated in H_2O)
2C	< 0.1 Ω	75 Ω	50 Ω
1-CN	< 0.1 Ω	< 0.1 Ω	< 0.1 Ω
II-CP	15×10^4 Ω	1.5×10^4	1.5×10^4
4c	< 0.1 Ω	< 0.4 Ω	2.5 Ω
9N	< 0.2 Ω	< 0.2 Ω	< 0.2 Ω
6C	< 0.2 Ω	< 0.2 Ω	3.15 Ω

* Details of the methods of preparation can be obtained from the reports of the Bureau of Mines.

Electrochemical tests have so far been carried out on samples 1-CN, II-CP, and 4C (Figs. 74-76). For these initial samples the surface areas, after exposure to air, have been measured and electron micrographs taken to establish the basic physical characteristics of these materials. These techniques will be used for future samples when interest warrants it.

Sample	Surface Area	Bulk Density by Centrifuging
1-CN	10.6 m^2/g	2.7 g/cm^3
II-CP	49.1 m^2/g	2.3 g/cm^2
4-C	14.1 m^2/g	1.77 g/cm^2

The electron micrographs are presented in Figs. 77, 78 and 79.

The electron micrograph of the iron carbonitride shows some very finely divided material — possibly a small quantity of residual iron and some more electron dense agglomerates, assumed to be the carbonitride — varying in size from 200 Å to more than 2 μ. The χ-Fe_2C was characterized by large agglomerates typified by the one shown in Fig. 79. The agglomerates are apparently formed from fairly uniformly sized particles of about 250 Å in diameter. As expected, the $Fe(OH)_3 + Ag_2O$ shows some extremely finely divided material forming agglomerates up to 500 Å in diameter. Some of these agglomerates are loosely grouped to give a lace-like structure.

ϵ Iron Carbonitride This material showed very little activity for the oxygen reduction process.

$Fe(OH)_3 + Ag_2O$ Since this material had been prepared at low temperatures, it was tested as a floating electrode, using Elvax as a plastic hydrophobic binder rather than PTFE which would require sintering at 275°C. The activity level was very low; there was no evidence of the activity normally observed with Ag.

$Fe_2C + Fe_3O_4$ A large anodic current, indicative of a surface oxidation process, was observed initially with this material; subsequent activity for oxygen reduction was low.

Ni_3C and $Ni_3C + Co_2C$ The results obtained with these materials have been fraught with irreproducibility and an irregular shape to the polarization curves; see, for example, Fig. 68. In order to try to understand the processes involved, an electrode was introduced to the electrolyte at a fixed potential of 800 mv and the current monitored as a function of time. The result is shown in Fig. 80. It is evident that most of the results have been obtained on the plateau where the current is reasonably constant. The unusual curves probably represent experiments that have run into the decay portion of the curve. Subsequent activities of these electrodes have always been at a low level, as evidenced by Fig. 73. This decay process must cast doubt on the figures presented in the results section, but it is encouraging to note that the pattern of the decay process (a plateau extending for > 2 hours) substantiates the fact that the high initial activity shown by these electrodes is a real effect; i. e. the high cathodic currents cannot be associated with the reduction of a surface oxide formed in some way during the preparation of the catalyst. The experimental evaluation of these catalysts will be closely defined as a function of time of immersion in the electrolyte in all future work.

E. Ti_3Au Powder

Ti_3Au powder was prepared by grinding glass brittle ingots, in an agate mortar and pestle and sieving for -325 mesh particles. A porous electrode was fabricated from about 50 mg of this powder and 20% Teflon on a nickel screen. An attempt was made to operate this electrode on oxygen in the floating electrode apparatus. It was found, however, that the electrode began evolving gas immediately upon immersion in solution. The powder, initially gray-gold, turned bluish-black and expanded significantly in volume. The currents observed were only nominally larger than those of the platinum wire clamps of the electrode holder itself.

In order to investigate these phenomena further, some of the original Ti_3Au powder was boiled in 2N KOH for 7 hours at which time gas evolution ceased. A BET analysis of the resultant powder yielded 133 m^2/gm of surface area. The electrical resistance of the compressed powder was of the order of 200 K Ω. An electrode made from the material showed no gain in performance over the original electrode.

Chemical analysis of the powder for Au and Ti showed Ti 22.75% and Au 56.3% by wt. This indicates a loss of 44.5 wt % Ti, if it is assumed that there was no loss of gold. The balance of the analysis, taken to be oxygen. gives a formula $Au\ Ti_{1.65}O_{4.53}$, an oxygen content in excess of the TiO_2 stoichiometry. This does not at all approach the formula for nonstoichiometric titanium oxide, $Au_{1.0}\ (TiO_{1.75})_3$ which is expected to show good electronic conductivity.

It is intended to make a deliberate attempt to prepare nonstoichiometric oxides of Ti_3Au and pure Ti to understand this behavior better and also to look at the other intermetallic compounds of Ti and Au. (TiAu has been described elsewhere in this report.)

F. Summary of Results

Activity presented in terms of current observed at 800 mv and at 600 mv vs. RHE (iR corrected).

Tyco-Prepared Materials

	800 mv	600 mv	
#44 $Ni_3C + Co_2C$	80	> 400	ma/cm^2
#47 Ni_3C	15	236	ma/cm^2
#39 Ni_3C	6	180	ma/cm^2
#48 $Ni_3C + Co_2C$	20	132	ma/cm^2
#41 $Ni_3C + Co_2C$	8	30	ma/cm^2
#42 $Ni_3C + Co_2C$	2	6	ma/cm^2
Graphite	22.2	95.5	ma/cm^2
Acetylene Black	7	94.5	ma/cm^2

Bureau-of-Mines-Prepared Materials

	800 mv	600 mv	
#1-CN^{+} ϵ-Iron carbonitride		1	ma/cm^2
#II-CP $Fe(OH)_3$ + Ag_2O	0-2	1	ma/cm^2
#4C Fe_2C + Fe_3O_4	anodic current		

REFERENCES

1. Fishman, J.H., and Rissman, E.F., Extended Abstracts, Spring Meeting of the Electrochemical Society, San Francisco, May 1965.
2. Rao, M.L.B., Damjanovic, A., and Bockris, John, J. Phys. Chem. 67, 2508, (1963).
3. Beer, S.Z., and Sandler, Y.I., J. Electrochem. Soc. 112, 1133, (1965).
4. Fourth Quarterly Report, Contract No. NASW-1233, June 30, 1966.
5. Stern, M., and Makrides, A.C., J. Electrochem. Soc. 107, 782 (1960).
6. Parsons, R., Surface Science 2, 418 (1964).
7. Frumkin, A.N., J. Electroanal. Chem. 9, 173 (1965).
8. Amelins Handbuch Part 41; pp 214-251 - Weinheim, (1951).
9. Douglass, D.L., St. Pierre, D.R., and Spieser, R., Met. Soc. Conf. 8, 705 (1961).
10. Gilles, J.C., Lejus, A.M., and Collonguy, R., Corrosion and Anticorrosion 12, (3) 99 (1964).
11. Hollander, L.E., and Castro, P.L., Phys. Rev. 119, 1882 (1960).
12. Dorin, V.A., and Tartakovskaya, F.M., Zhur. Neorg. Khim. 4, 2635 (1959).
13. Boltaks, B.I., Vesenin, F.I., and Salunina, A.E., Zhur. Tekh. Fiz. 21, 532 (1951).
14. Greener, E.H., Diss. Abstr. 21, 1514 (1960).
15. Ariya, S.M., and Bogdanova, N.I., Fiz. Tverdogo Tela 1, 1022 (1959).
16. Morin, F.J., Phys. Rev. Letters 3, 34 (1959).
17. Sawai, I., Terada, K., Okamura, T., and Ueno, A., Repts. Inst. Chem. Research Kyoto Univ. 17, 55 (1949).
18. Grunewald, H., Z. Ann. Physik 14, 121 (1954).

19. Long, J., and Tiechner, S.J., Bull. Soc. Chim. France, (9) 2625 (1965).

20. Mysanikov, I.A., Zhur. Fiz. Khim. 33, 2564 (1959).

21. Mazza, F., Mussoni, T., and Trasatti, S., Chim. e Ind. (Milan) 45 (4), 417 (1963).

22. Mazza, F., Chim. e Ind. (Milan) 43, 1424 (1961).

23. Dean, R.S., and Hornstein, I., U.S. Government Research Reports 32, 251 (1959).

24. Smirnov, M.V., Ivanovskii, L.E., and Krasnov, Yu. N., Akad. Nauk. S.S.S.R., Ural Filial, 2, 177 (1958).

25. Schmets, J., and Pourbaix, M., Proc. 6th Meeting C.I.T.C.E. p. 118 (1955).

26. DeVries, R.C., and Roy, R., Ceramic Bulletin 33, 370 (1954).

27. Philipsborn, H.V., and Laves, R., Acta Cryst. 17, 213 (1964).

28. Giner, J., and Smith, S., to be published in Jan/Feb 1967 issue, Electrochem. Tech.

29. Particle Size: Measurement Interpretation and Application, Irani and Callis, Wiley, New York (1963) p. 9.

30. Rienäcker, G., and Mohl, K.H., Z. Anorg. Allgem. Chem. 333, 291 (1964).

31. Leicester, J., and Redman, M.J., J. Appl. Chem. 12, 356 (1962).

32. Juza, R., and Sachze, W., Z. Anorg. Chem. 253, 95 (1945).

APPENDIX 1

i(E)-CURVES

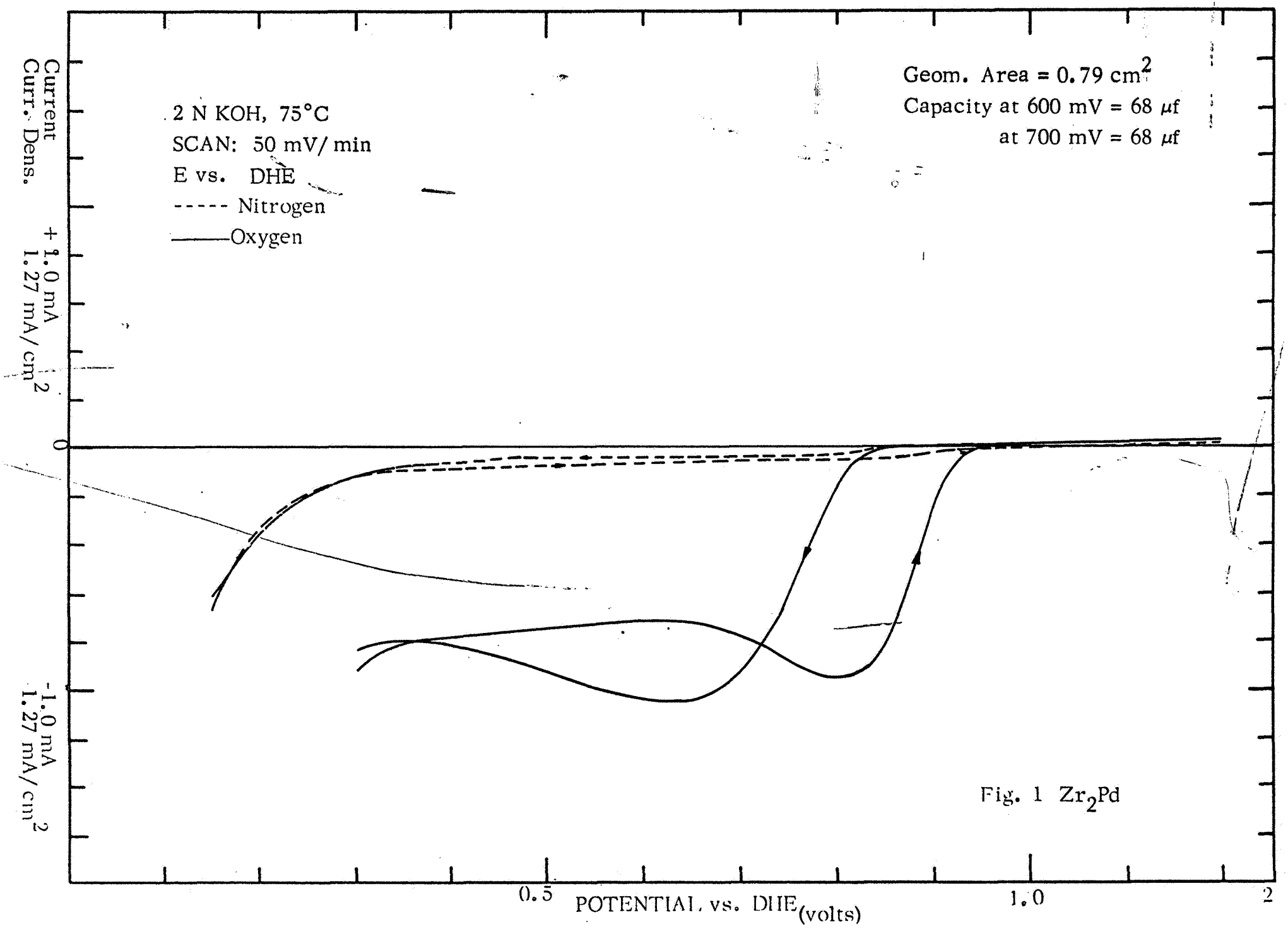
Current
Curr. Dens.
+1.0 mA
1.27 mA/cm2
0
-1.0 mA
1.27 mA/cm2
2 N KOH, 75°C
SCAN: 50 mV/ min
E vs. DHE
----- Nitrogen
——Oxygen
Geom. Area = 0.79 cm2
Capacity at 600 mV = 68 μf
at 700 mV = 68 μf
0.5
POTENTIAL vs. DHE (volts)
1.0
2

Fig. 1 Zr_2Pd

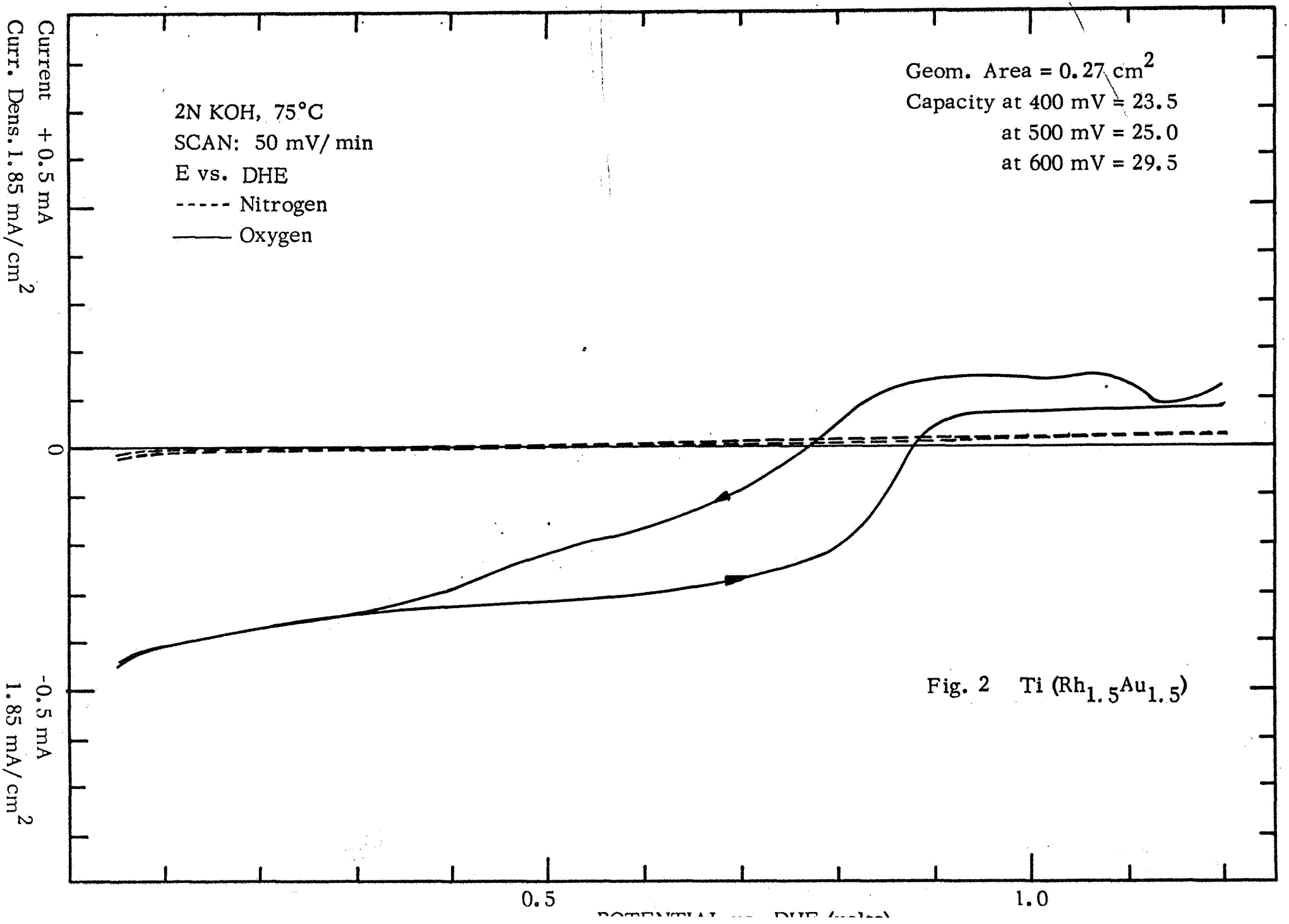

Fig. 2 Ti ($Rh_{1.5}Au_{1.5}$)

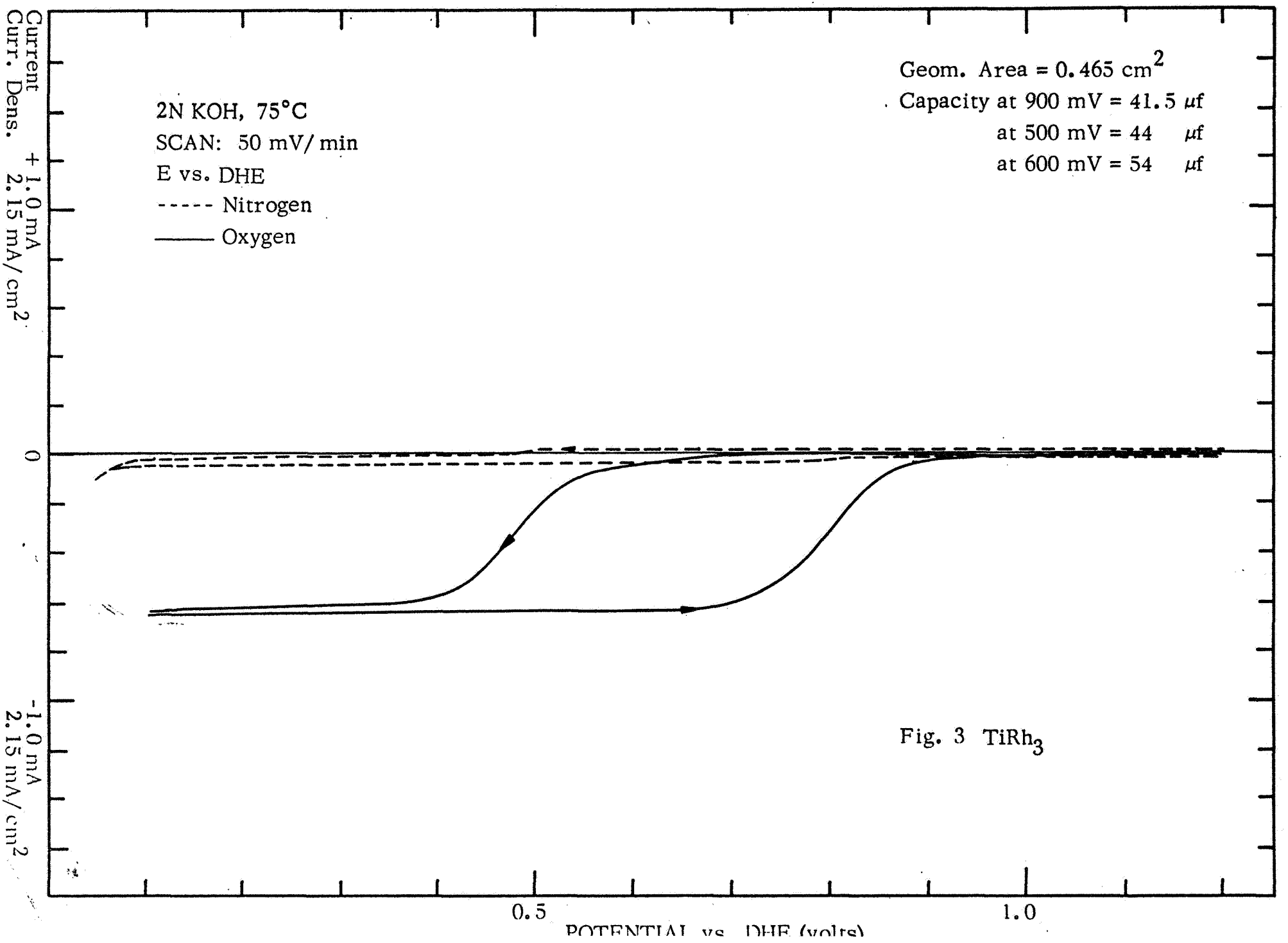
Current
Curr. Dens.
+1.0 mA
2.15 mA/cm²
0
-1.0 mA
2.15 mA/cm²
2N KOH, 75°C
SCAN: 50 mV/min
E vs. DHE
----- Nitrogen
—— Oxygen
Geom. Area = 0.465 cm²
Capacity at 900 mV = 41.5 μf
at 500 mV = 44 μf
at 600 mV = 54 μf
0.5
1.0
POTENTIAL vs. DHE (volts)

Fig. 3 $TiRh_3$

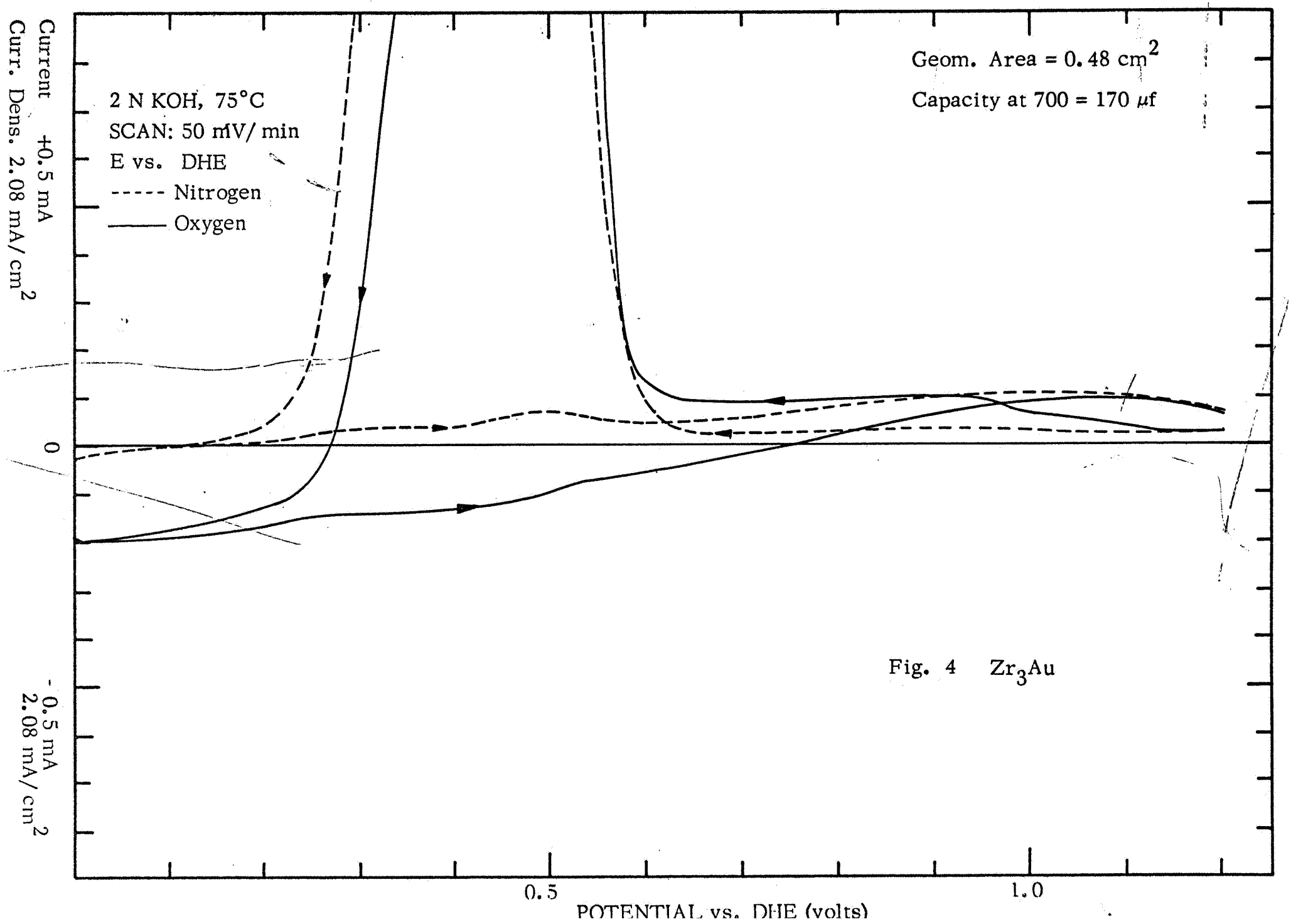
Current +0.5 mA
Curr. Dens. 2.08 mA/cm2
0
- 0.5 mA
2.08 mA/cm2
2 N KOH, 75°C
SCAN: 50 mV/ min
E vs. DHE
----- Nitrogen
—— Oxygen
Geom. Area = 0.48 cm2
Capacity at 700 = 170 μf
0.5
1.0
POTENTIAL vs. DHE (volts)

Fig. 4 Zr_3Au

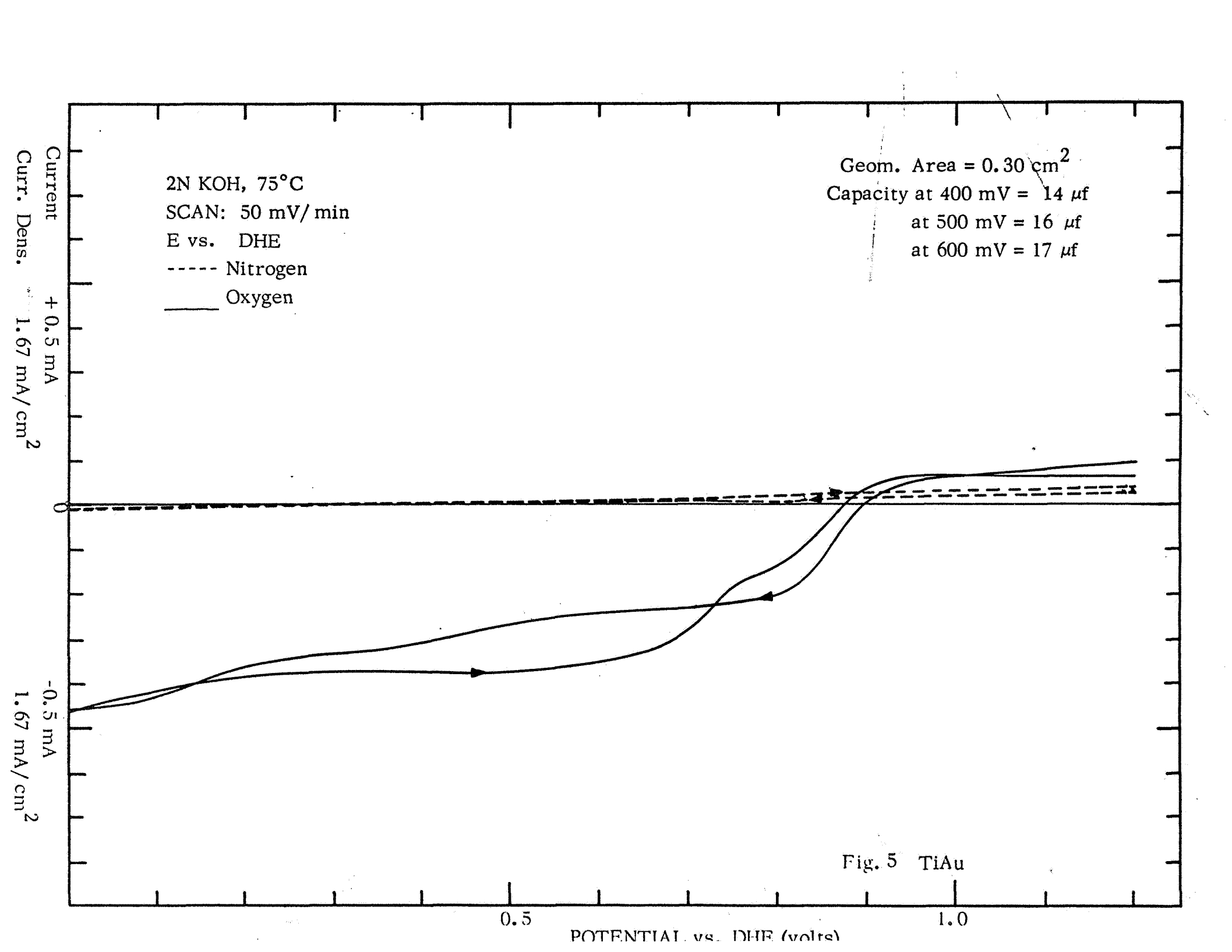
2N KOH, 75°C
SCAN: 50 mV/ min
E vs. DHE
----- Nitrogen
_____ Oxygen
Geom. Area = 0.30 cm2
Capacity at 400 mV = 14 μf
at 500 mV = 16 μf
at 600 mV = 17 μf
Current
Curr. Dens.
+0.5 mA
1.67 mA/cm2
0
-0.5 mA
1.67 mA/cm2
0.5
1.0
POTENTIAL vs. DHE (volts)

Fig. 5 TiAu

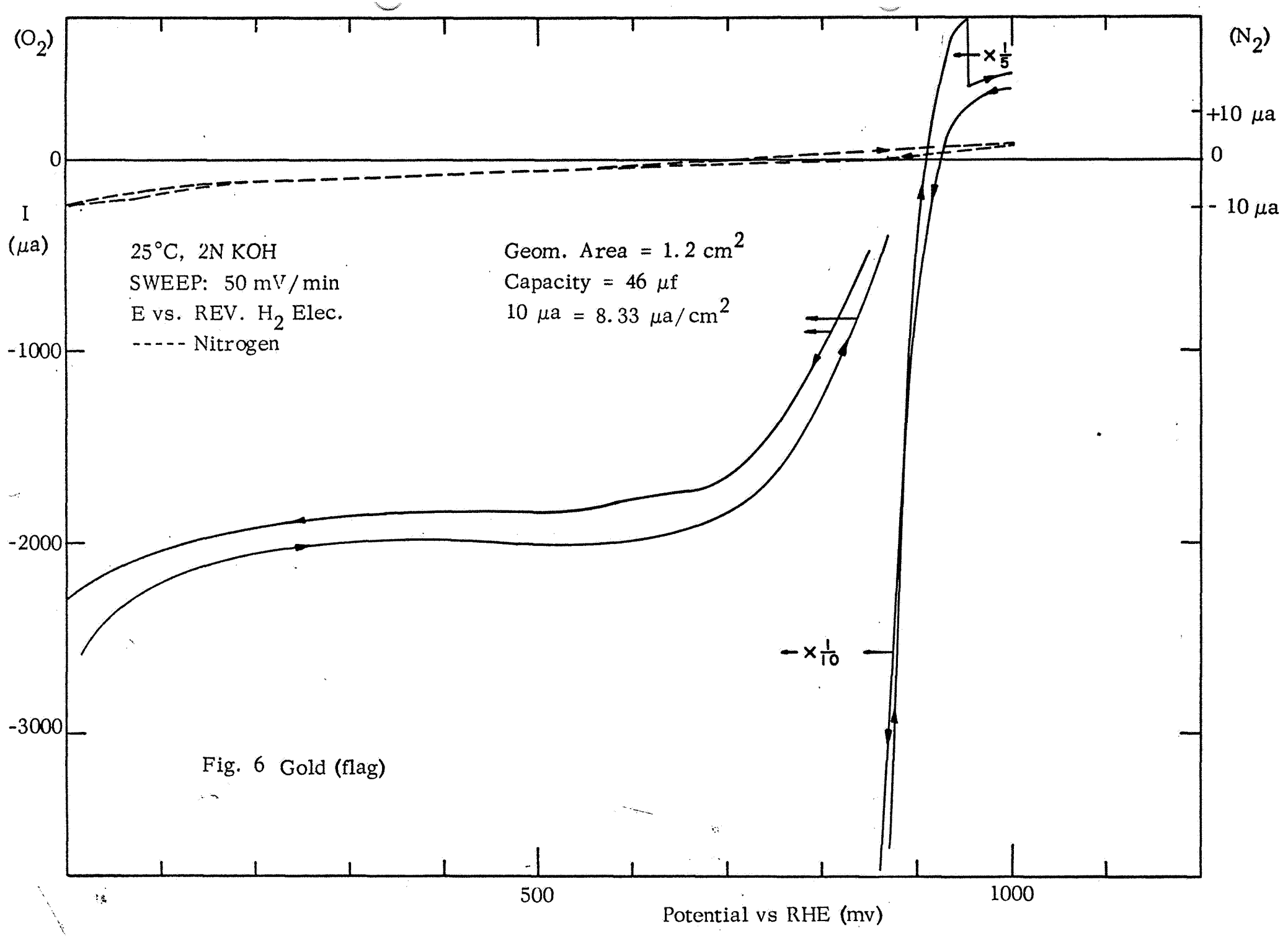

Fig. 6 Gold (flag)

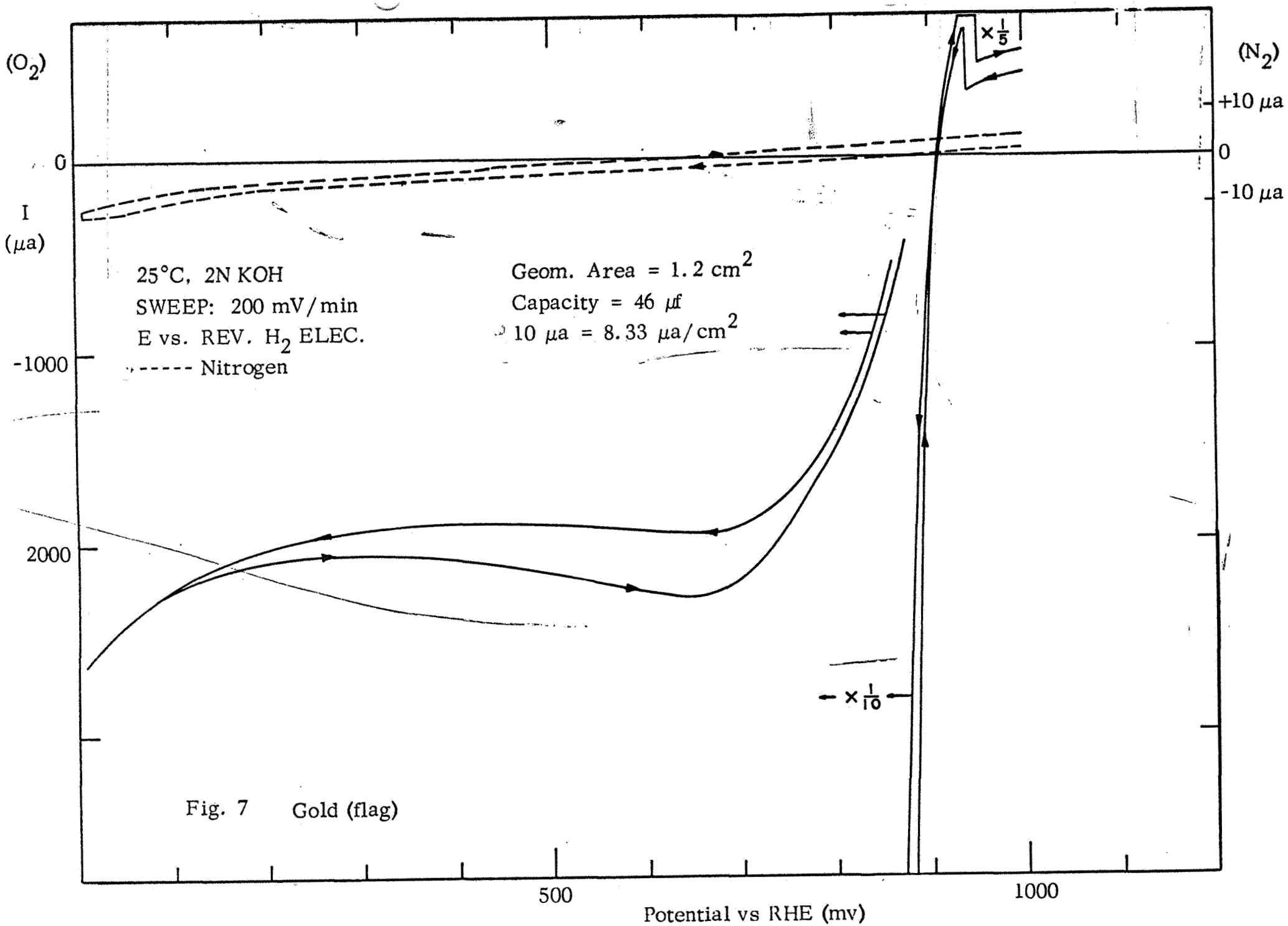

Fig. 7 Gold (flag)

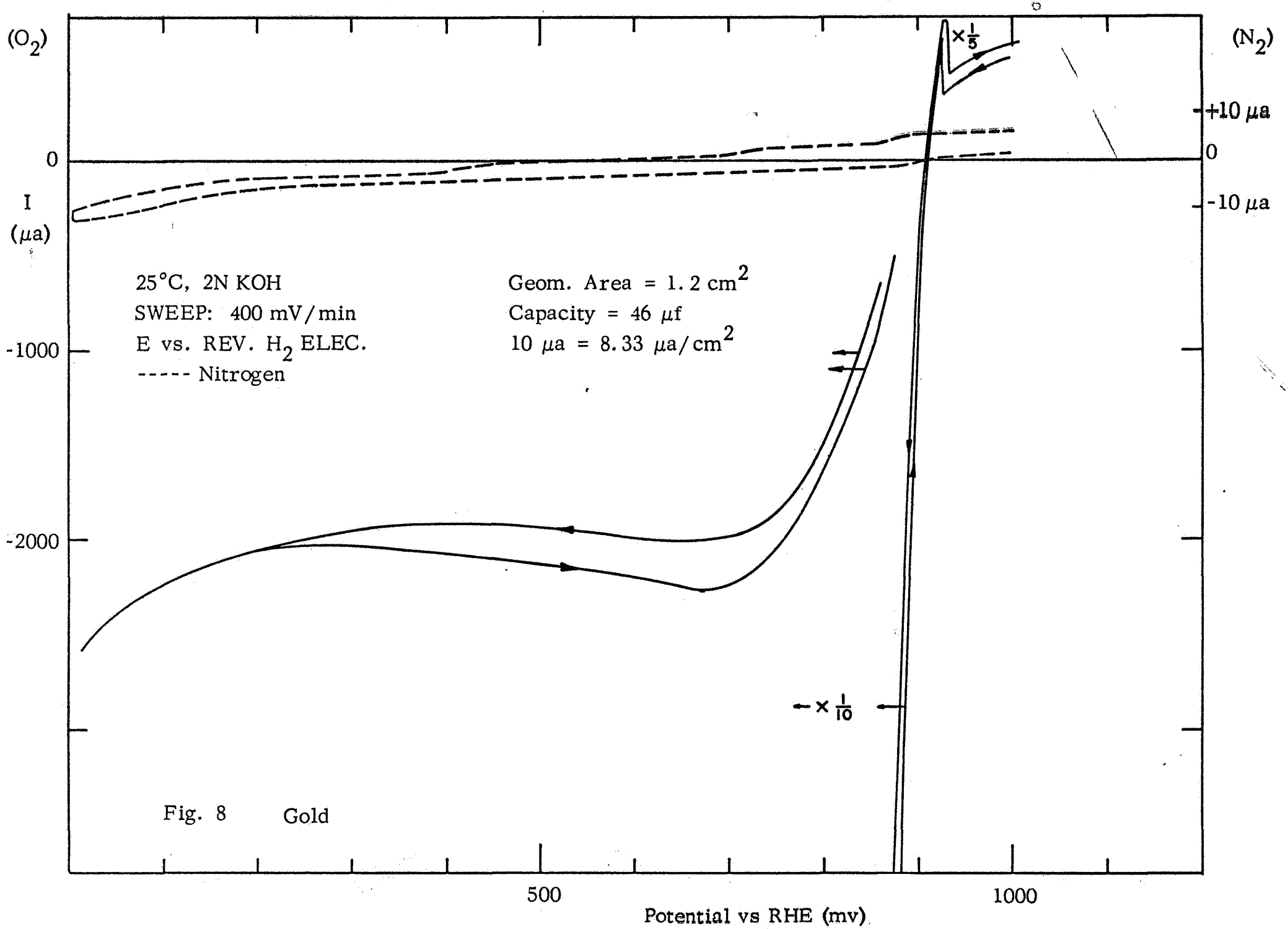
(O2)
(N2)
×1/5
+10 μa
0
0
I
(μa)
-10 μa
25°C, 2N KOH
SWEEP: 400 mV/min
E vs. REV. H2 ELEC.
----- Nitrogen
Geom. Area = 1.2 cm2
Capacity = 46 μf
10 μa = 8.33 μa/cm2
-1000
-2000
×1/10
500
1000
Potential vs RHE (mv)

Fig. 8 Gold

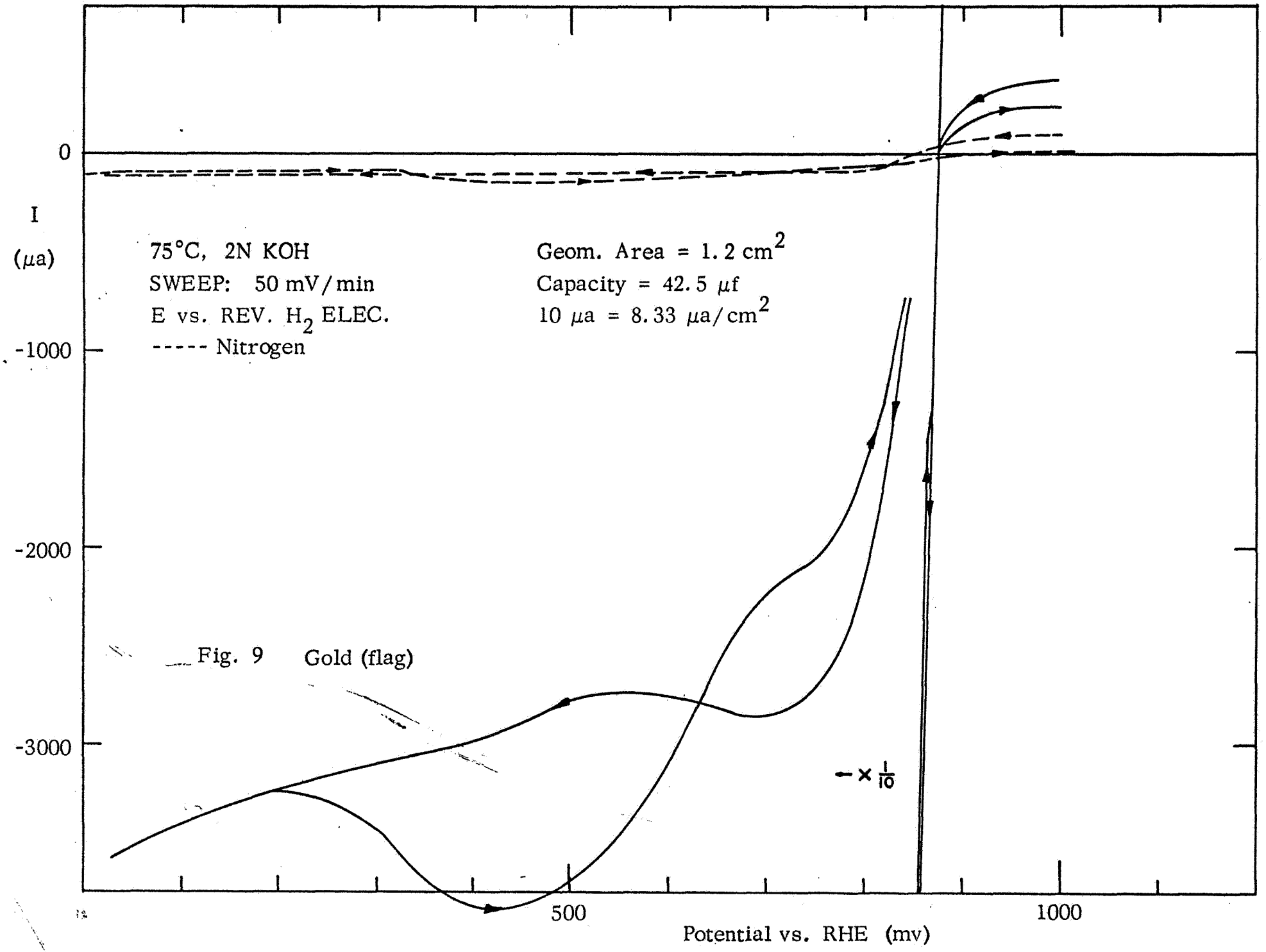
0
I
(μa)
75°C, 2N KOH
SWEEP: 50 mV/min
E vs. REV. H_2 ELEC.
----- Nitrogen
Geom. Area = 1.2 cm^2
Capacity = 42.5 μf
10 μa = 8.33 μa/cm^2
-1000
-2000
-3000
Fig. 9 Gold (flag)
← × 1/10
500
1000
Potential vs. RHE (mv)

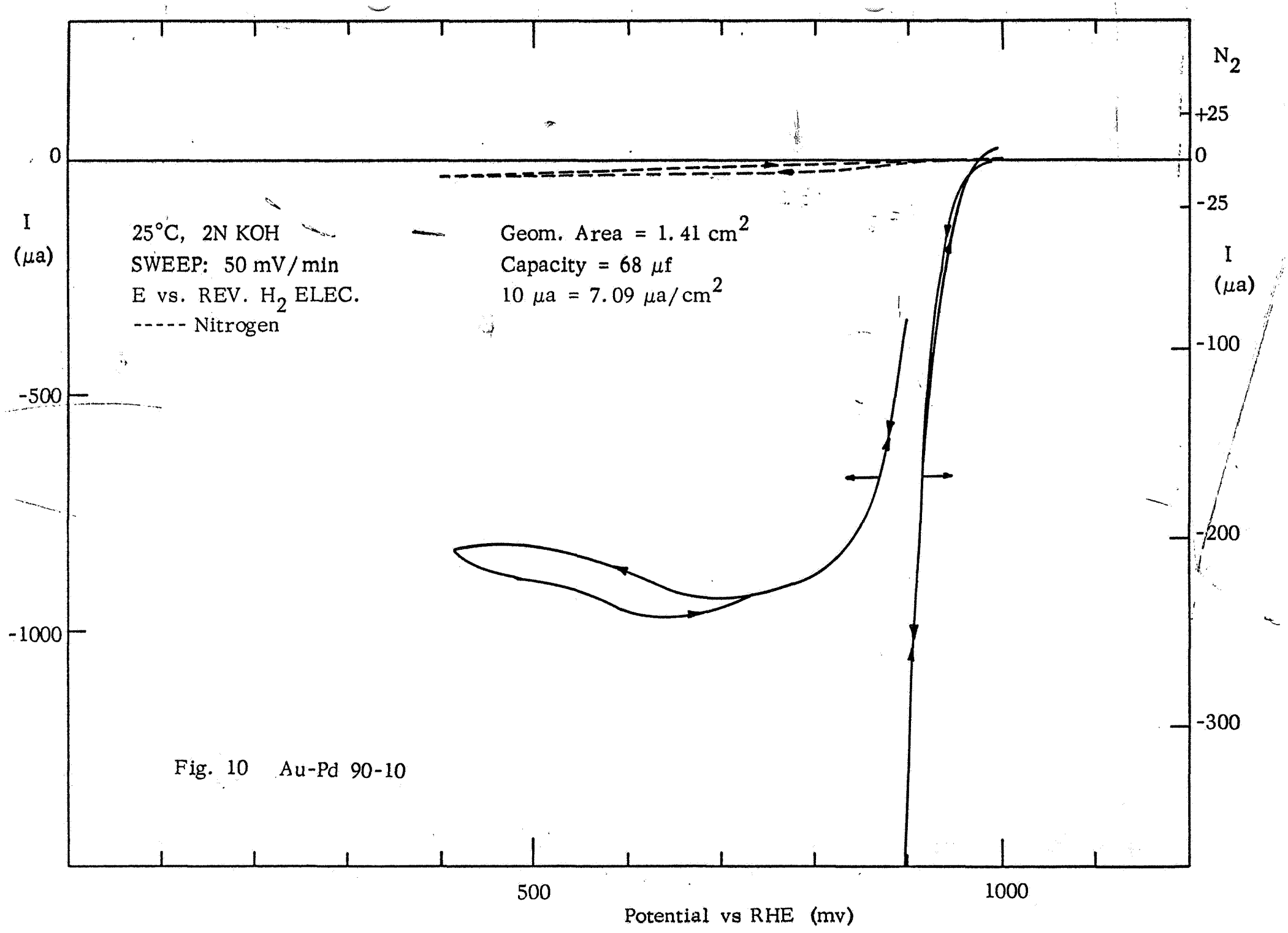

Fig. 10 Au-Pd 90-10

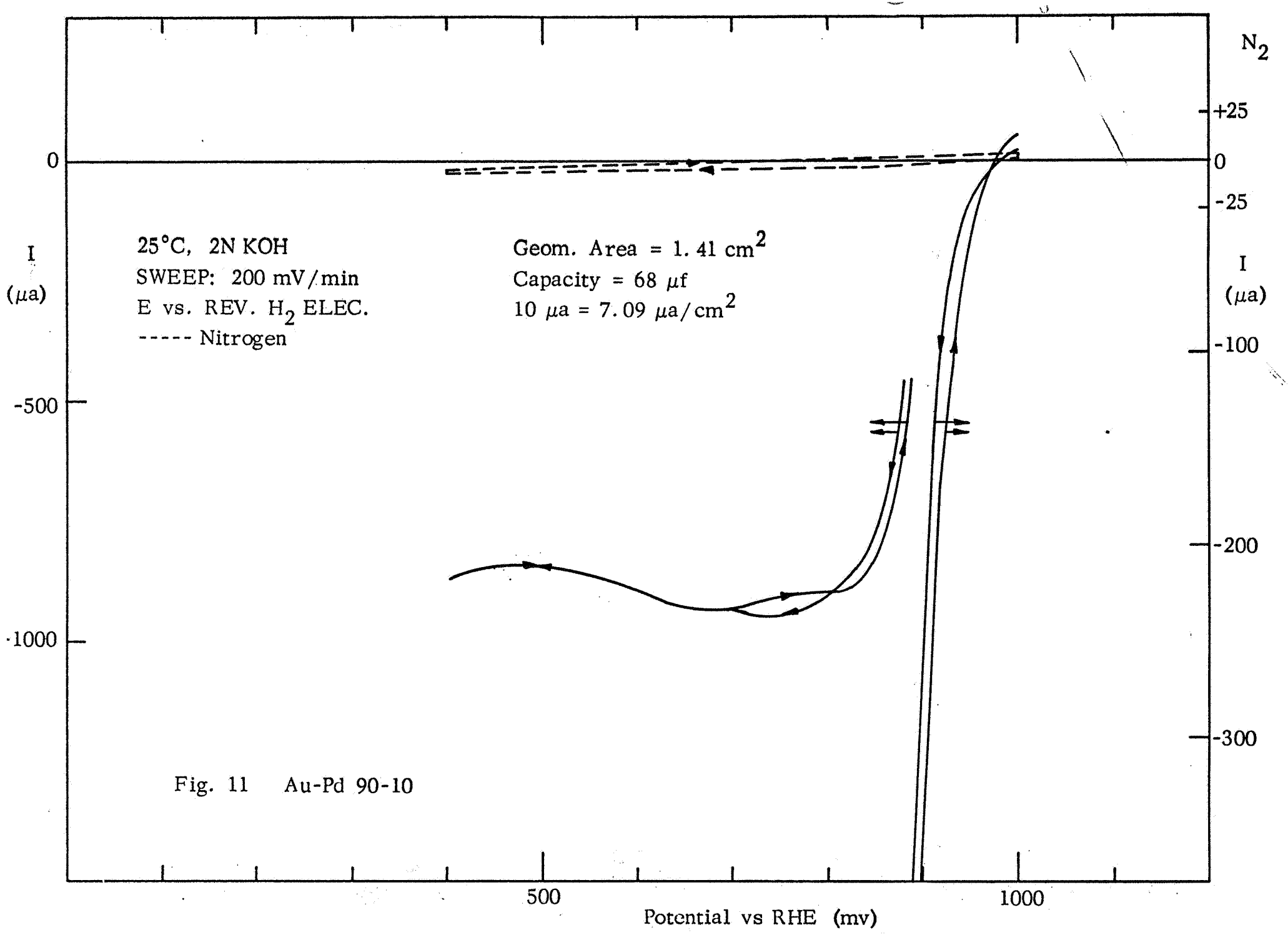

Fig. 11 Au-Pd 90-10

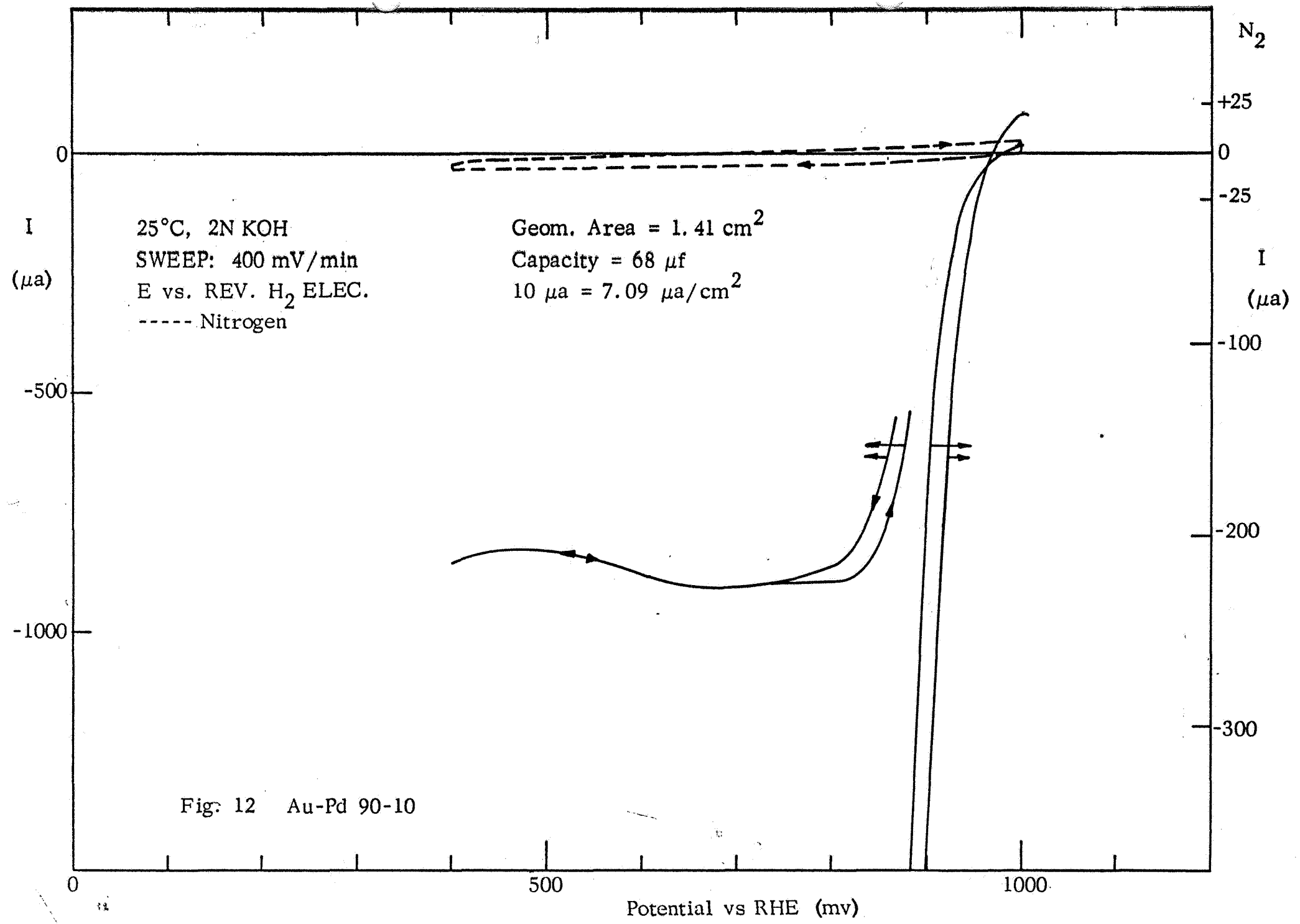

Fig. 12 Au-Pd 90-10

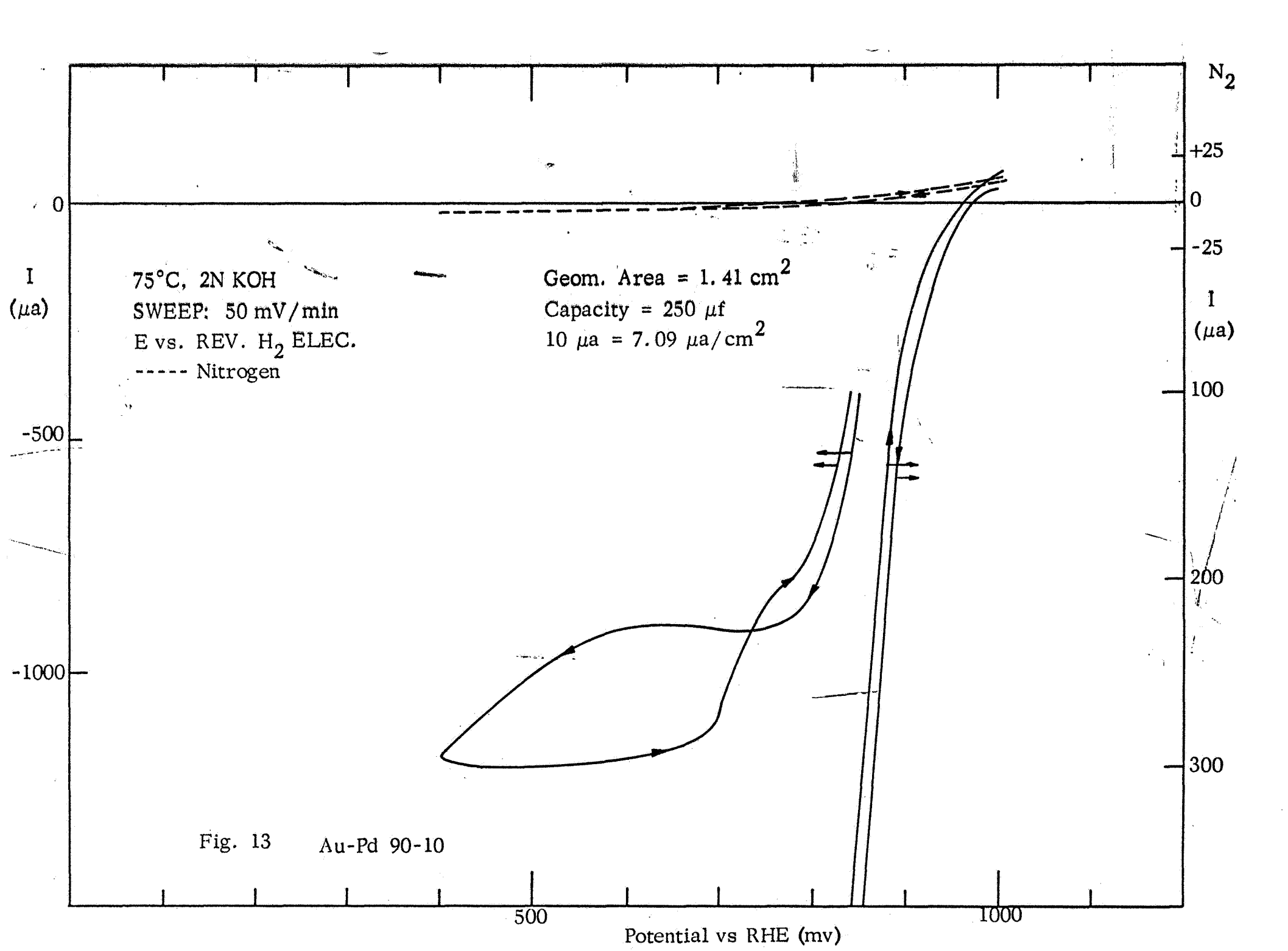

Fig. 13 Au-Pd 90-10

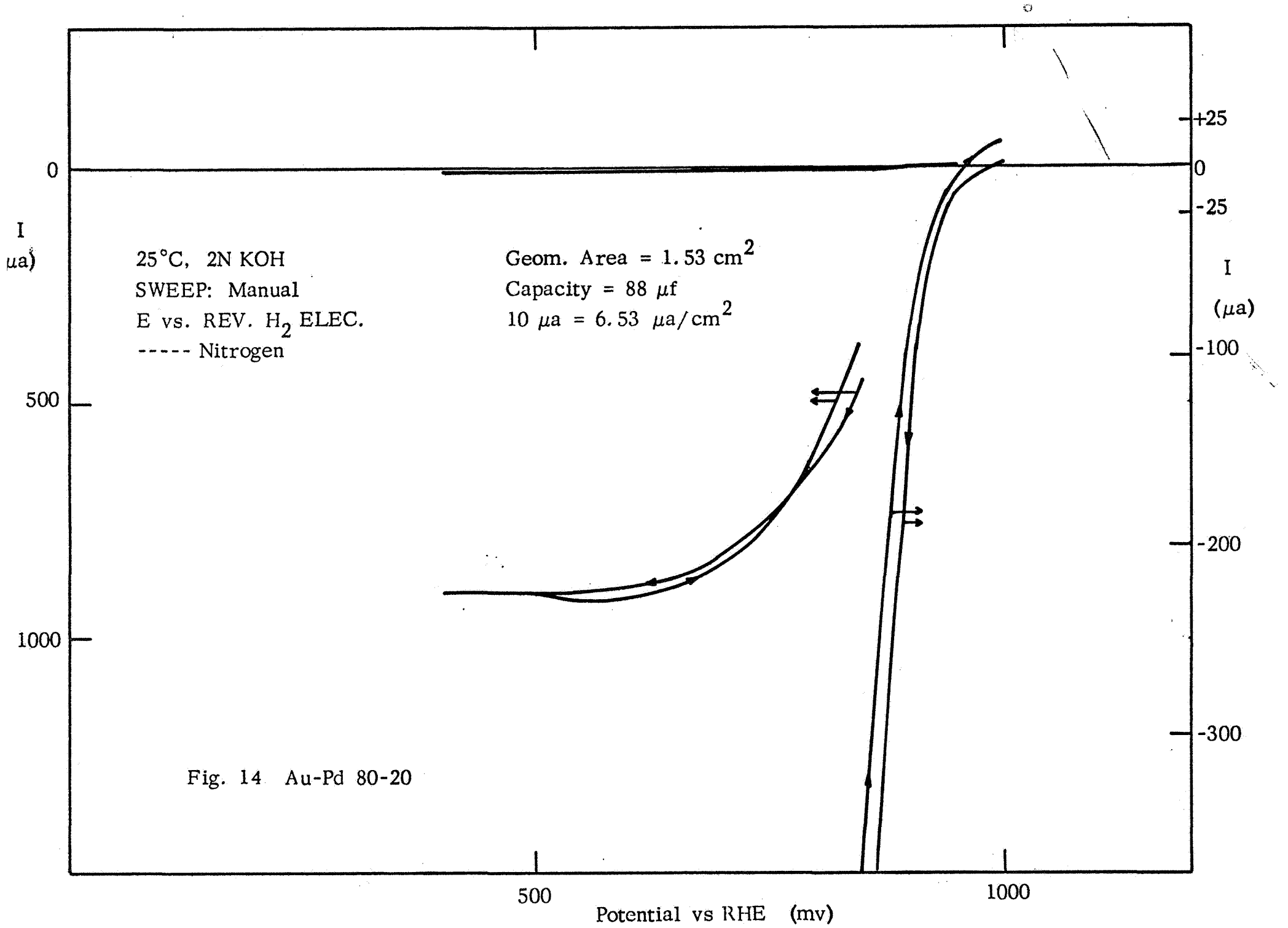

Fig. 14 Au-Pd 80-20

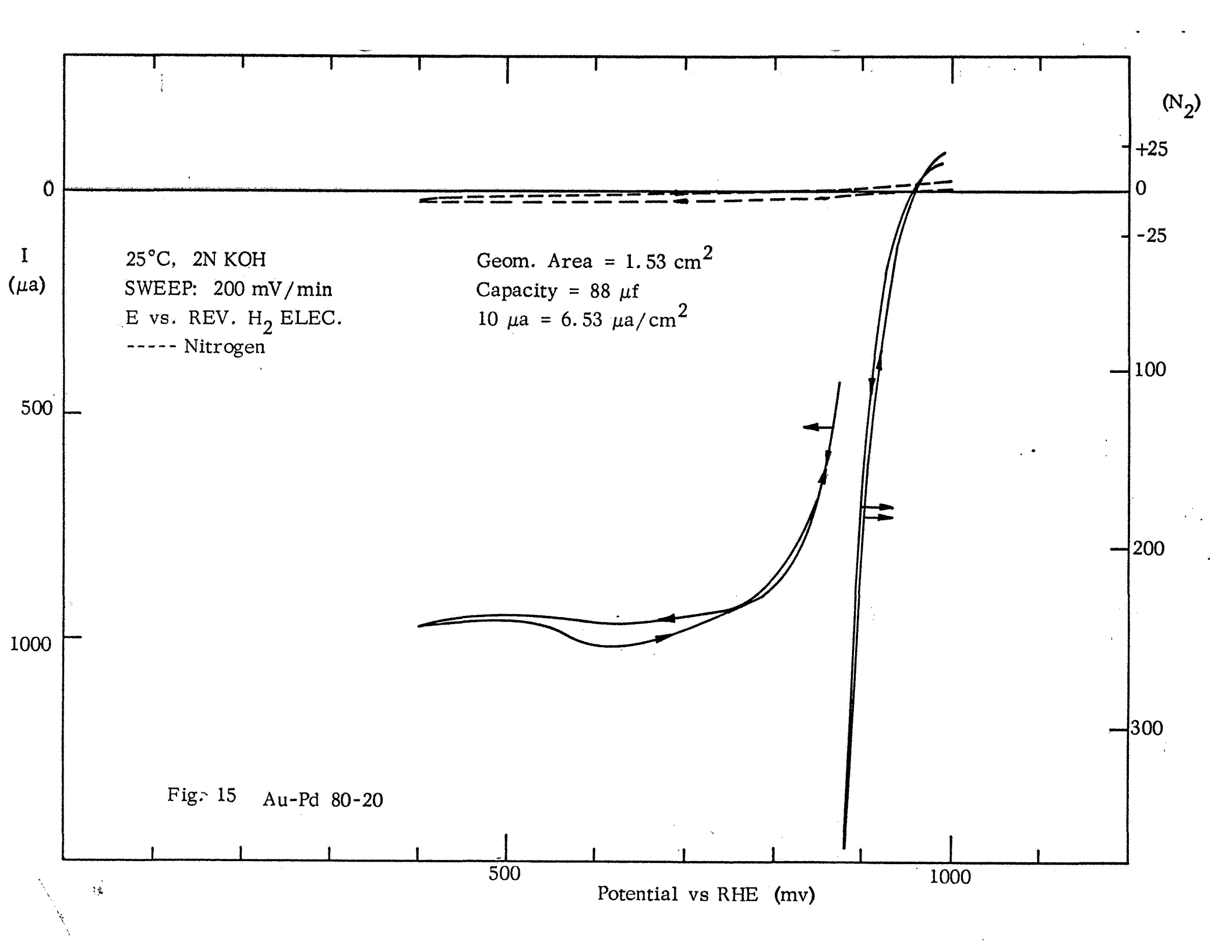

Fig. 15 Au-Pd 80-20

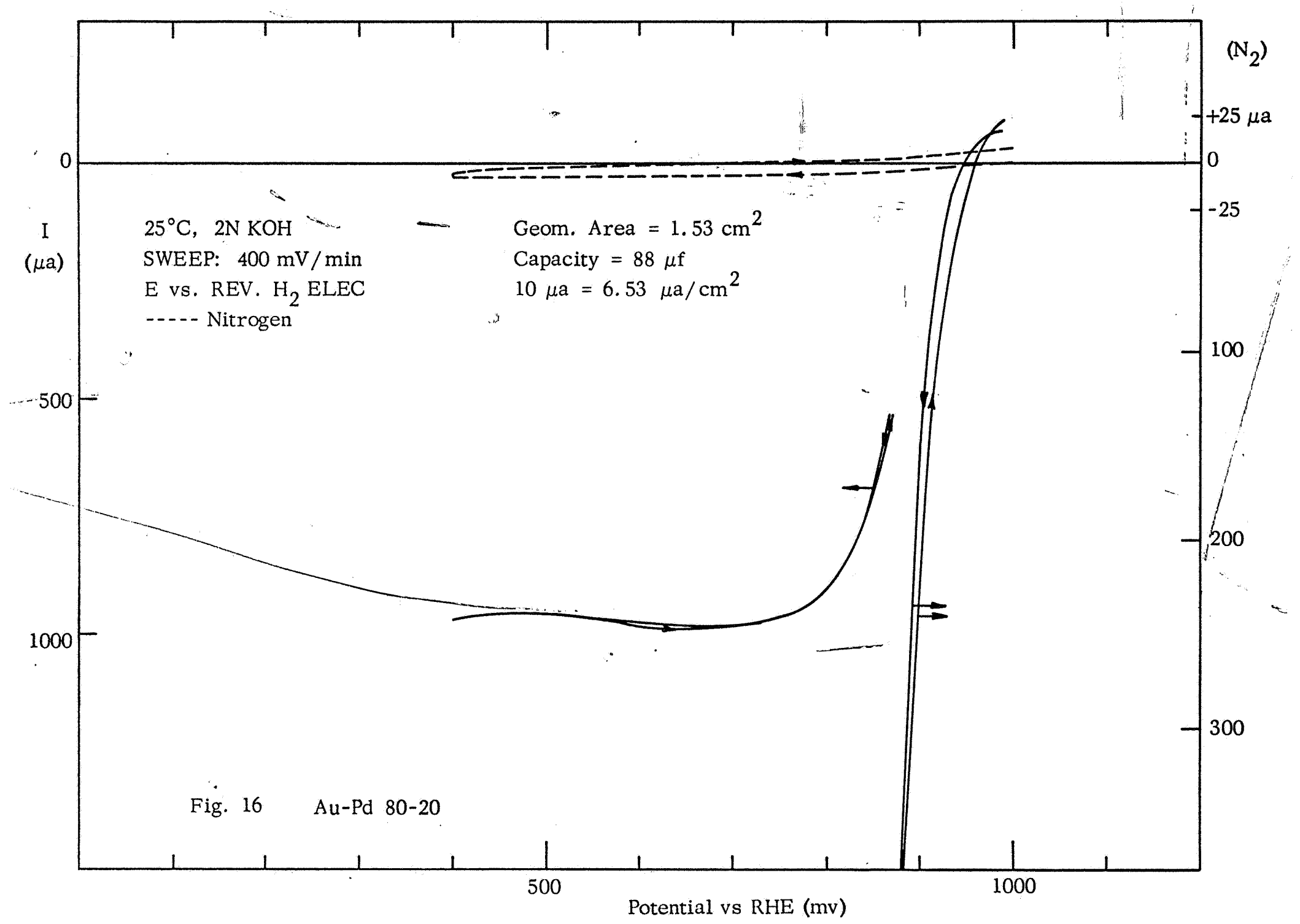

Fig. 16 Au-Pd 80-20

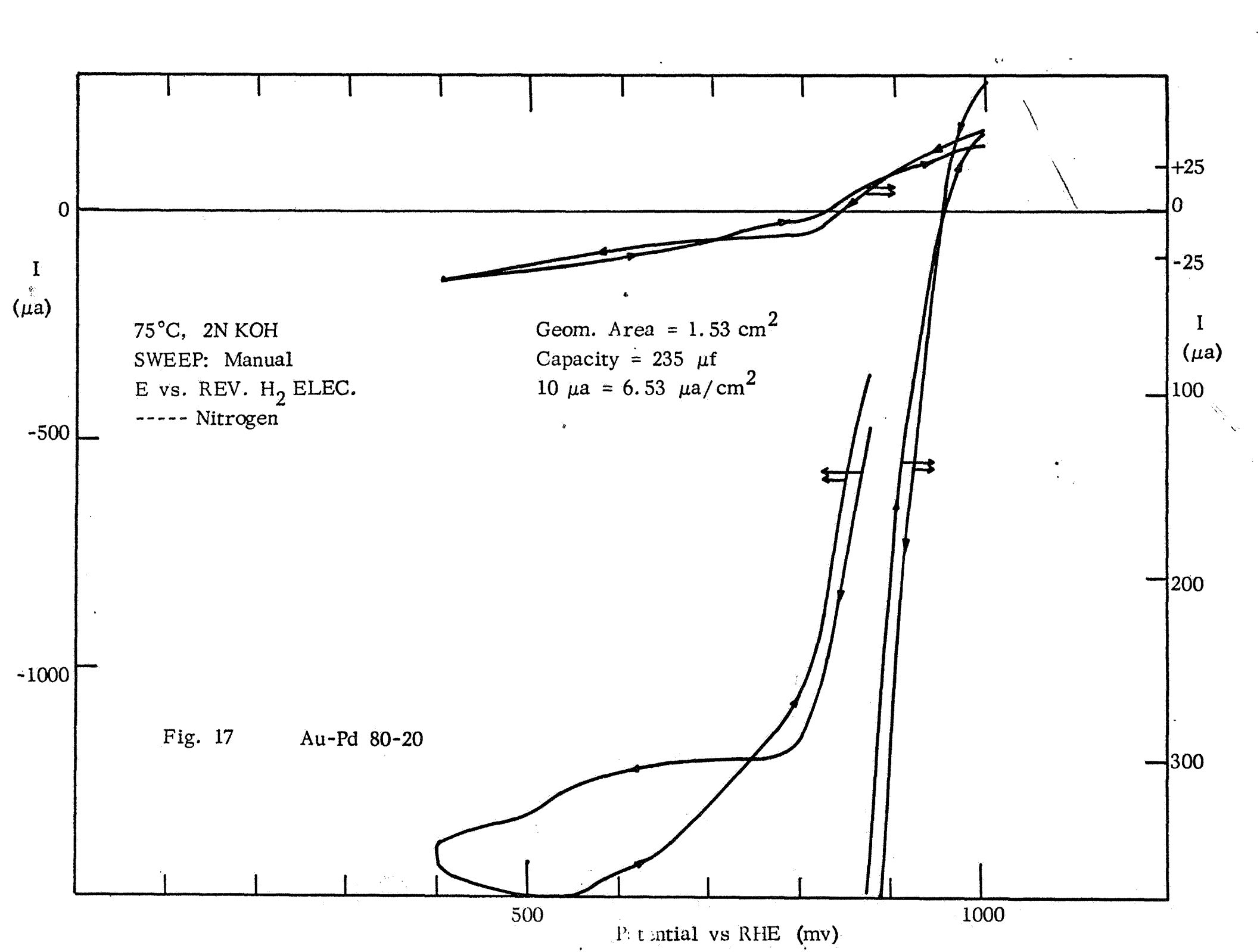

Fig. 17 Au-Pd 80-20

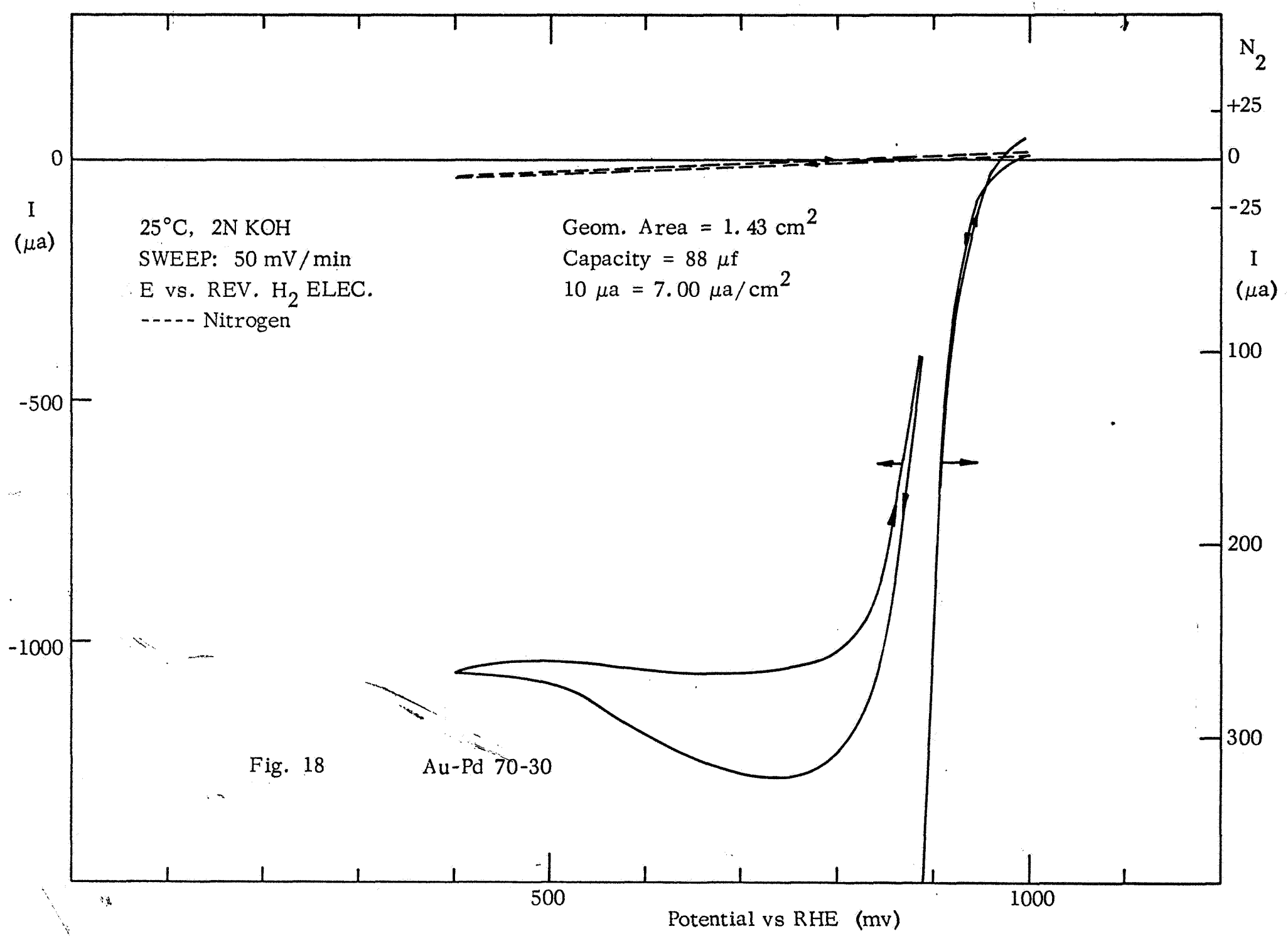

Fig. 18 Au-Pd 70-30

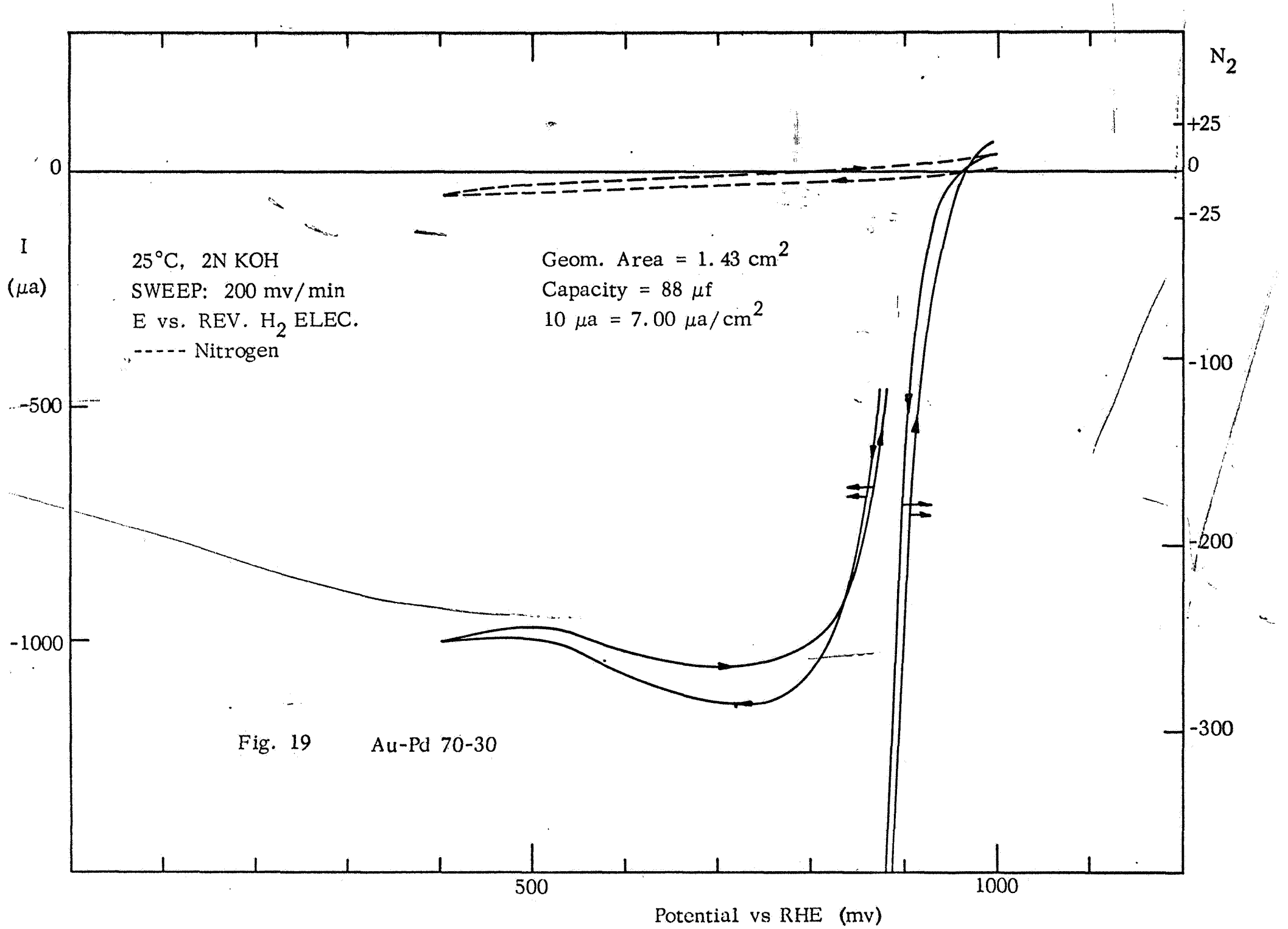

Fig. 19 Au-Pd 70-30

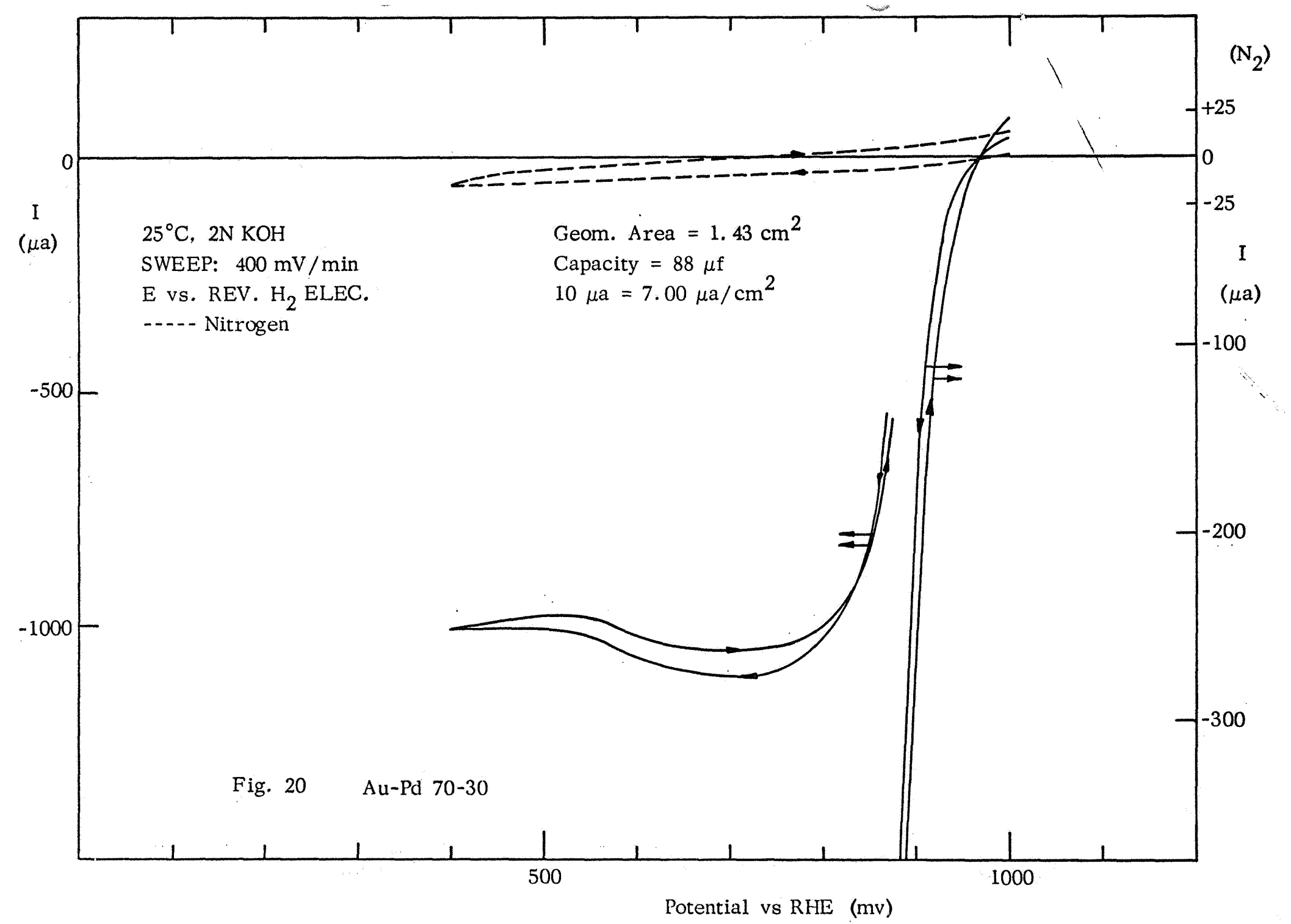

Fig. 20 Au-Pd 70-30

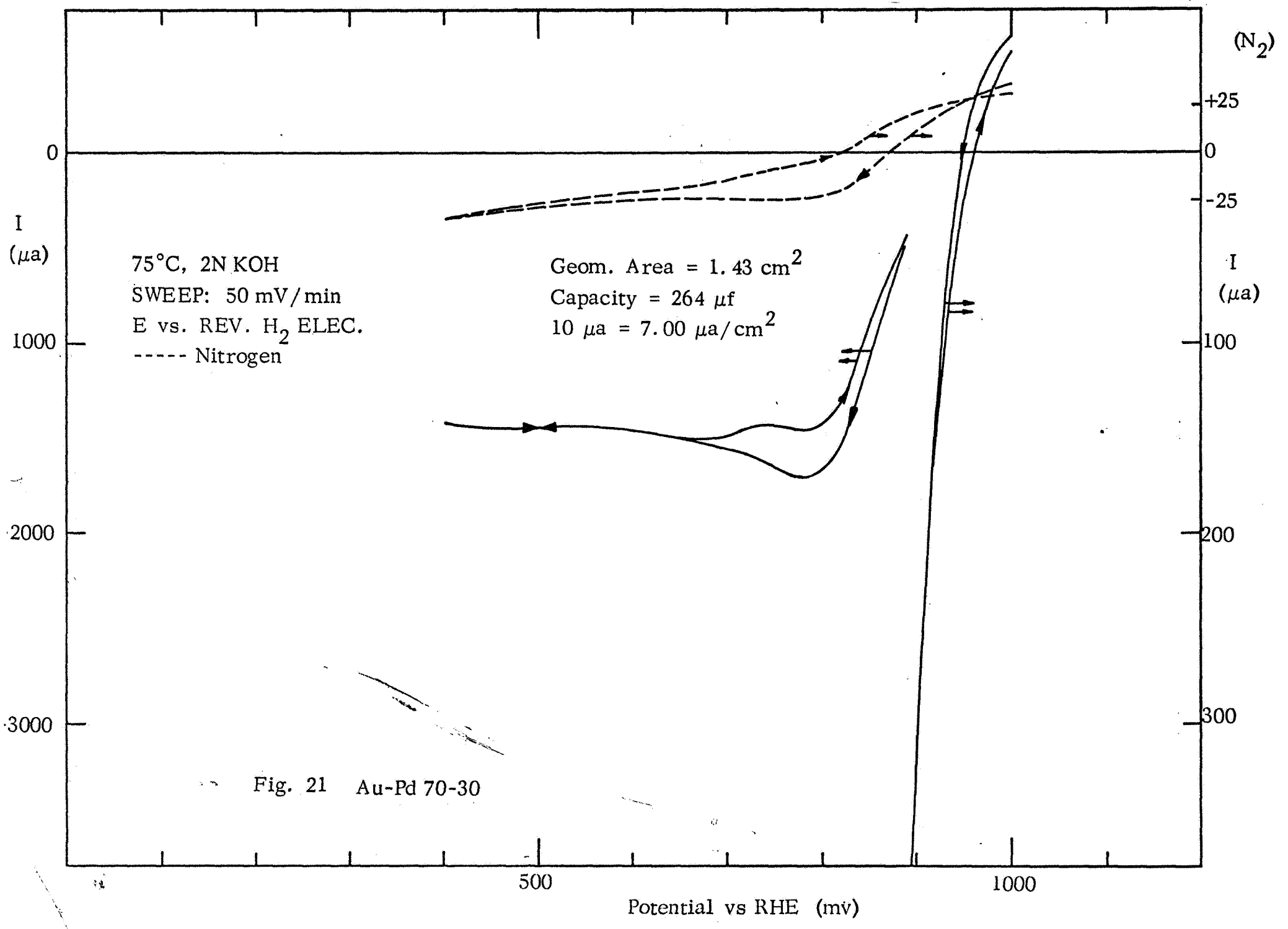

Fig. 21 Au-Pd 70-30

Fig. 22
Au

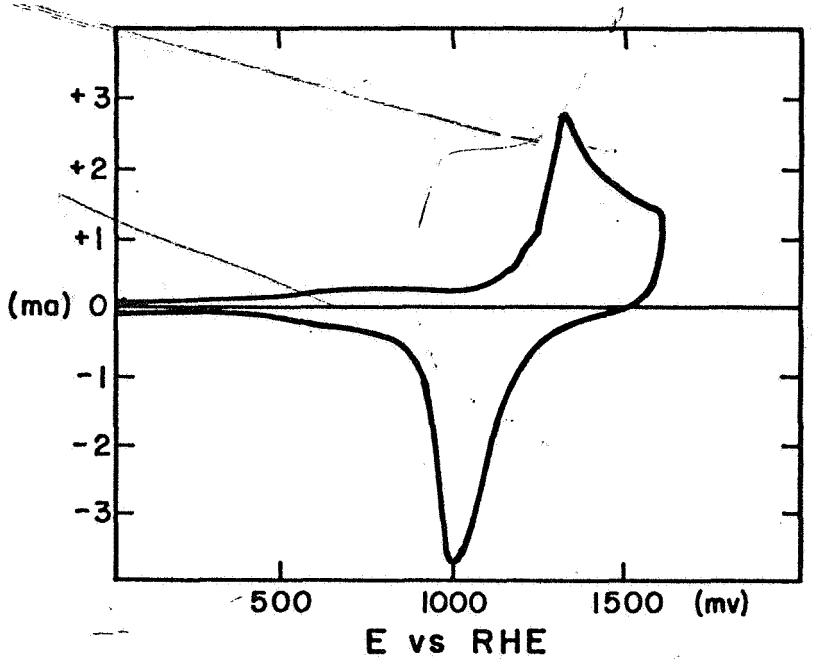

Fig. 23
Au - Pd
90-10

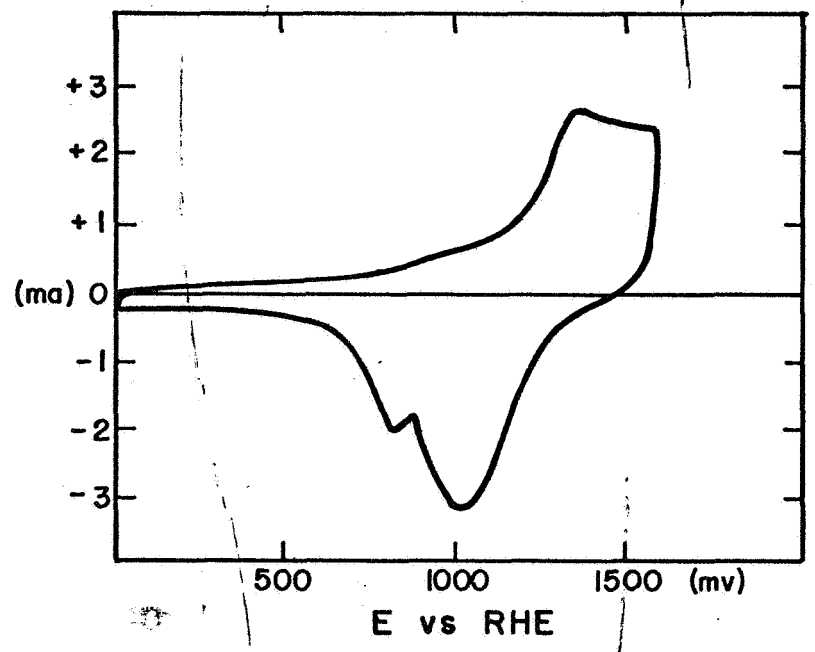

Fig. 24
Au-Pd
80-20

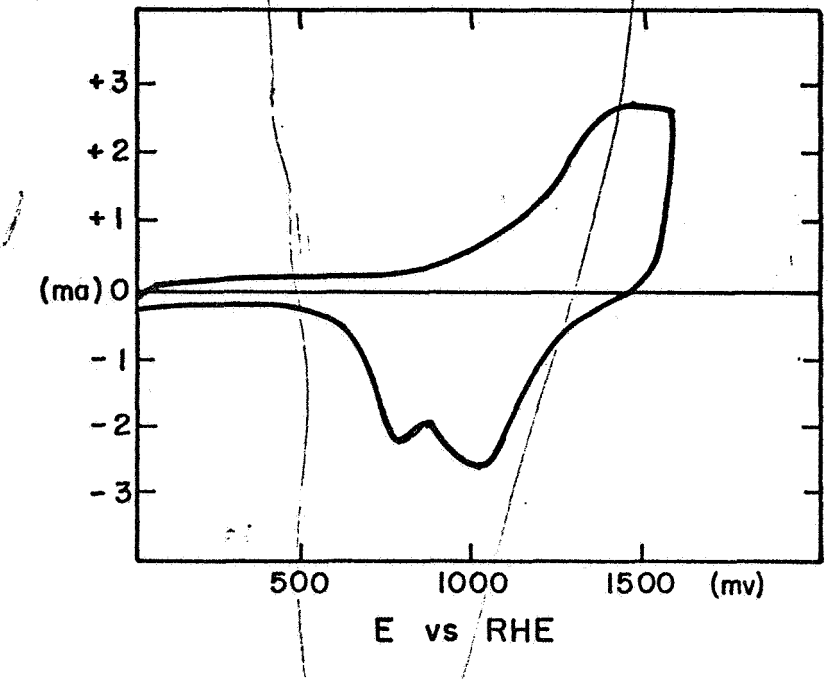

Fig. 25
Au-Pd
70-30

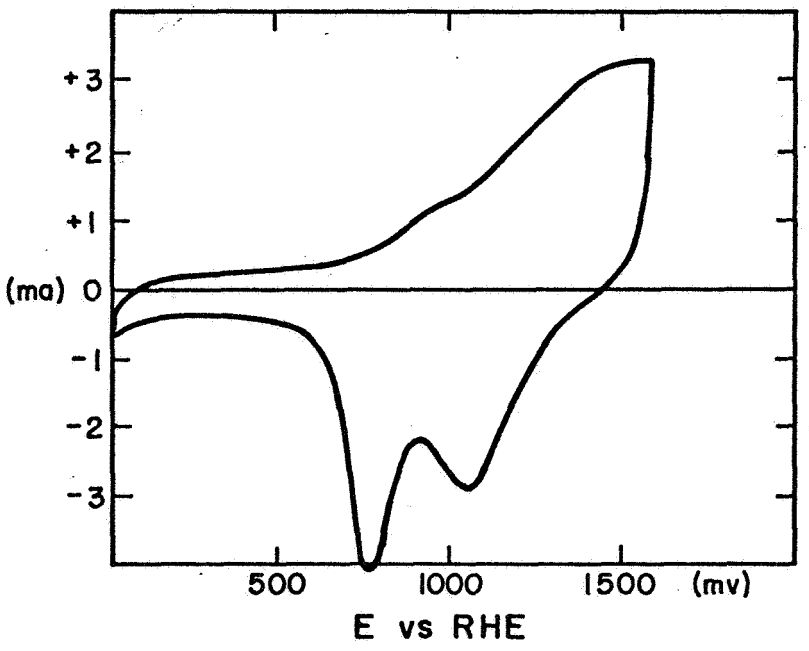

Fig. 26
Au-Pd
60-40

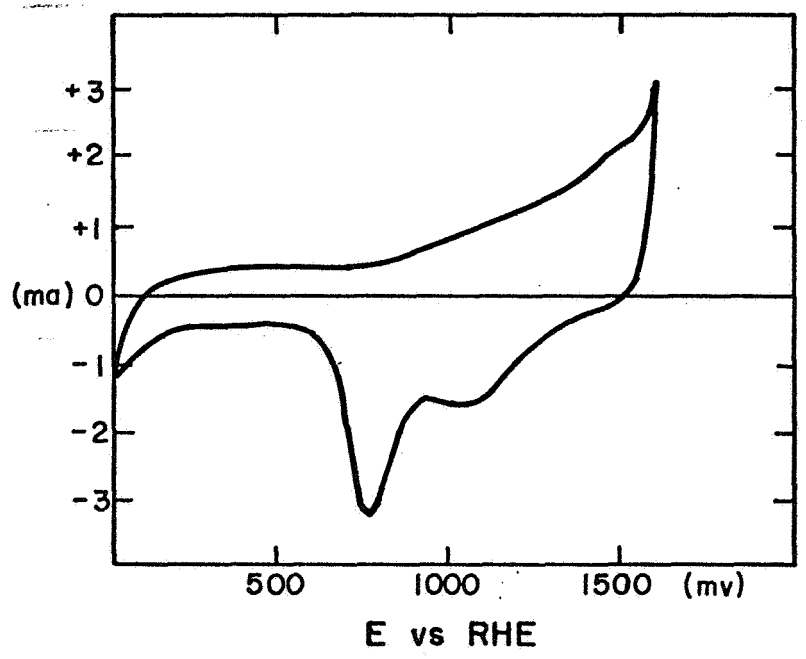

Fig. 27
Au-Pd
50-50

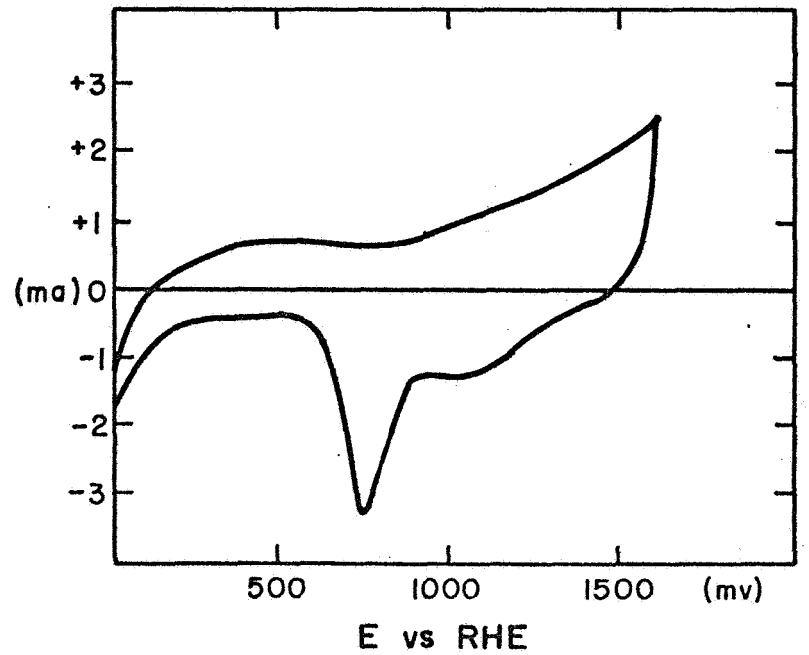

Fig. 28
Au-Pd
40-60

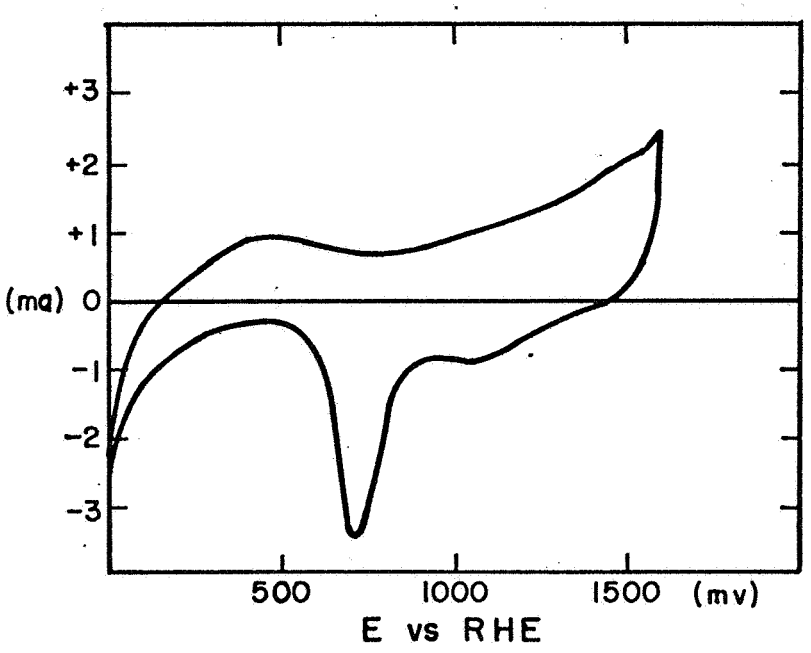

Fig. 29
Au-Pd
30-70

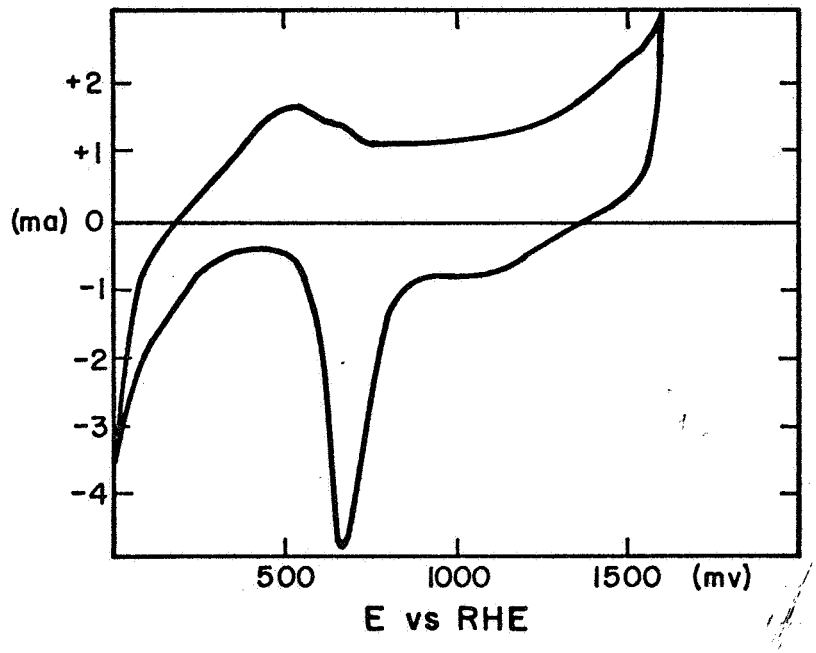

Fig. 30
Au-Pd
20-80

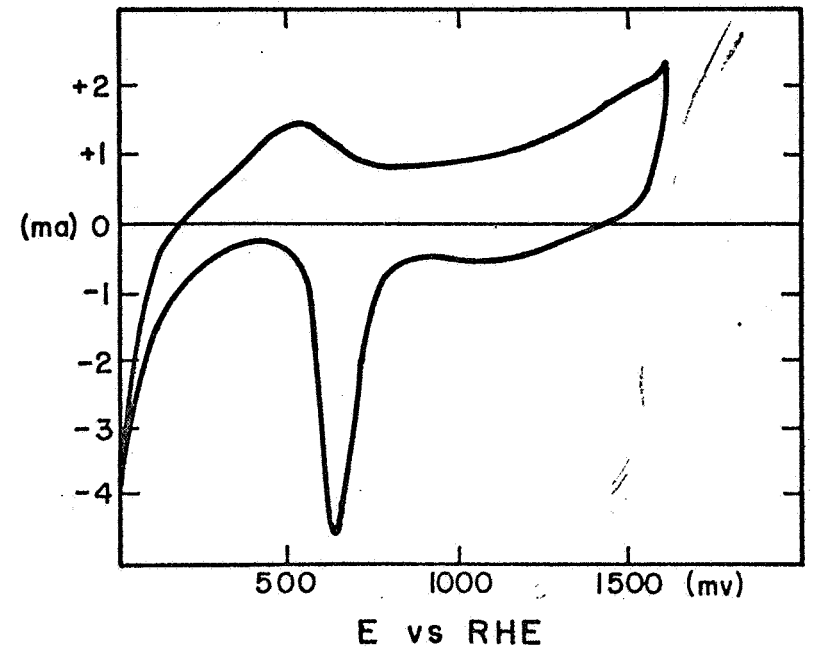

Fig. 31

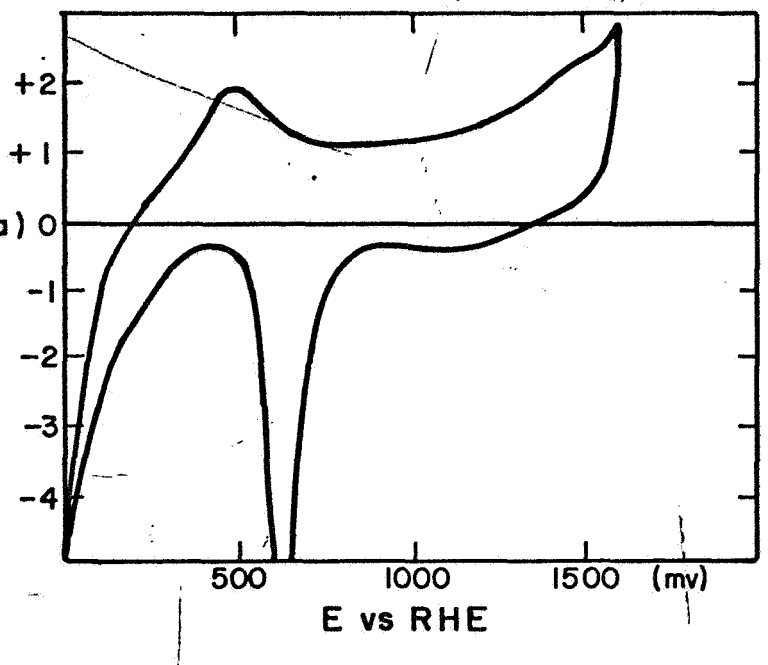

Fig. 32

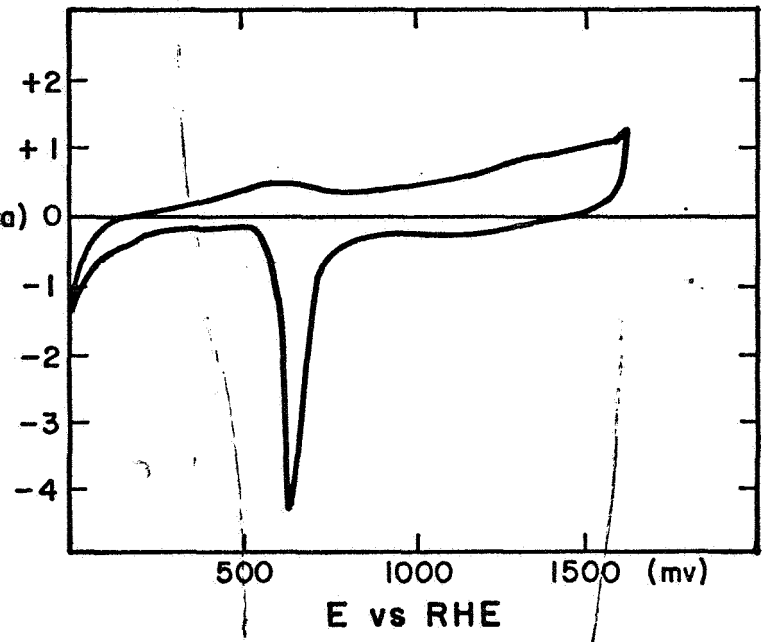

All of the above measurements (Au-Pd Series) were made under the following conditions:

N_2 – Saturated 2N KOH, 25°C

500 mv/sec, 4th sweep recorded

E vs Rev. H_2 elec., graphite counter electrode

Makrides-Stern electrode holder rotated at 600 RPM

Geometric area approx. 1.5 cm^2

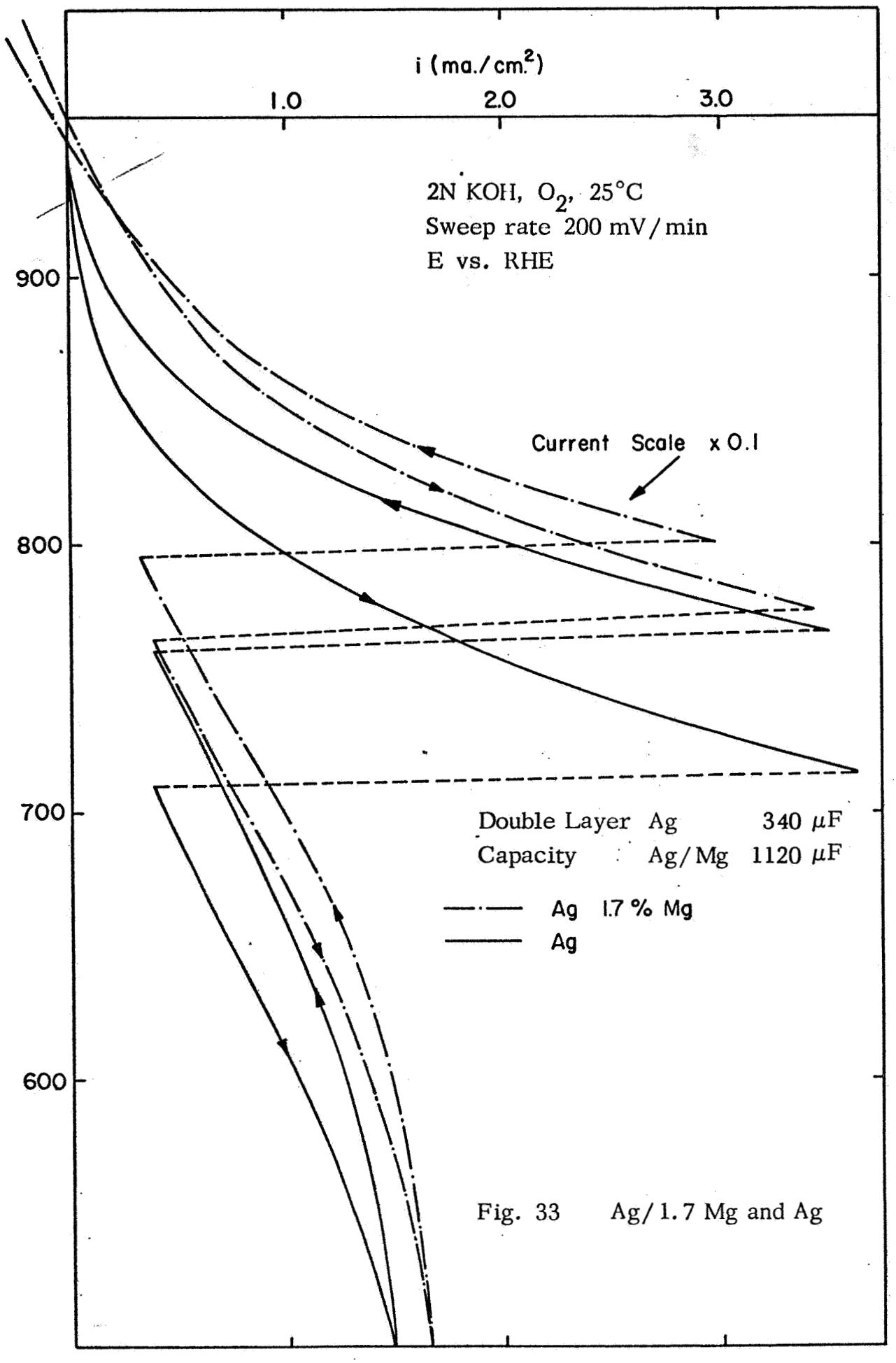

Fig. 33 Ag/1.7 Mg and Ag

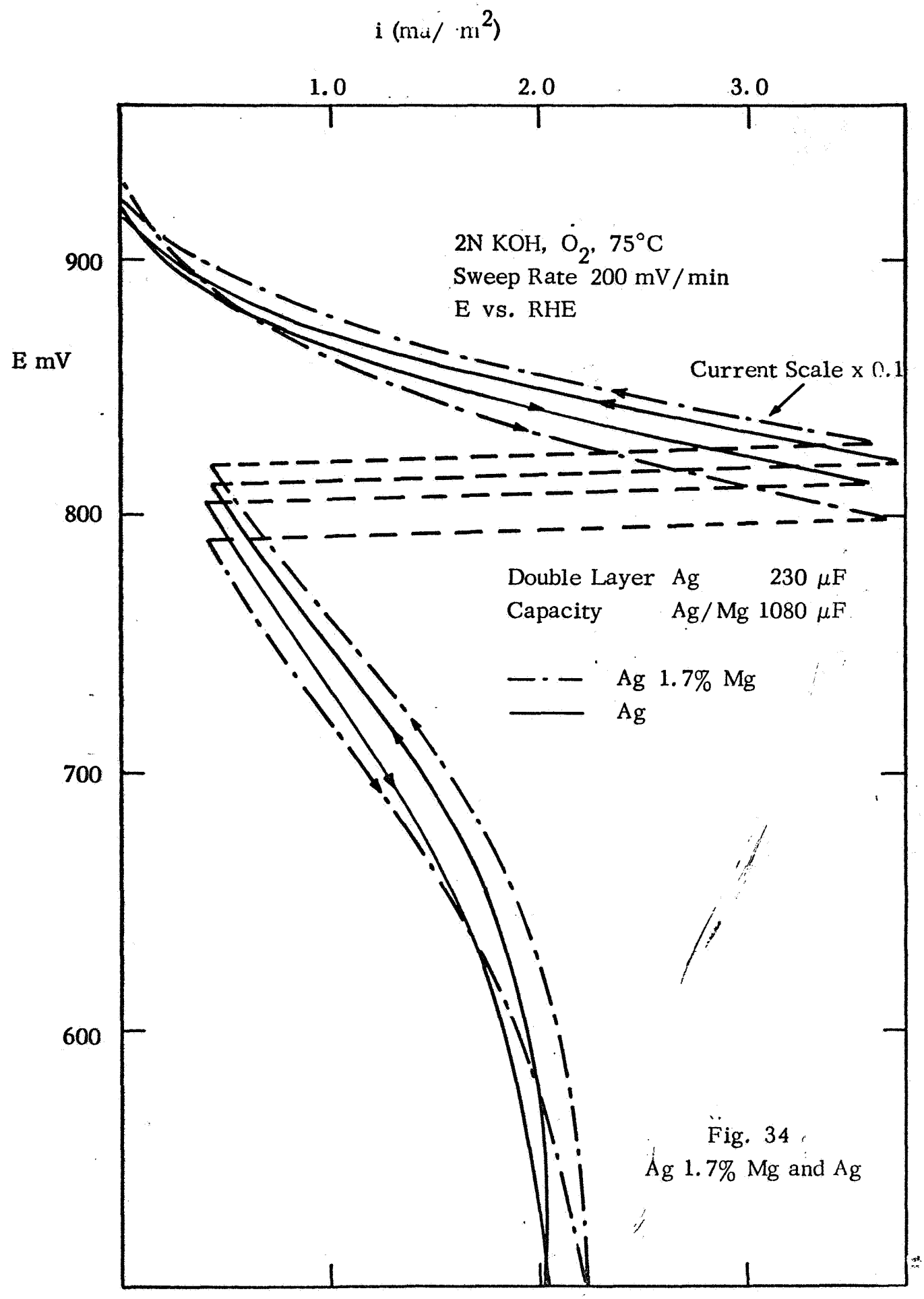

Fig. 34
Ag 1.7% Mg and Ag

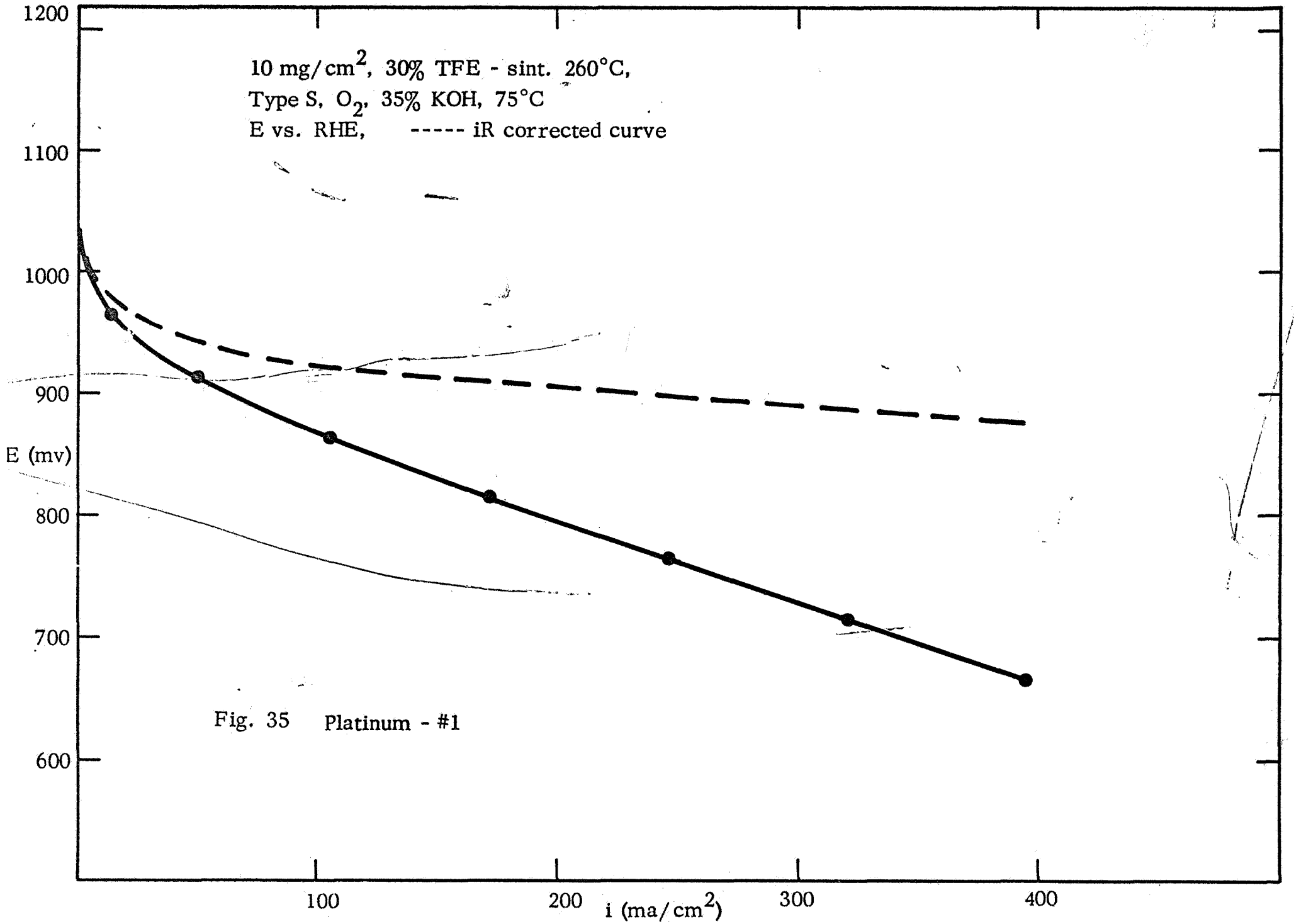

Fig. 35 Platinum - #1

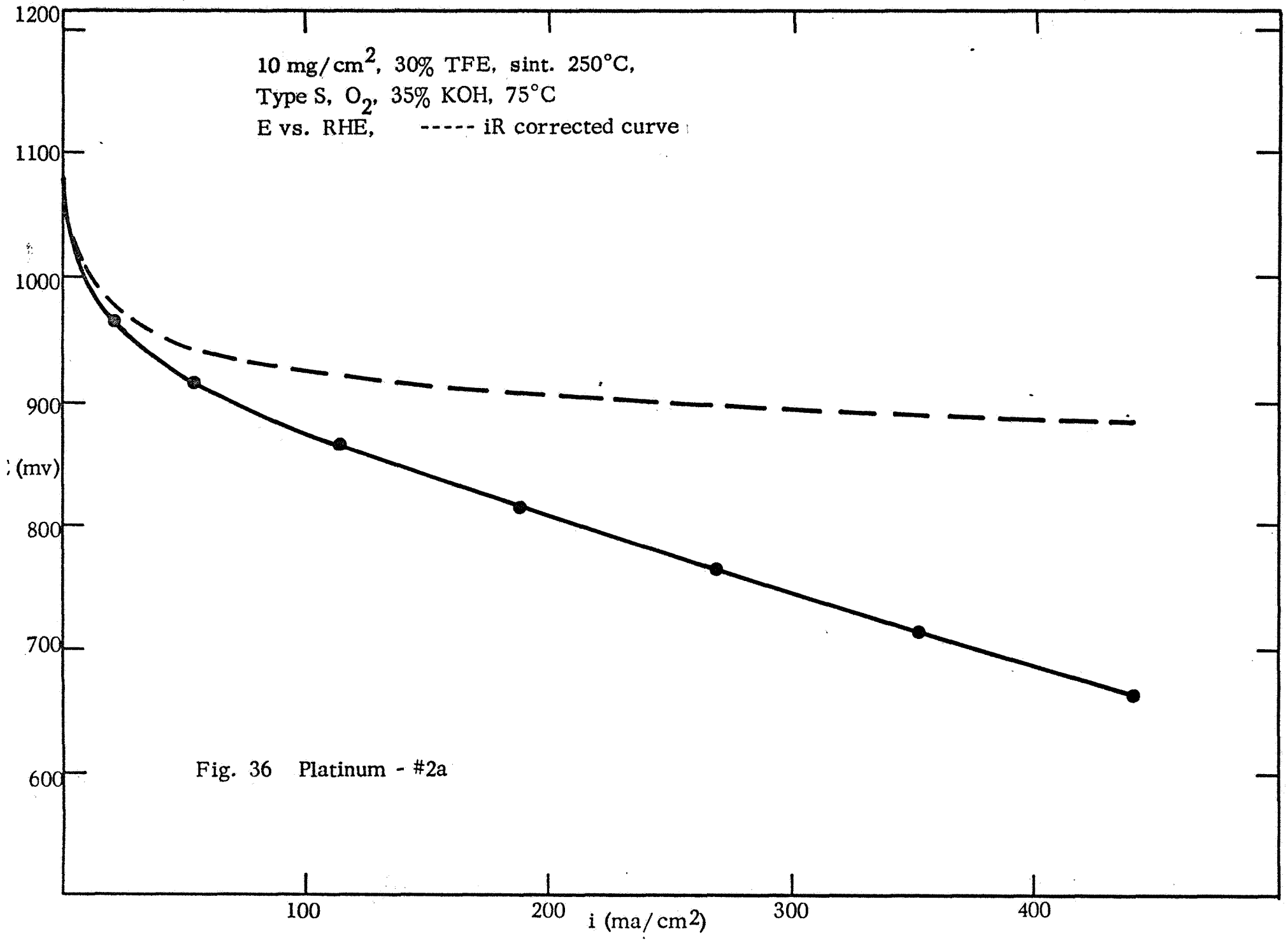

Fig. 36 Platinum - #2a

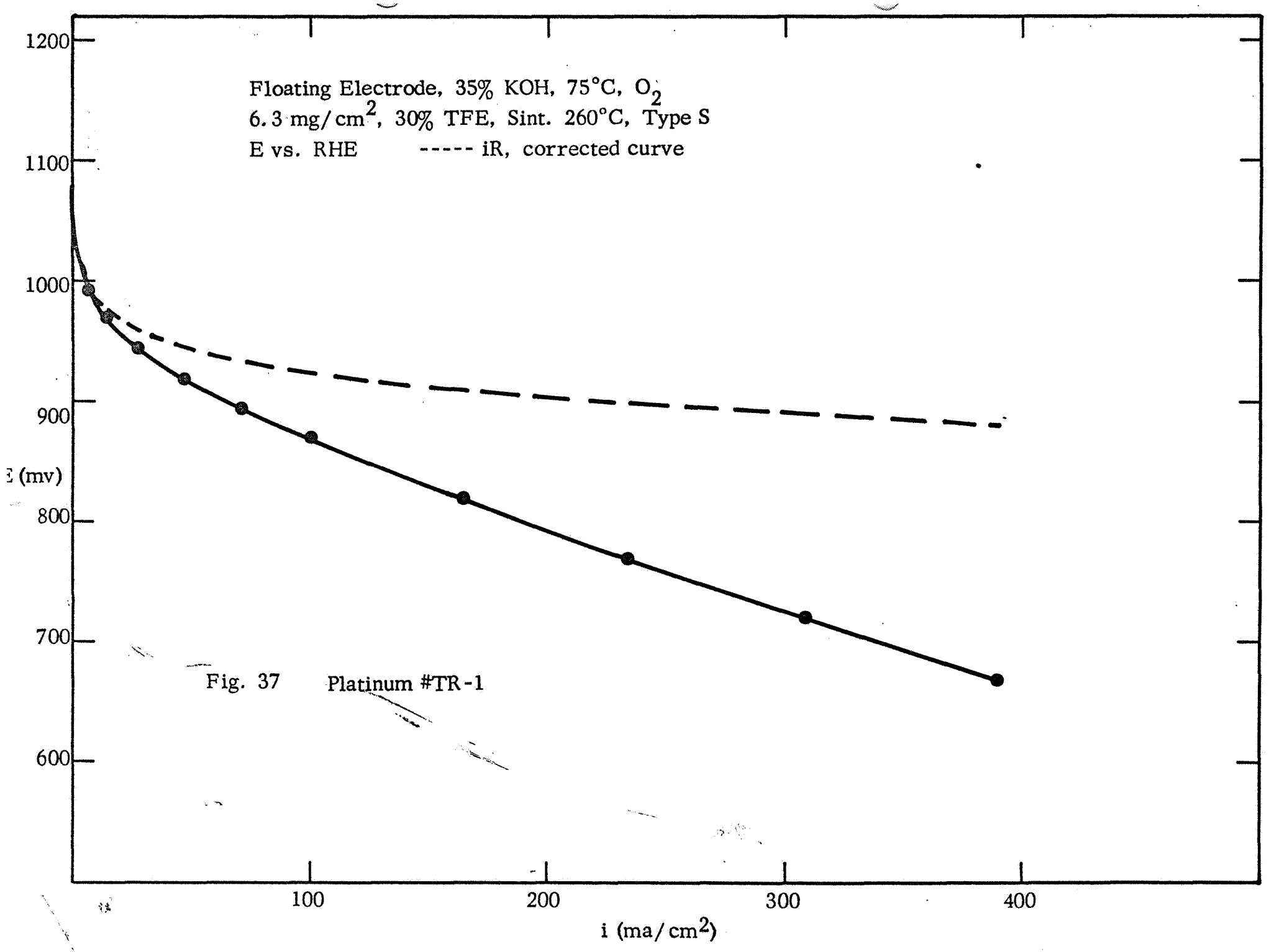

Fig. 37 Platinum #TR-1

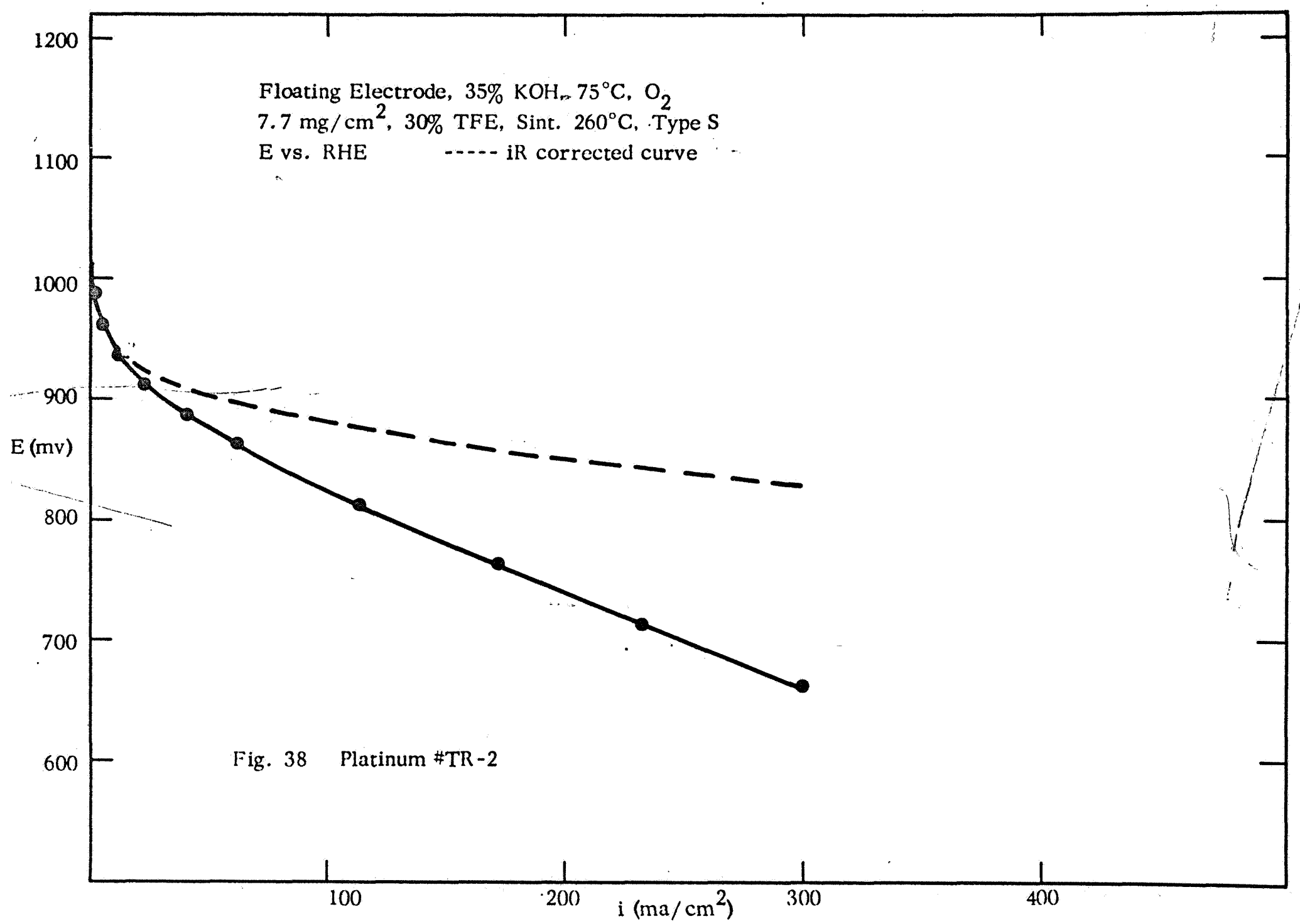

Fig. 38 Platinum #TR-2

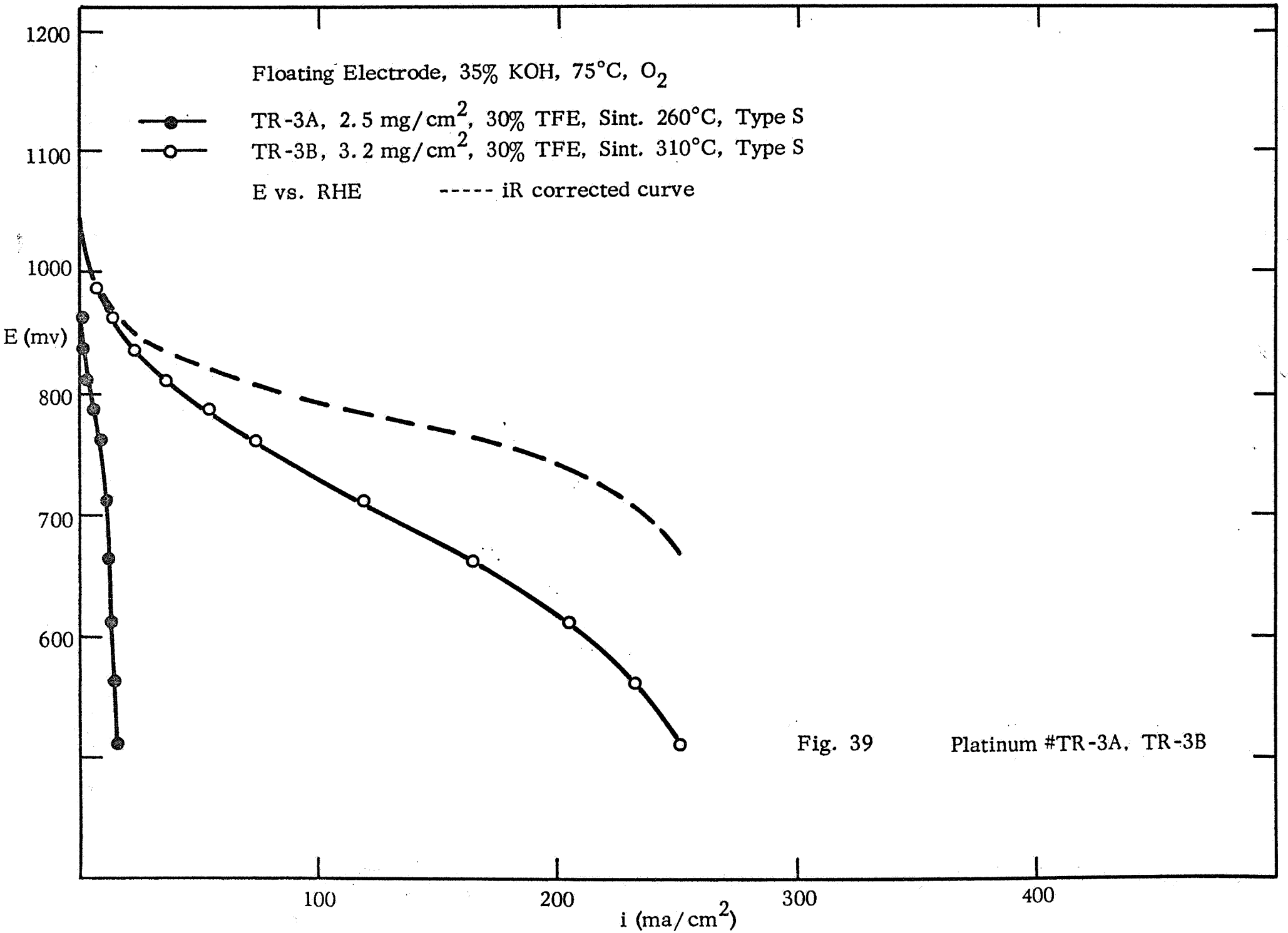

Fig. 39 Platinum #TR-3A, TR-3B

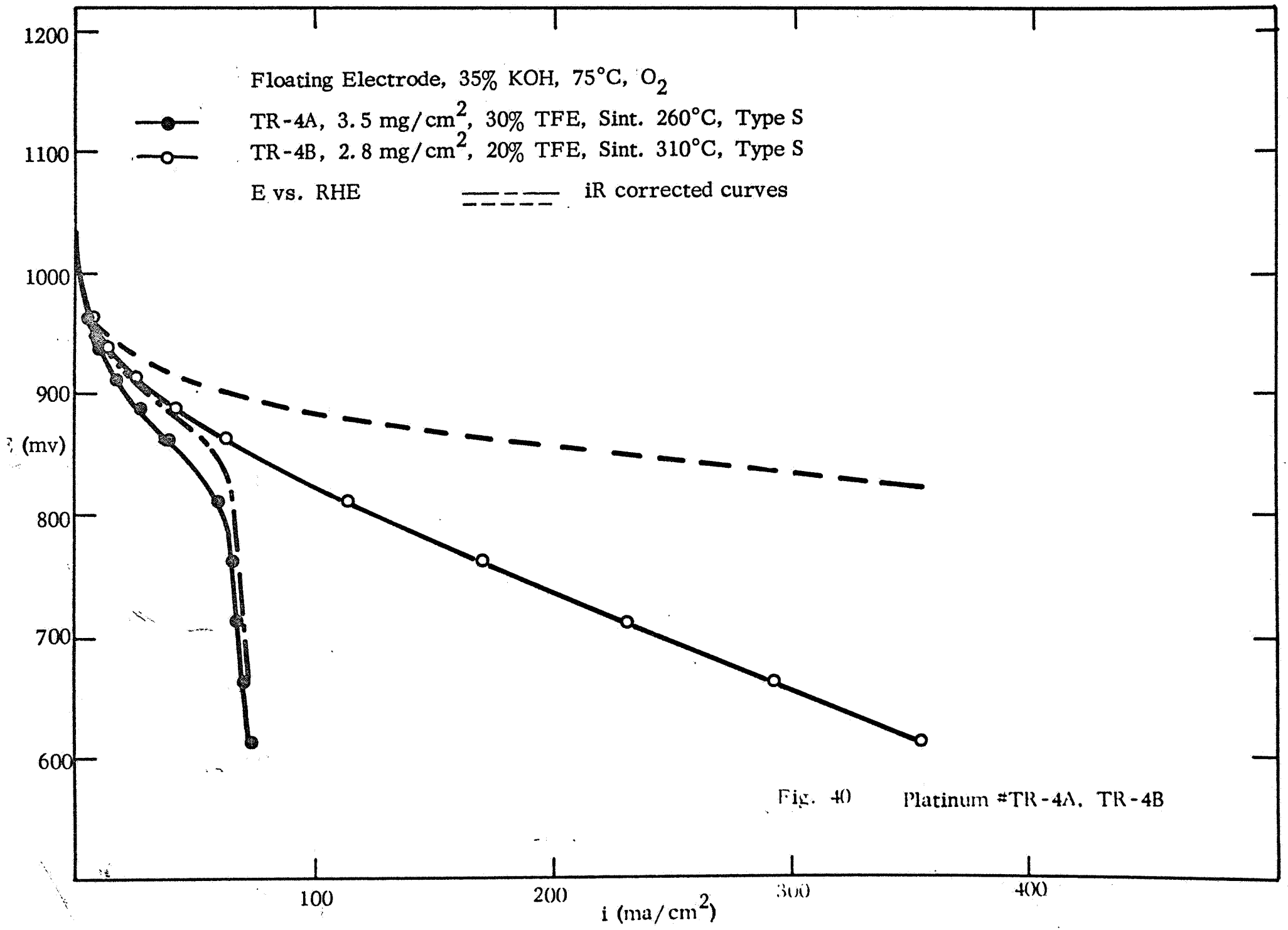

Fig. 40 Platinum #TR-4A, TR-4B

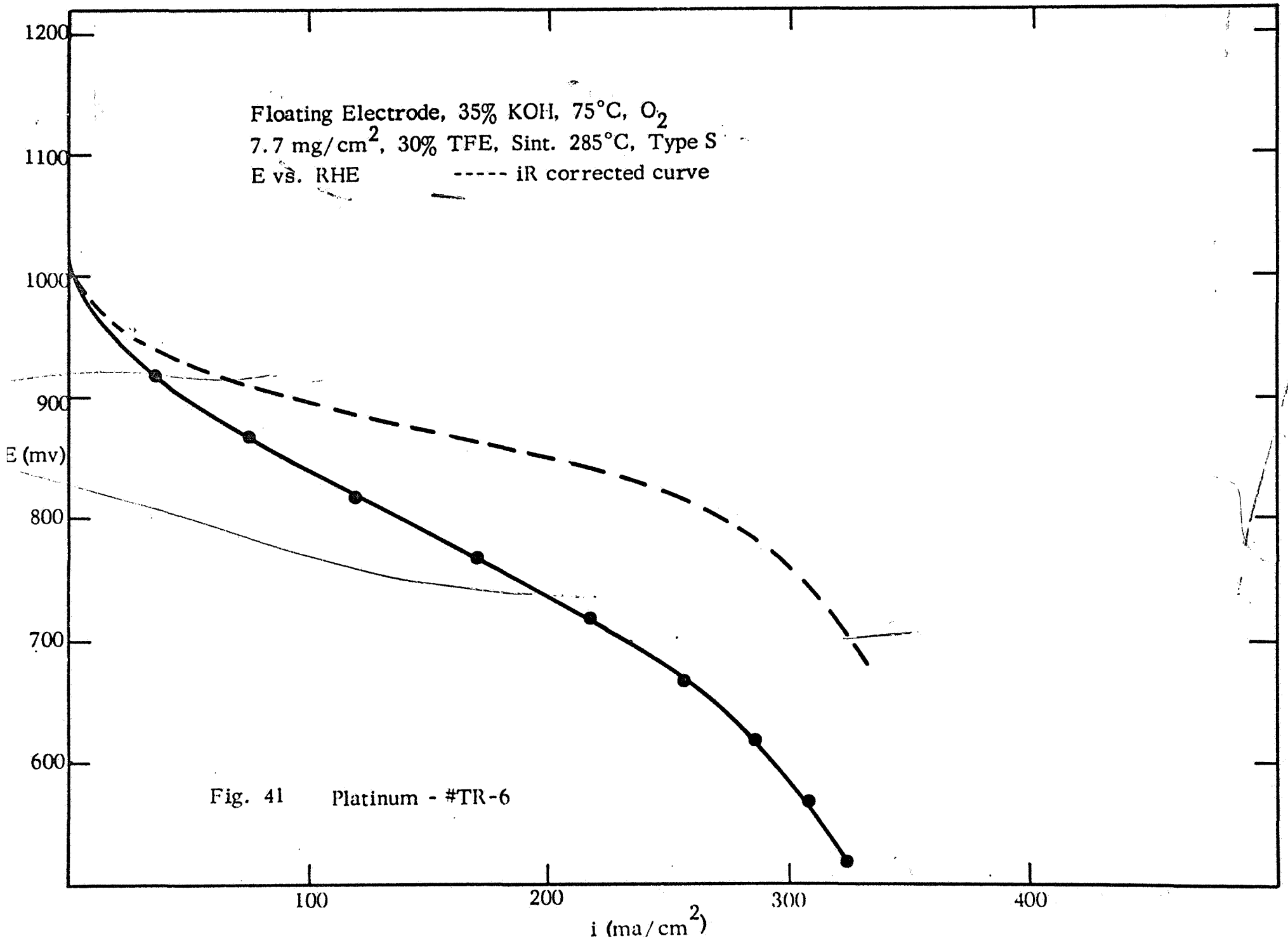

Fig. 41 Platinum - #TR-6

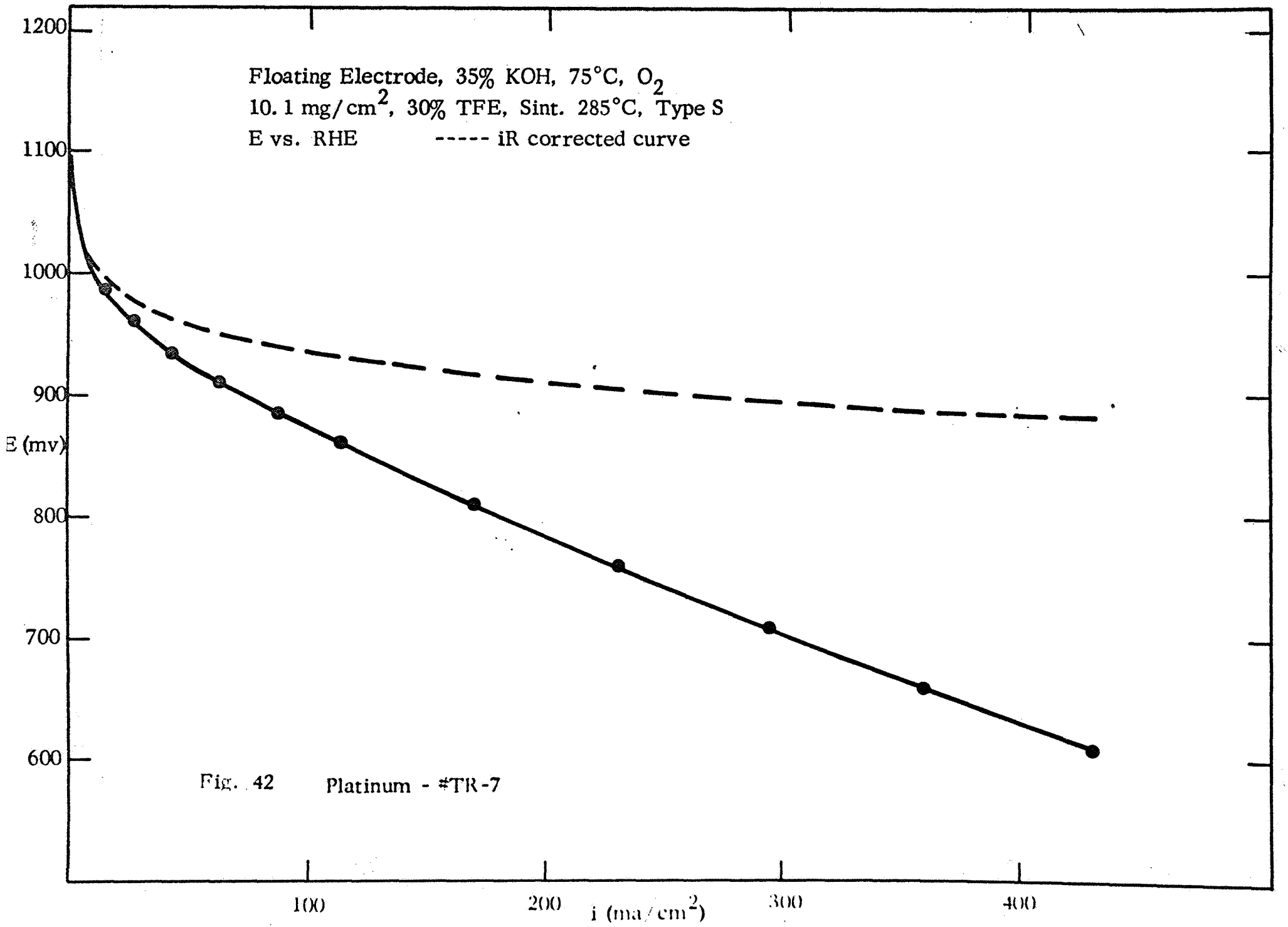

Fig. 42 Platinum - #TR-7

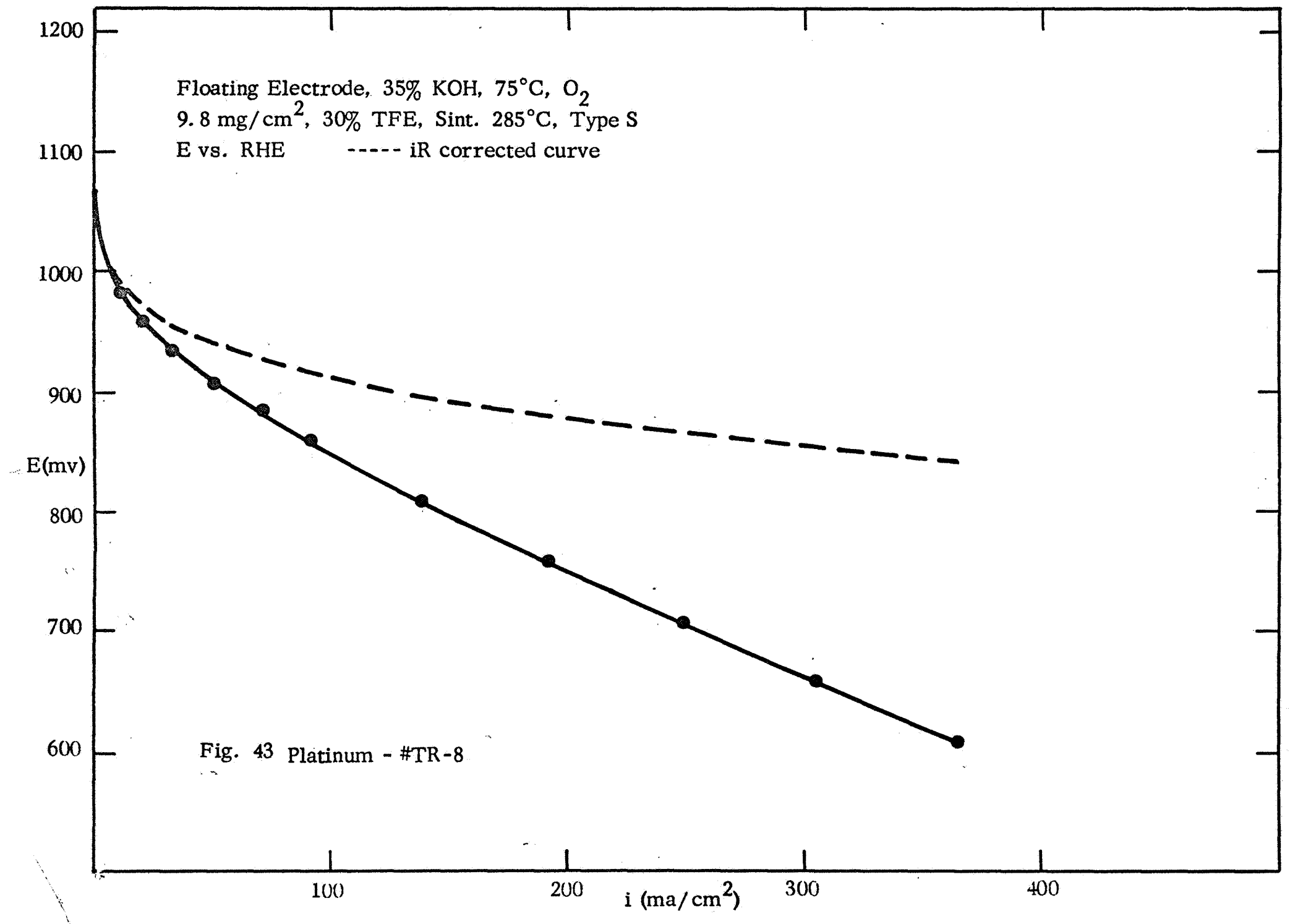

Fig. 43 Platinum - #TR-8

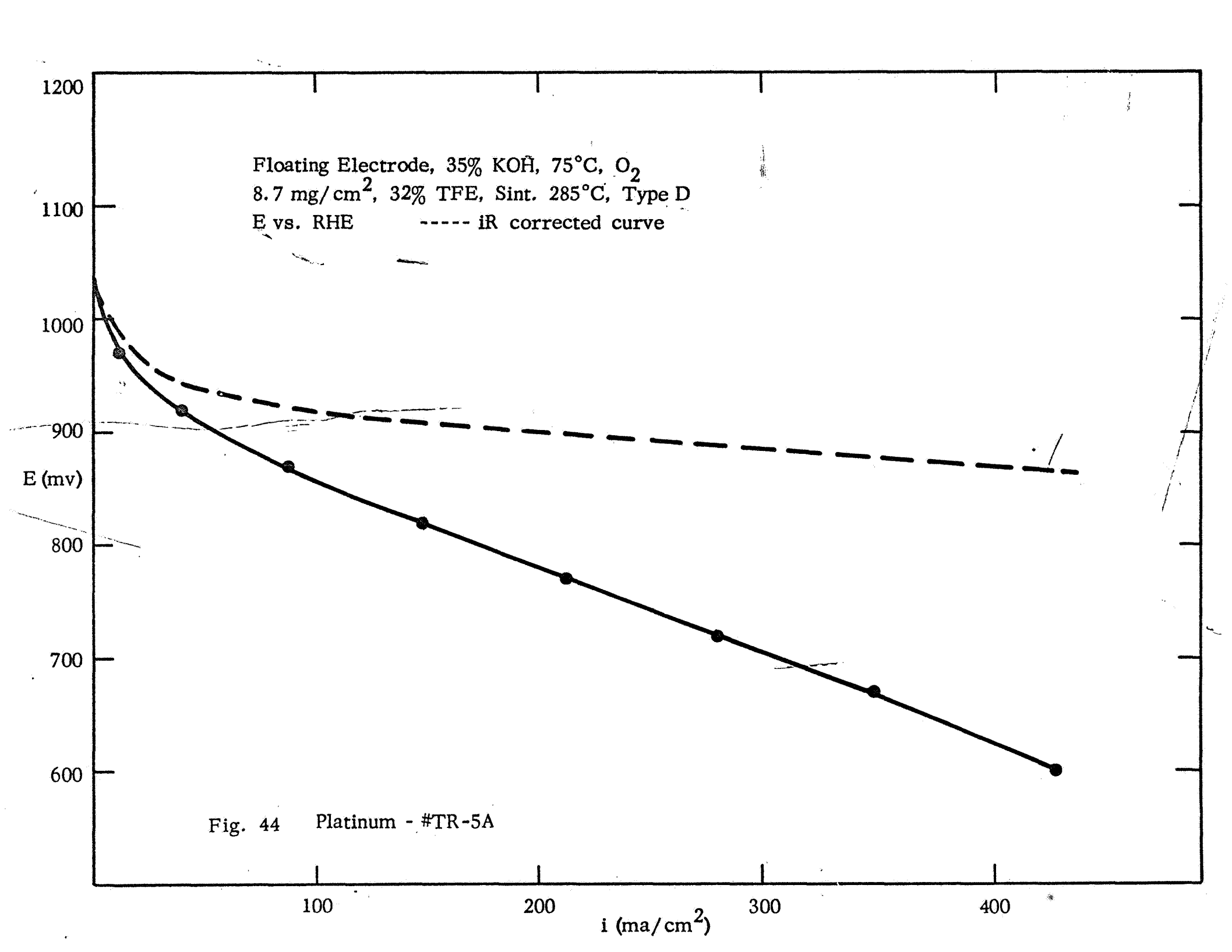

Fig. 44 Platinum - #TR-5A

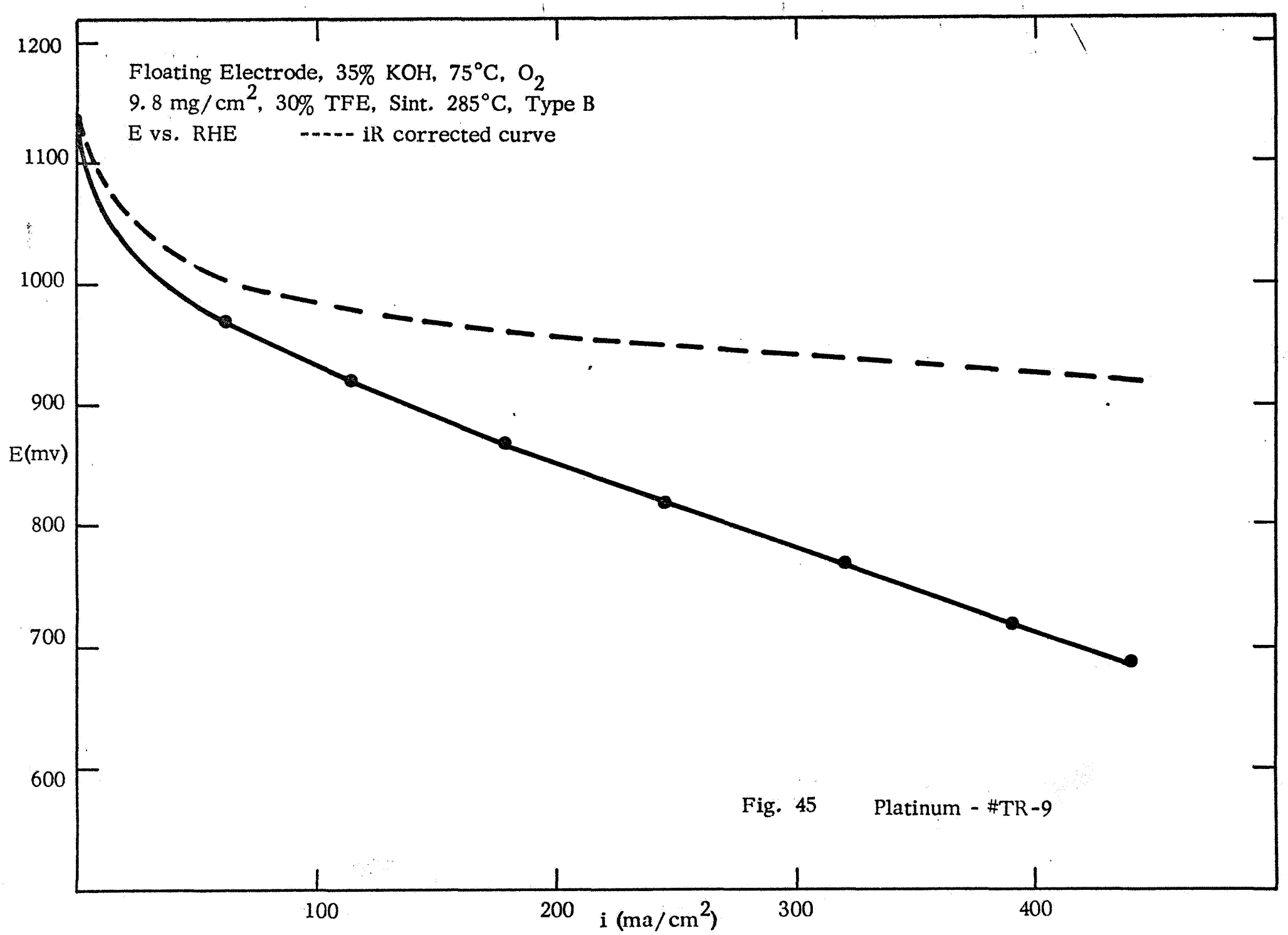

Fig. 45 Platinum - #TR-9

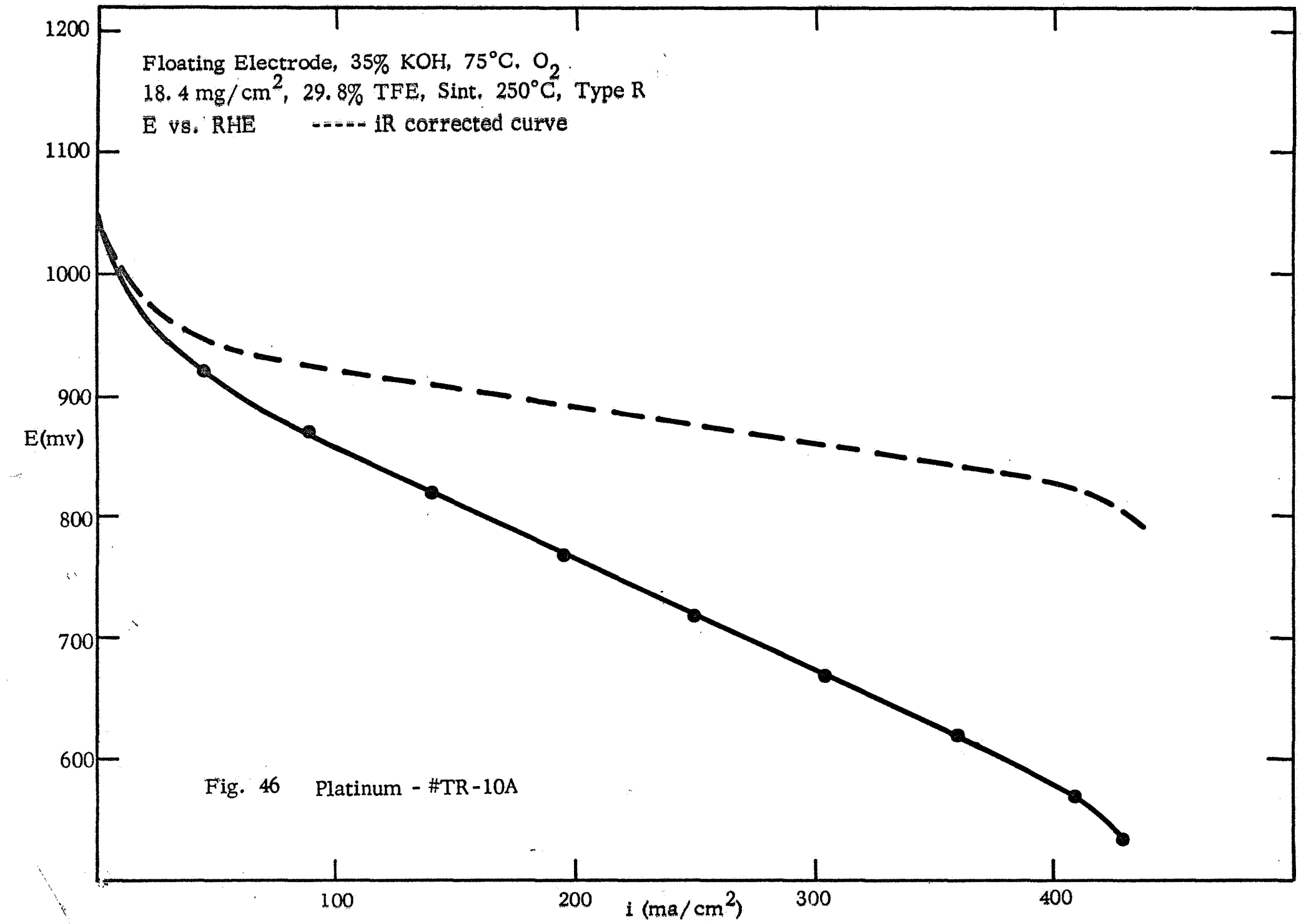

Fig. 46 Platinum - #TR-10A

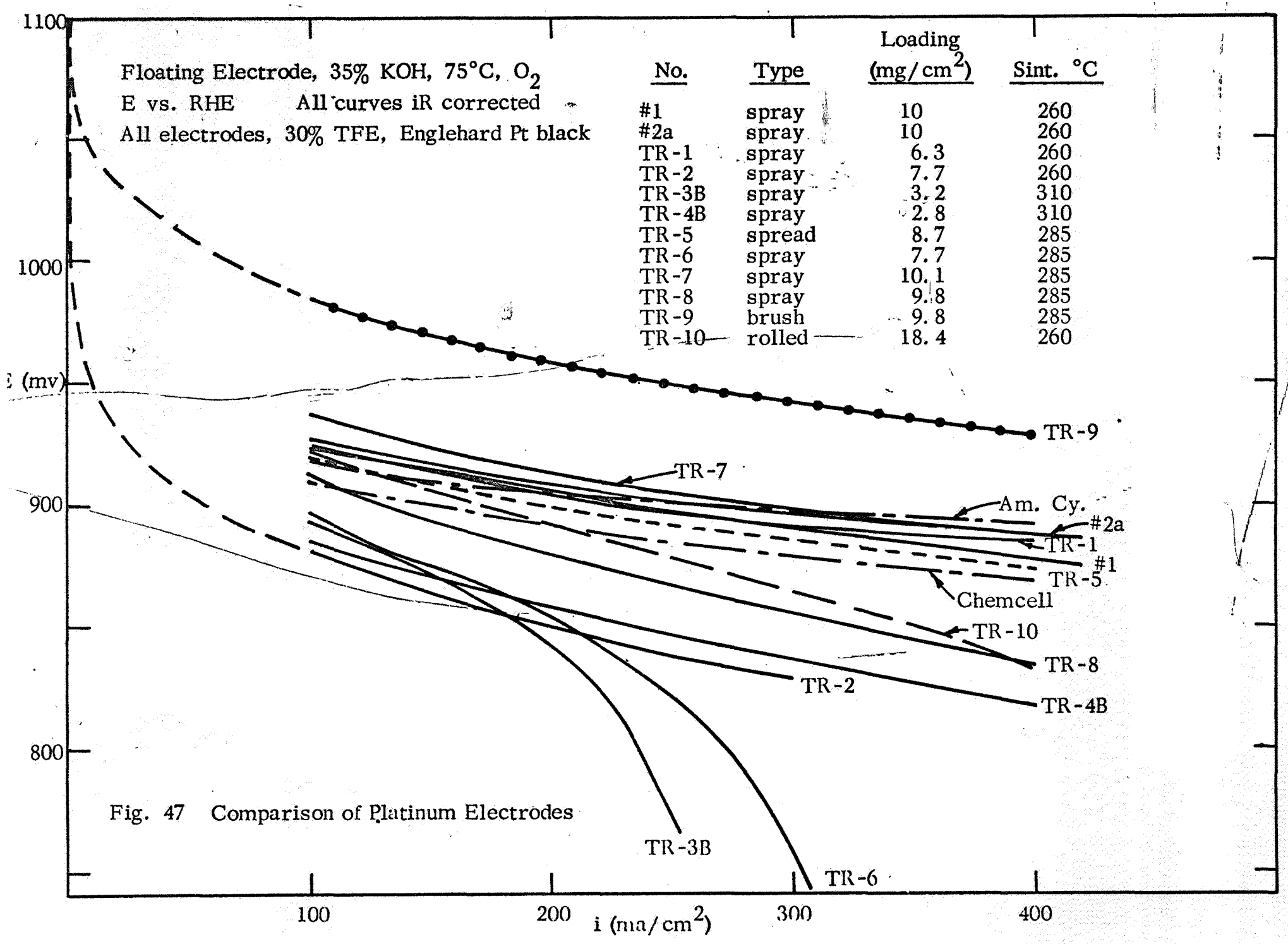

Fig. 47 Comparison of Platinum Electrodes

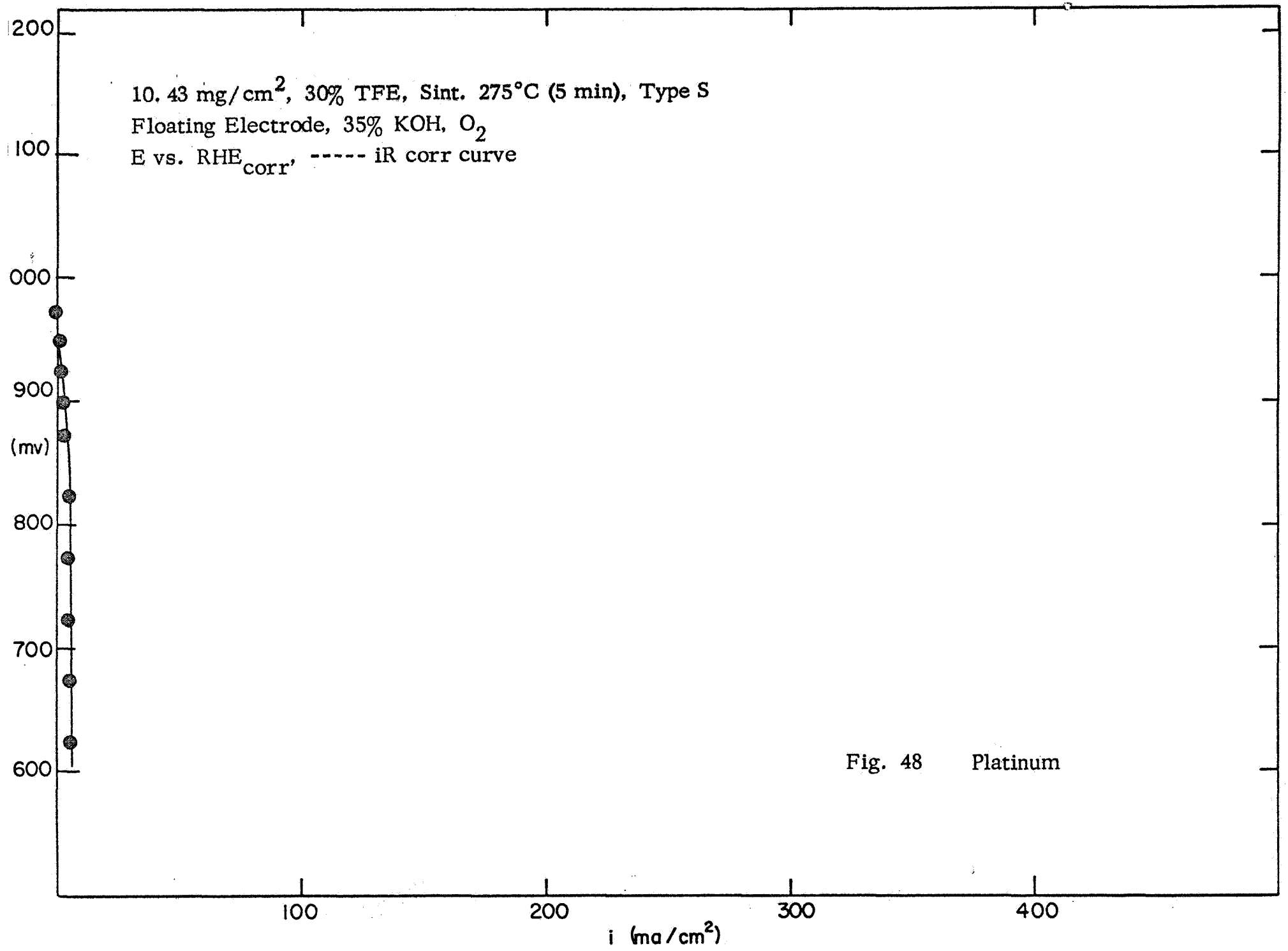

Fig. 48 Platinum

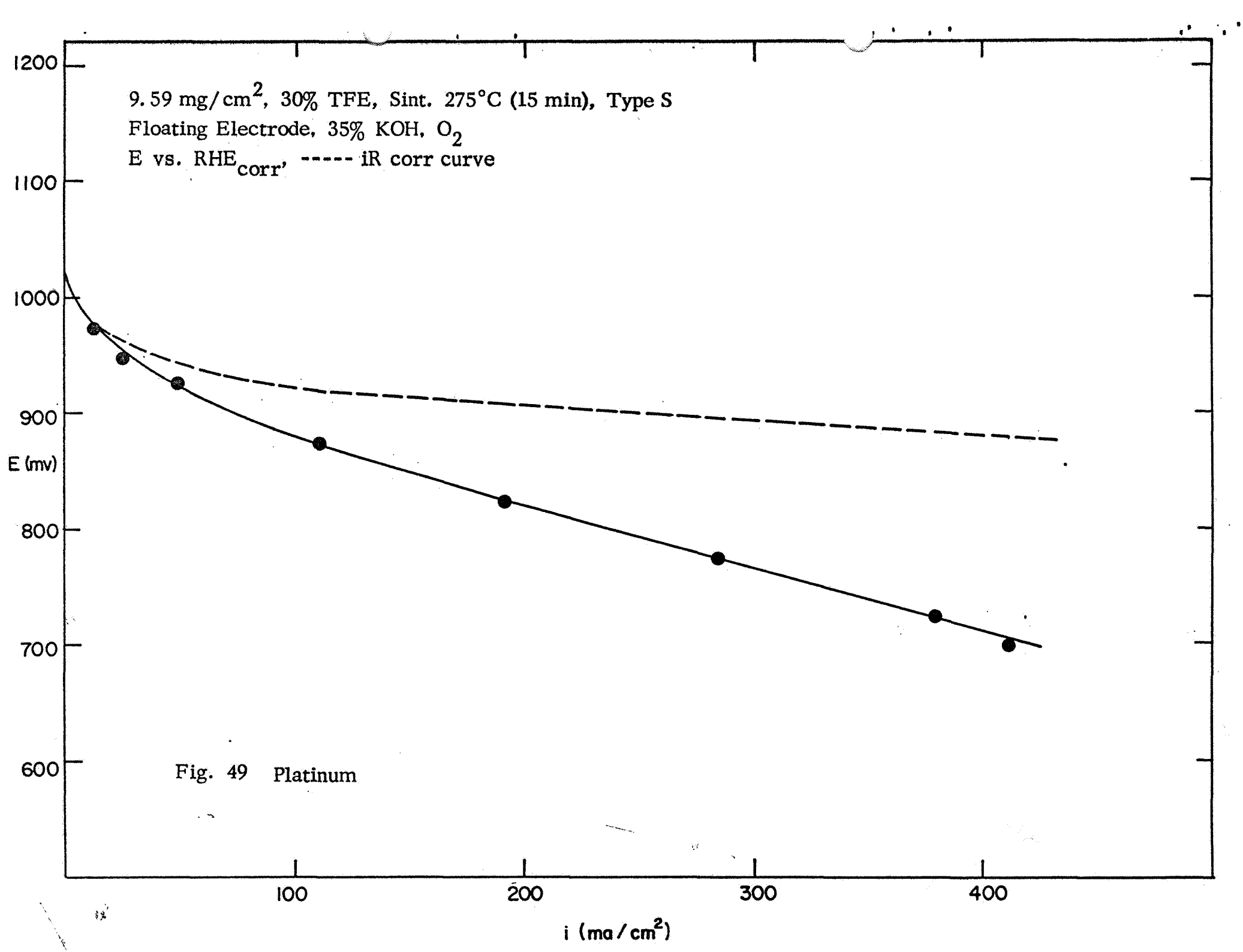

Fig. 49 Platinum

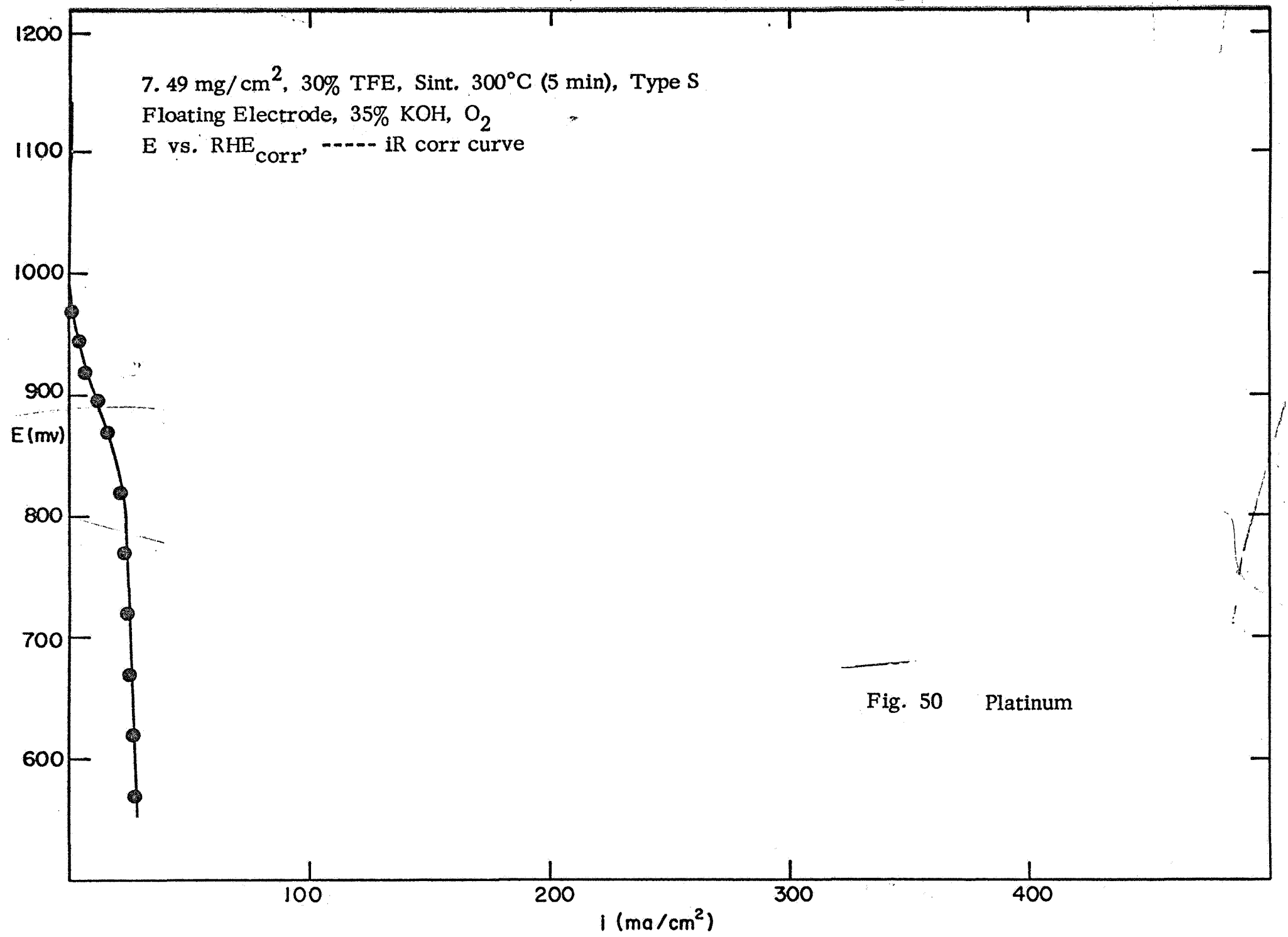

Fig. 50 Platinum

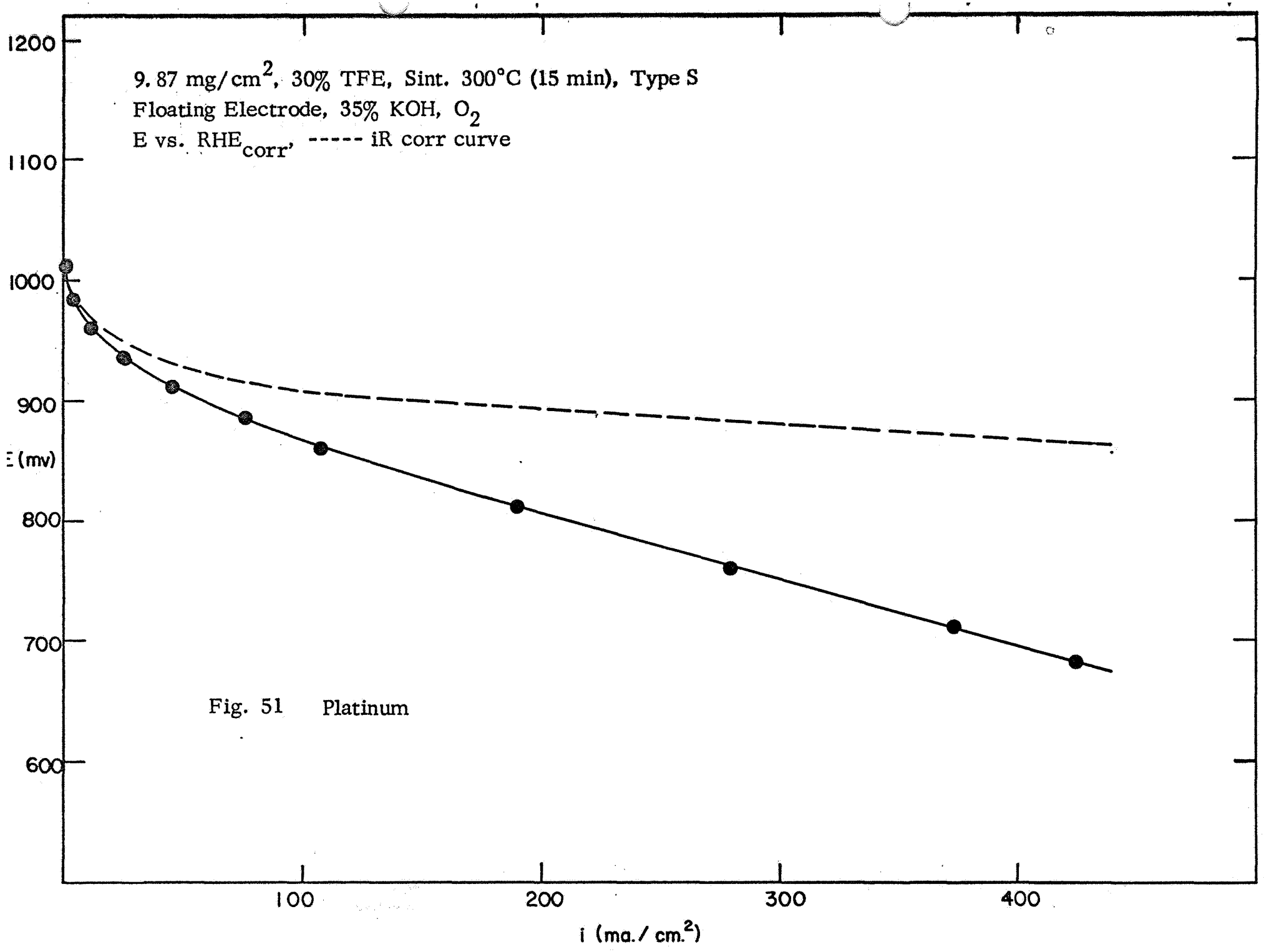

Fig. 51 Platinum

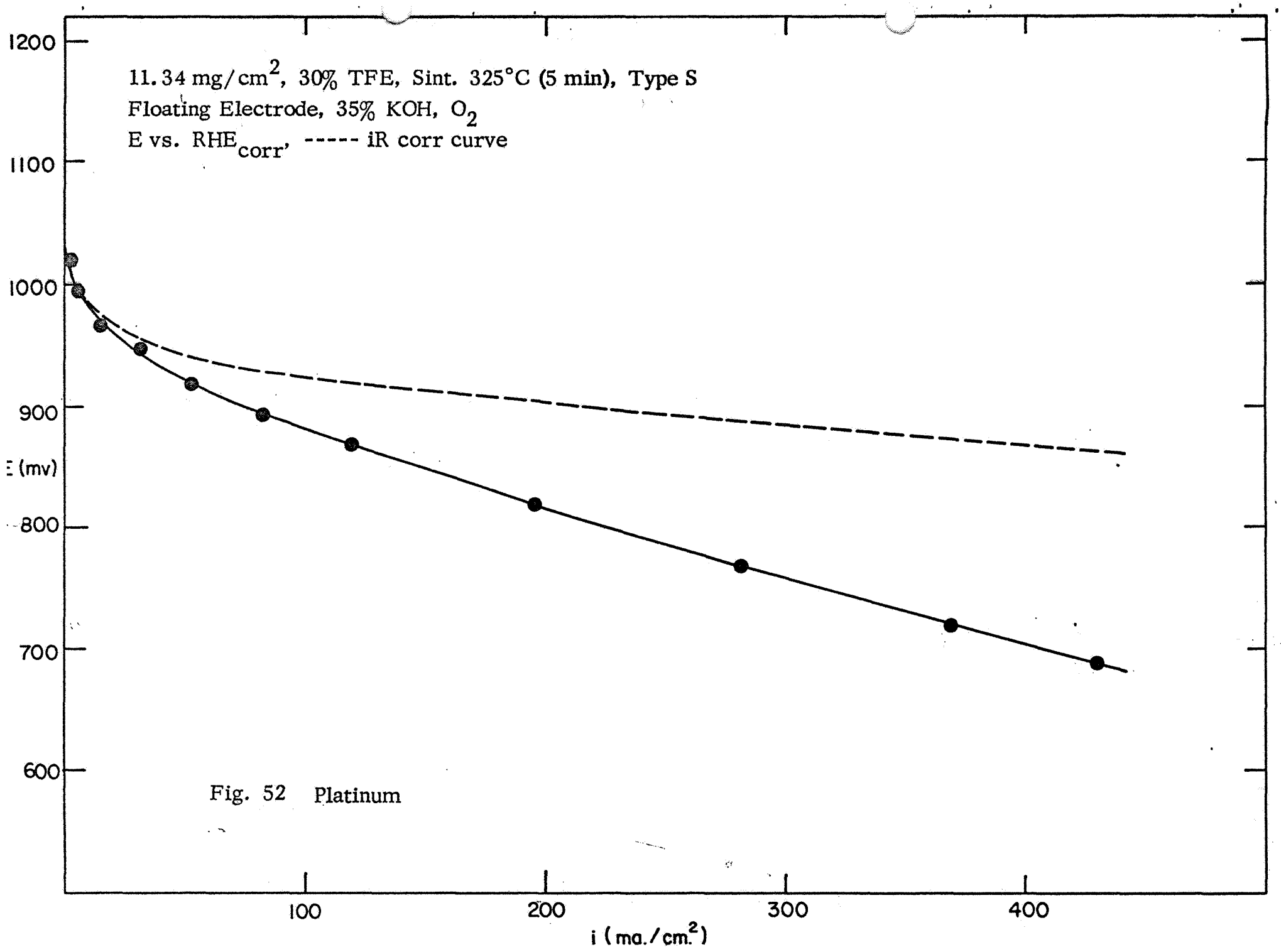

Fig. 52 Platinum

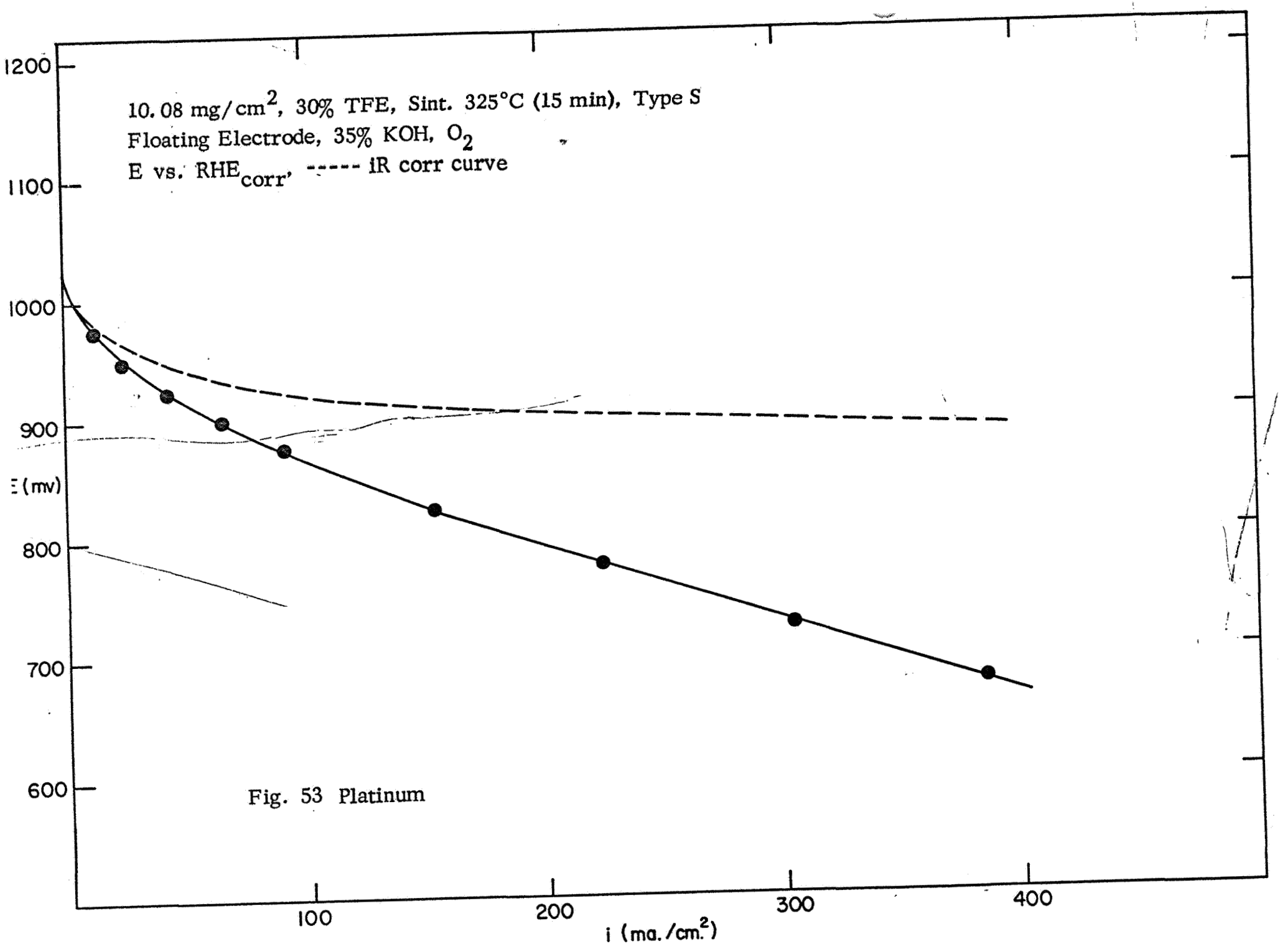

Fig. 53 Platinum

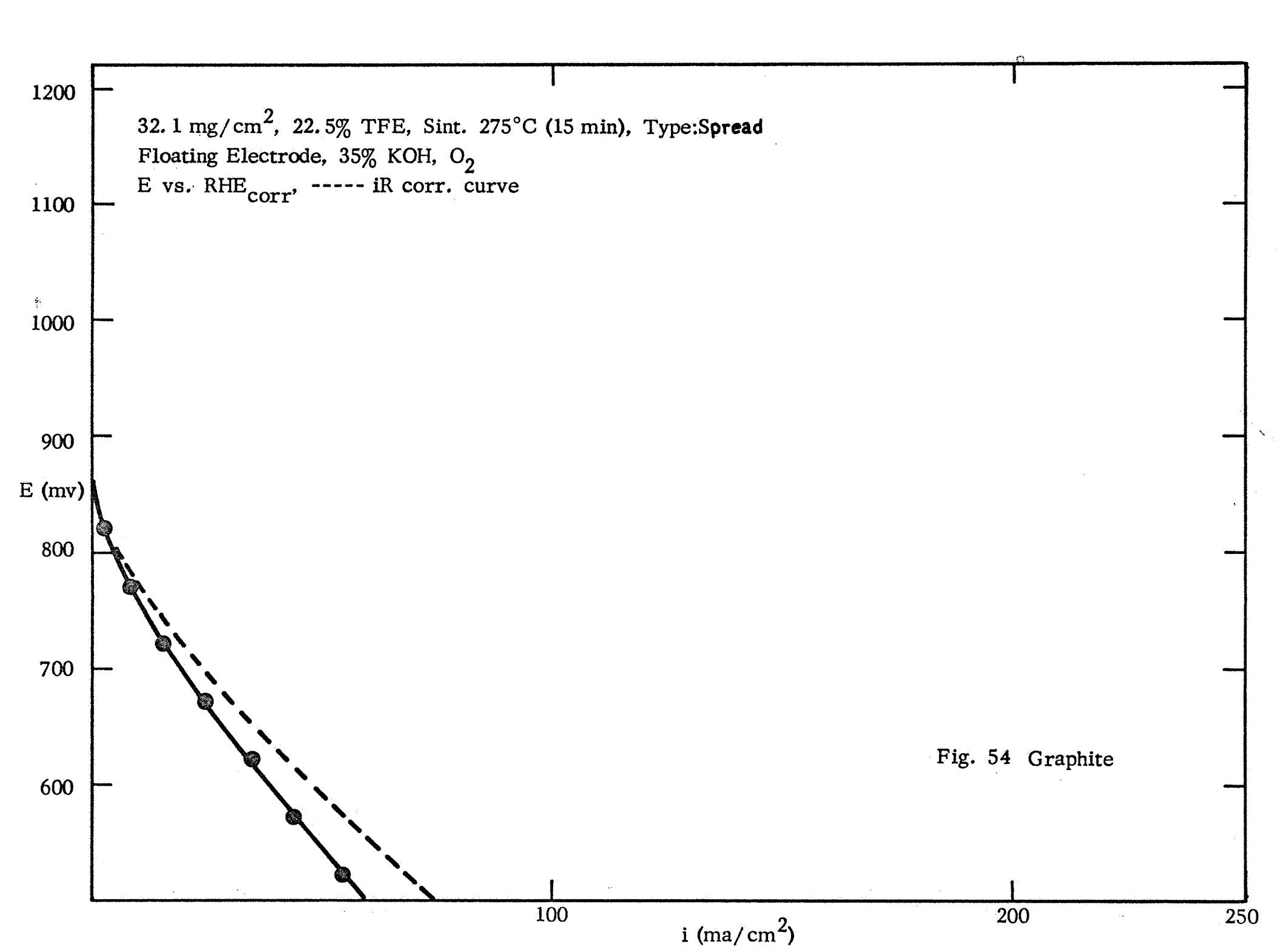

Fig. 54 Graphite

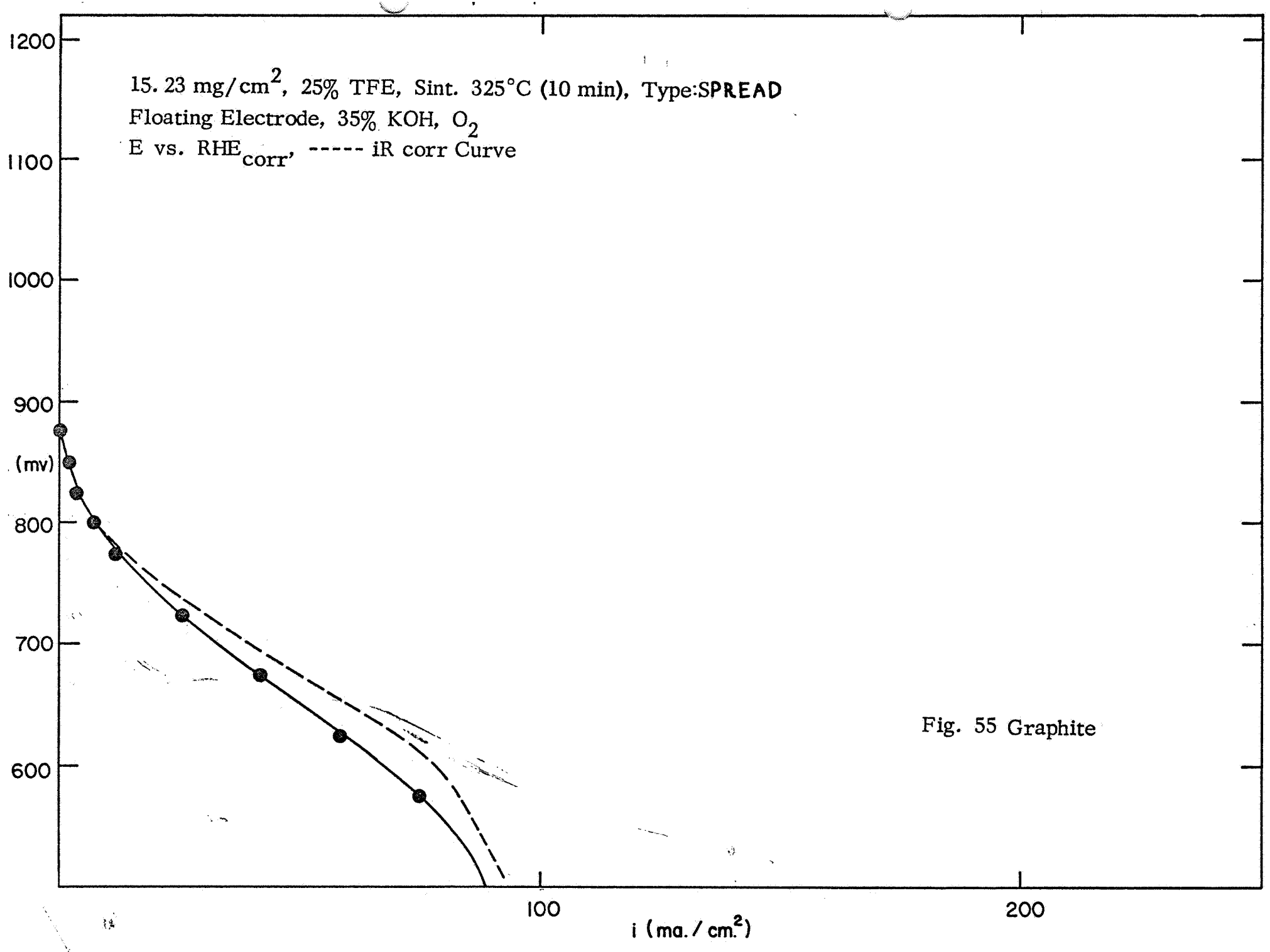

Fig. 55 Graphite

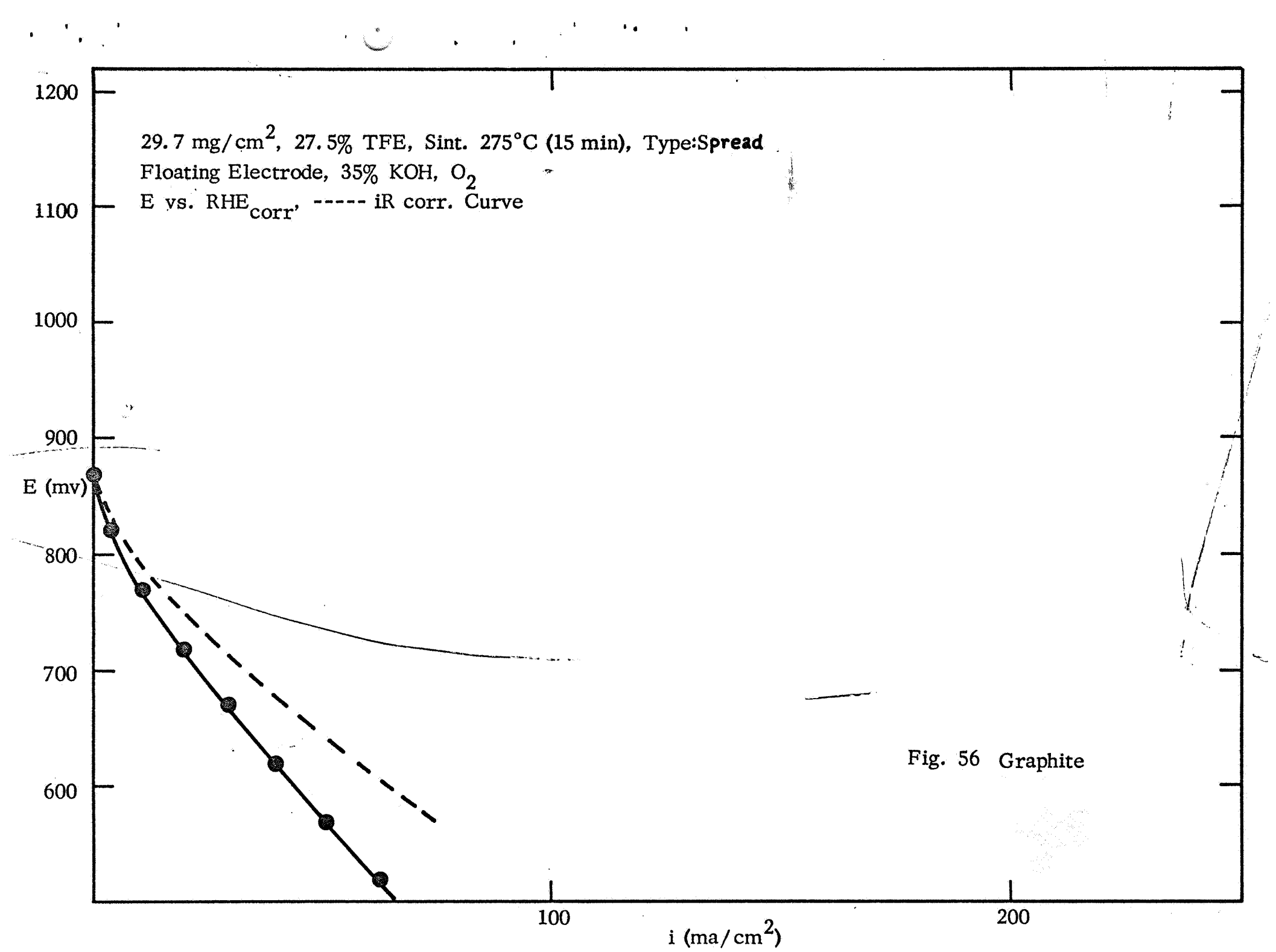

Fig. 56 Graphite

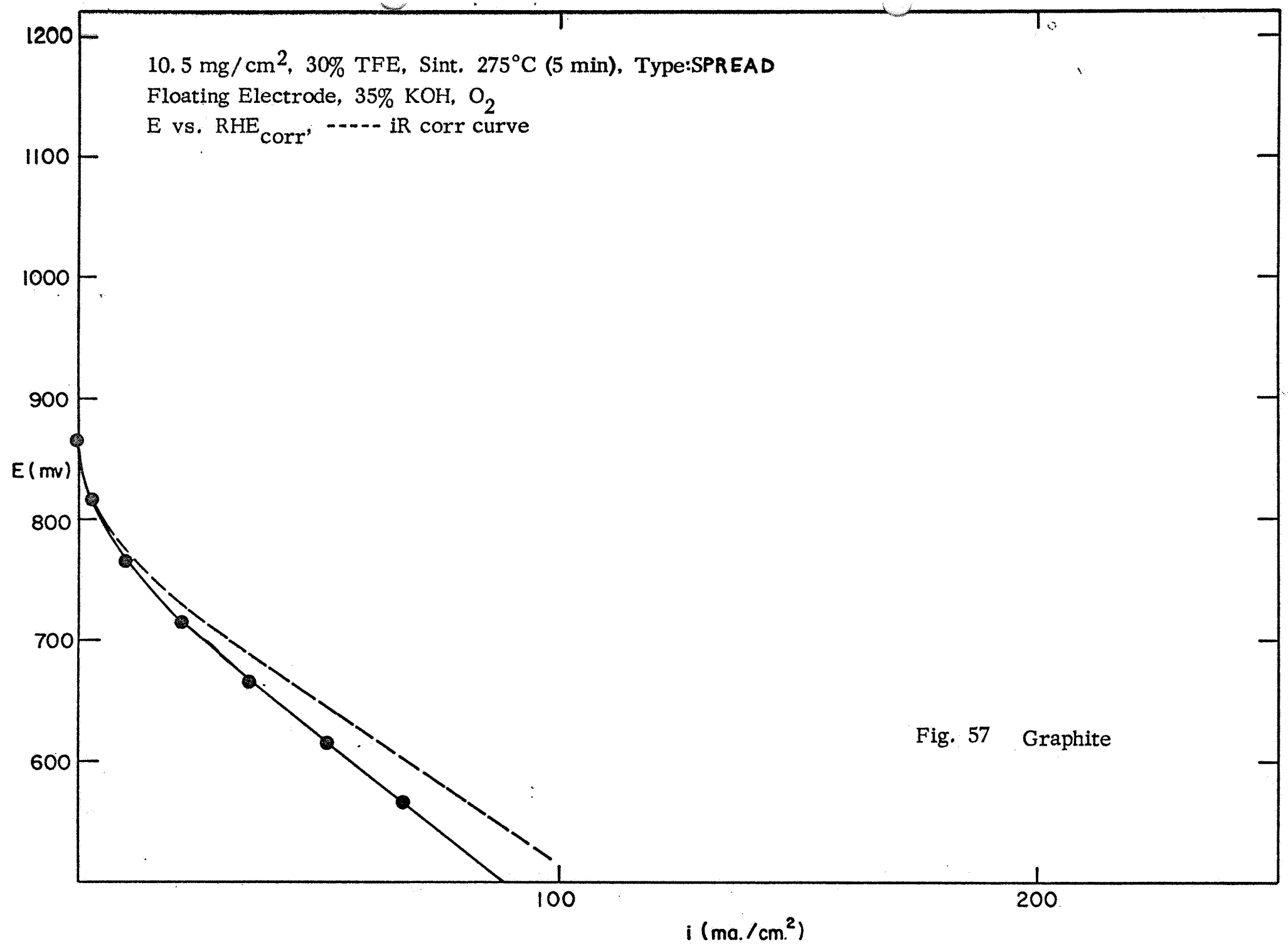

Fig. 57 Graphite

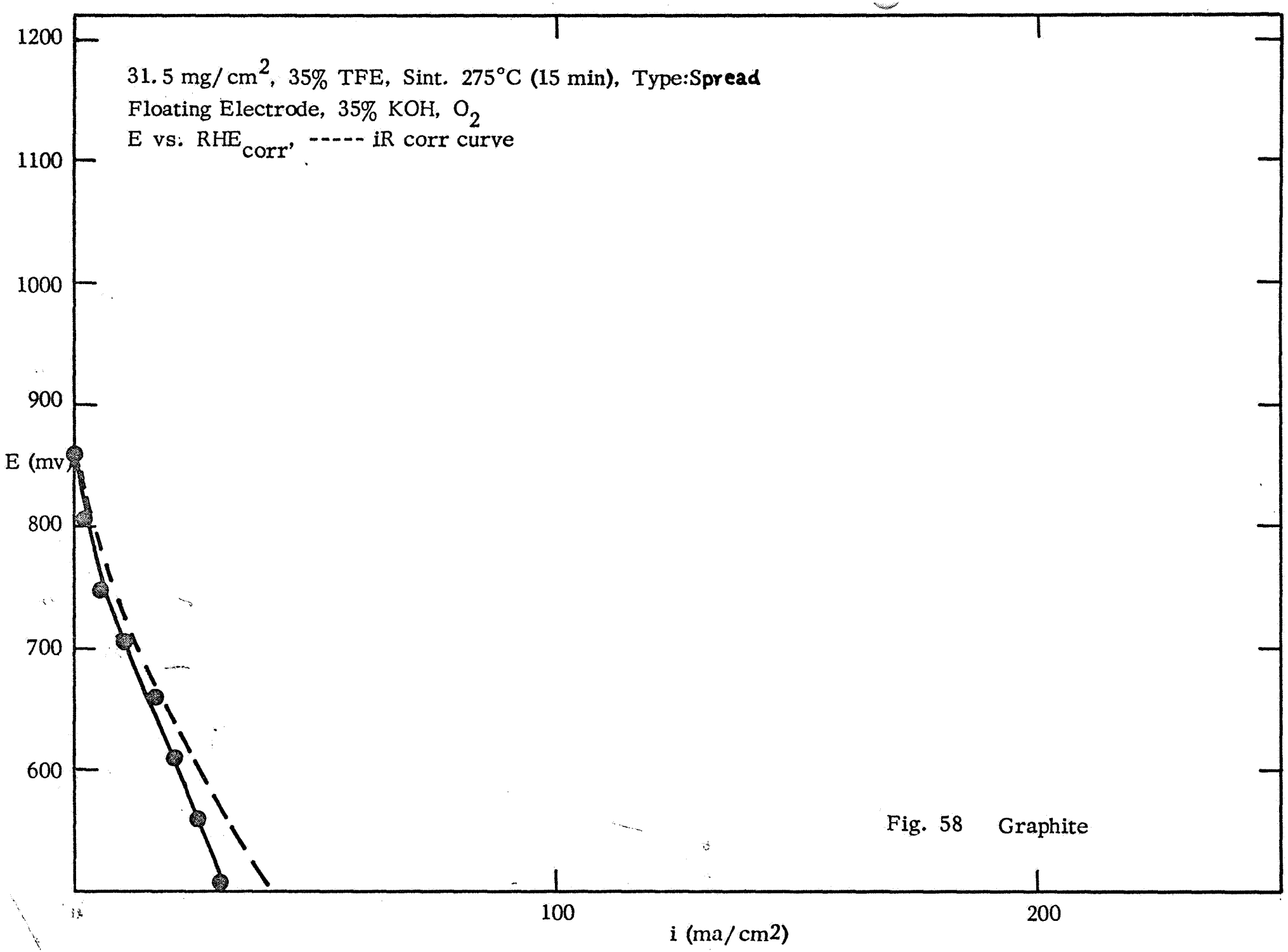

Fig. 58 Graphite

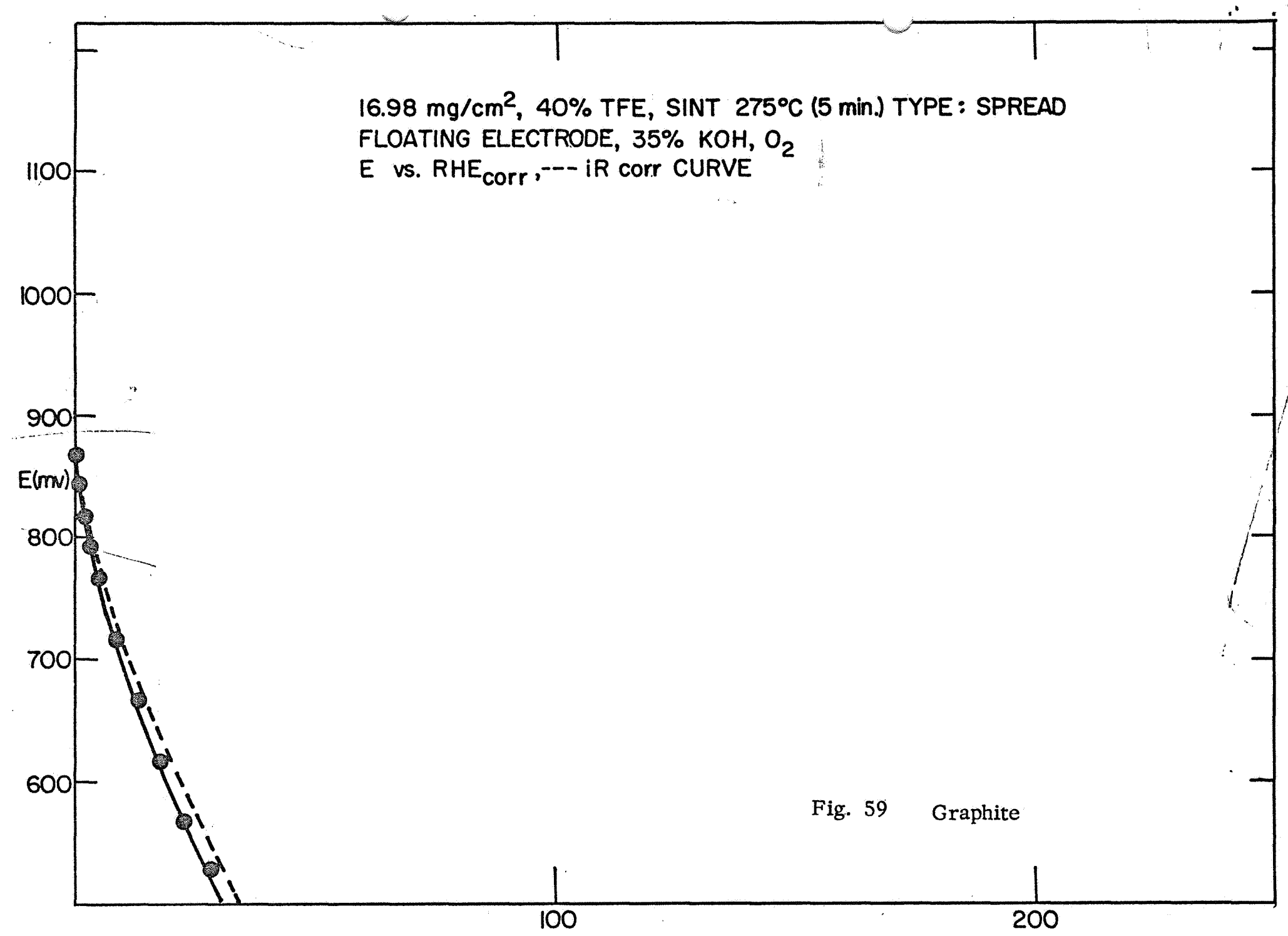

Fig. 59 Graphite

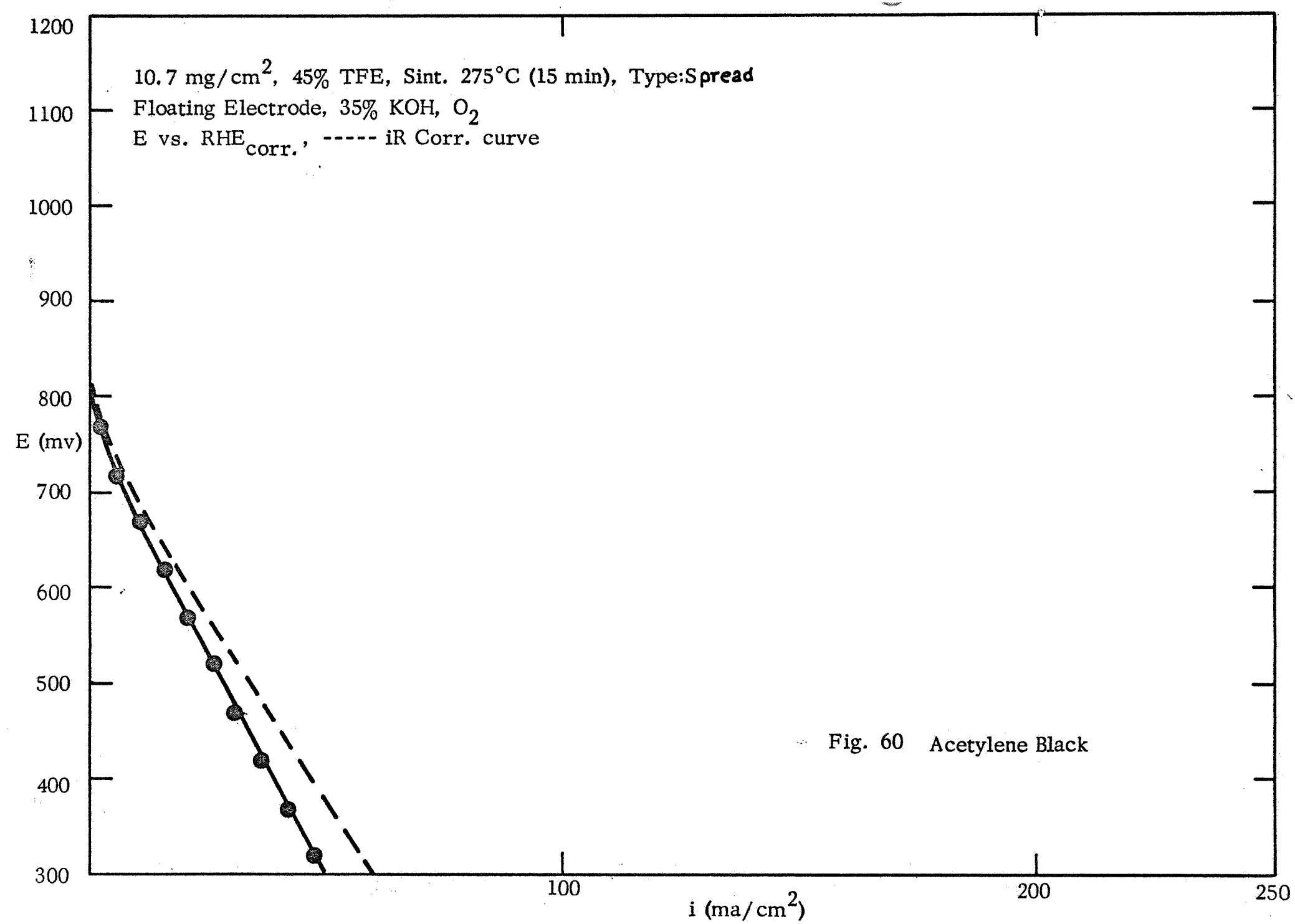

Fig. 60 Acetylene Black

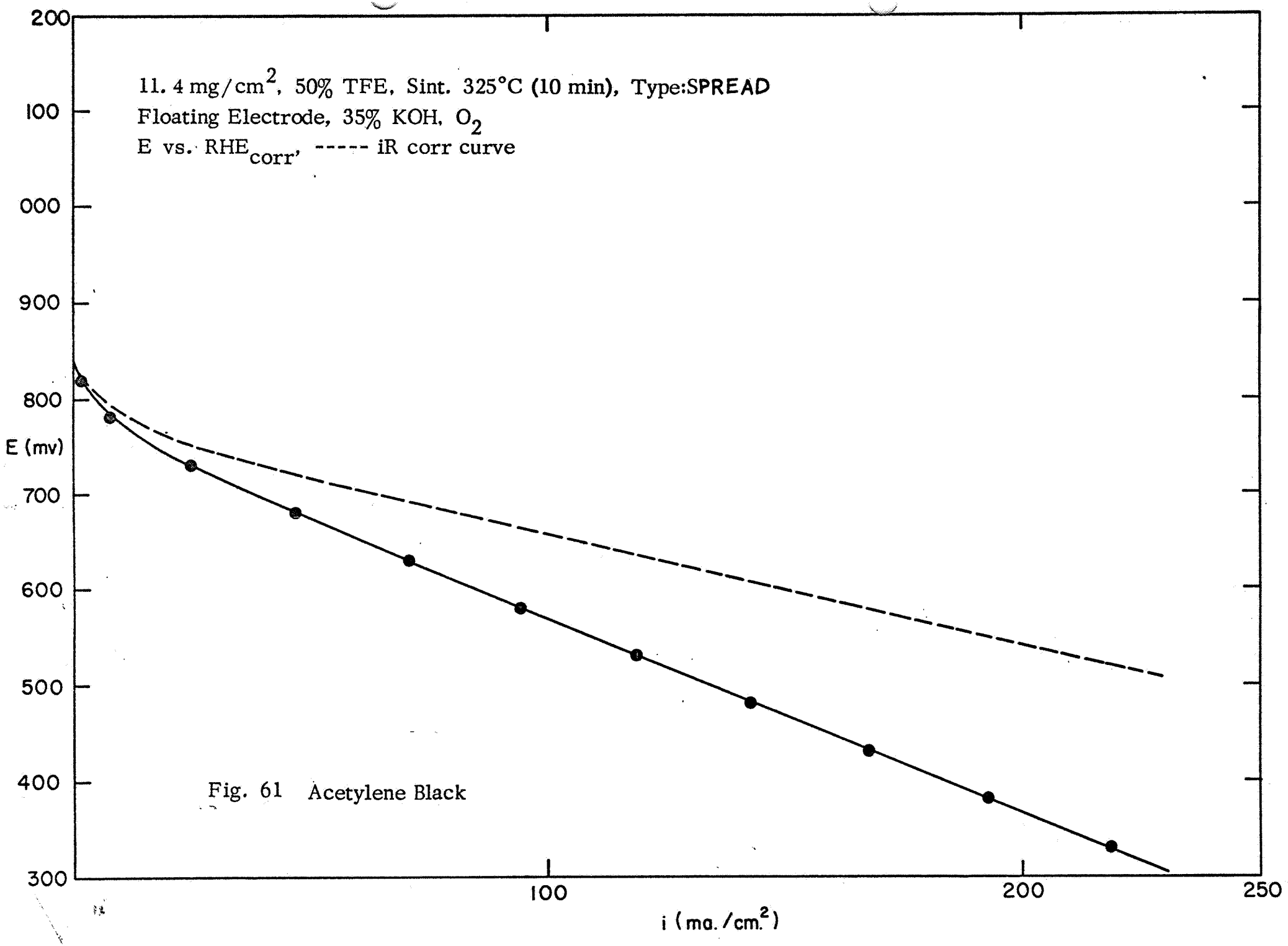

Fig. 61 Acetylene Black

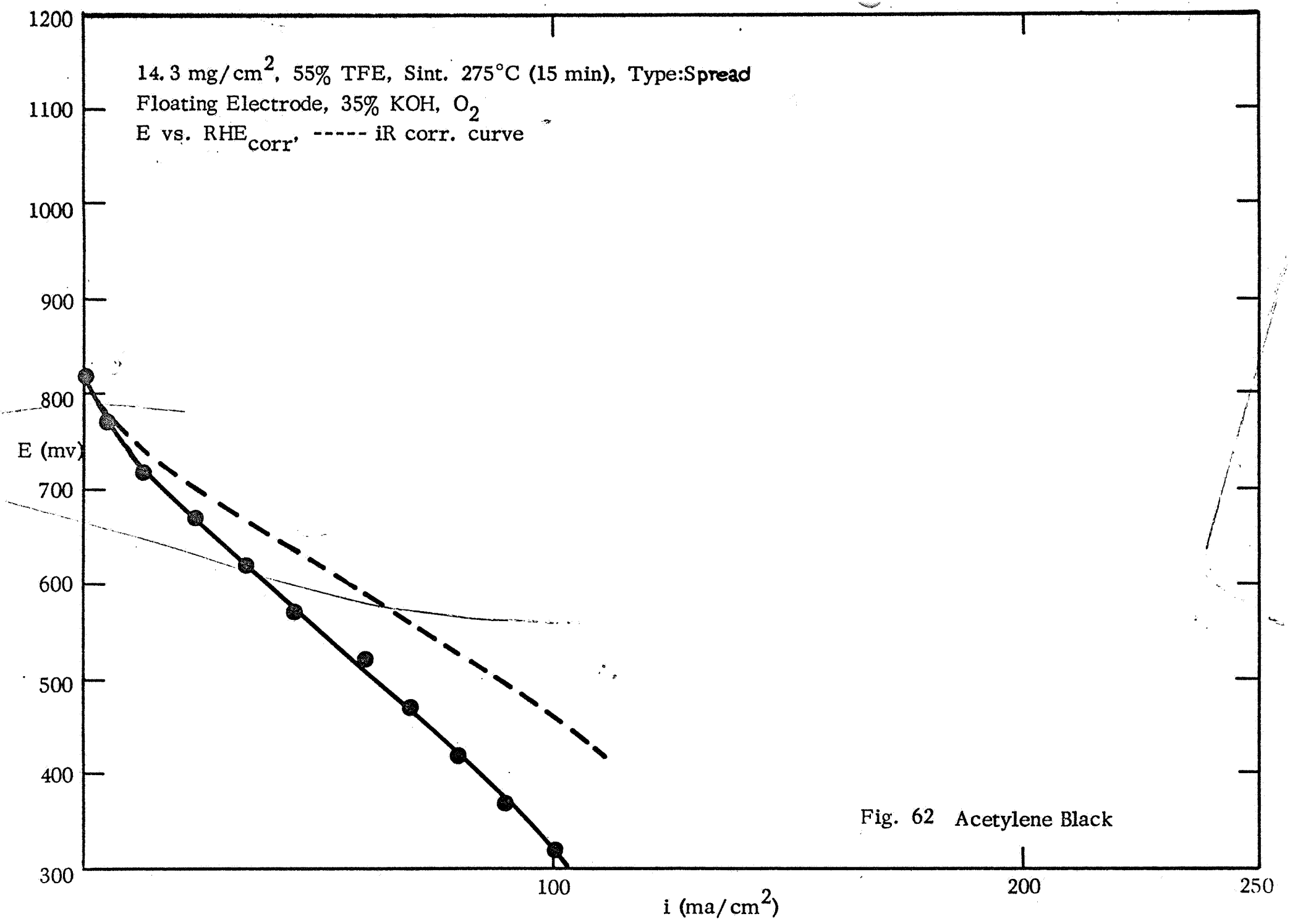

Fig. 62 Acetylene Black

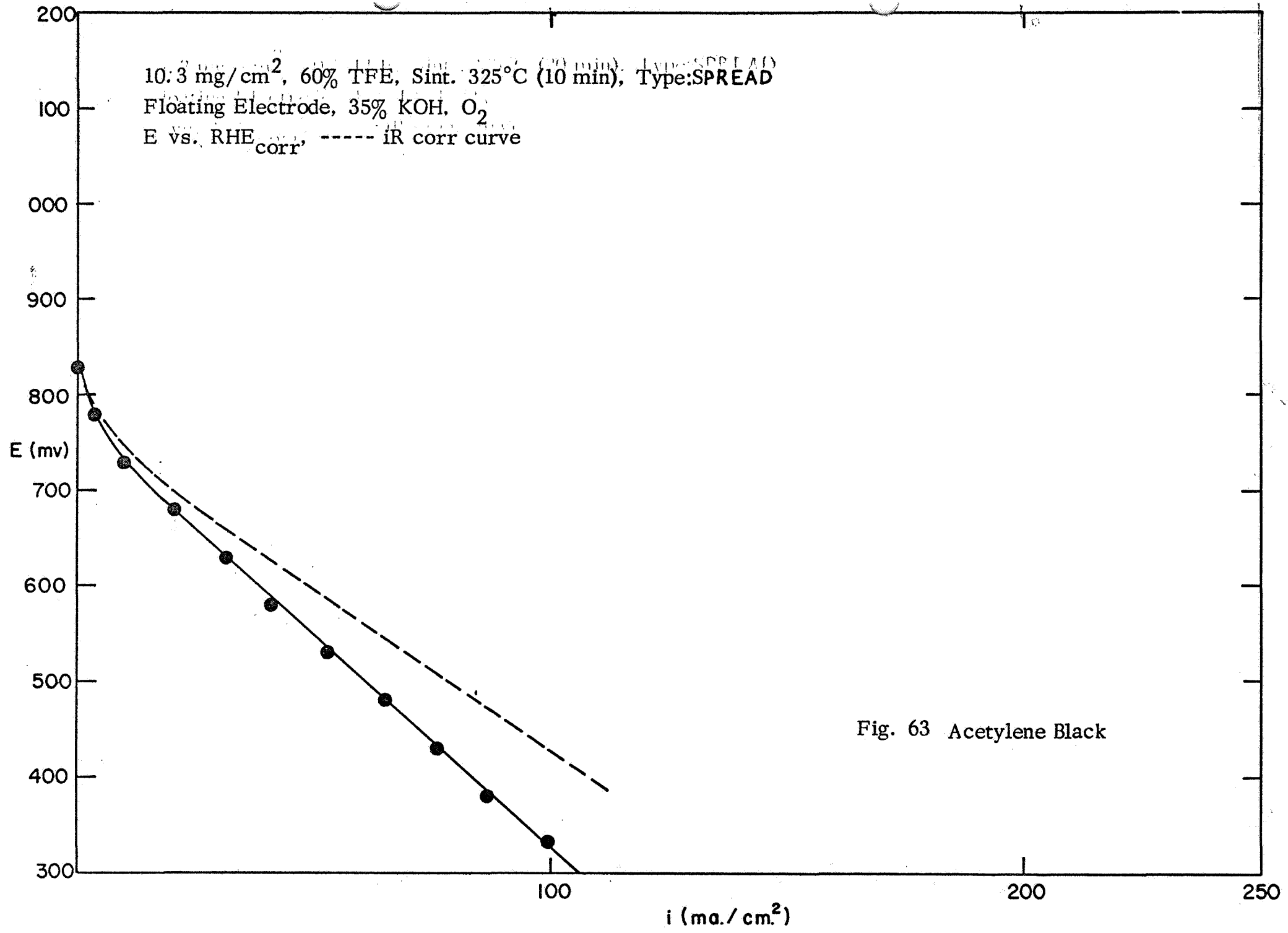

Fig. 63 Acetylene Black

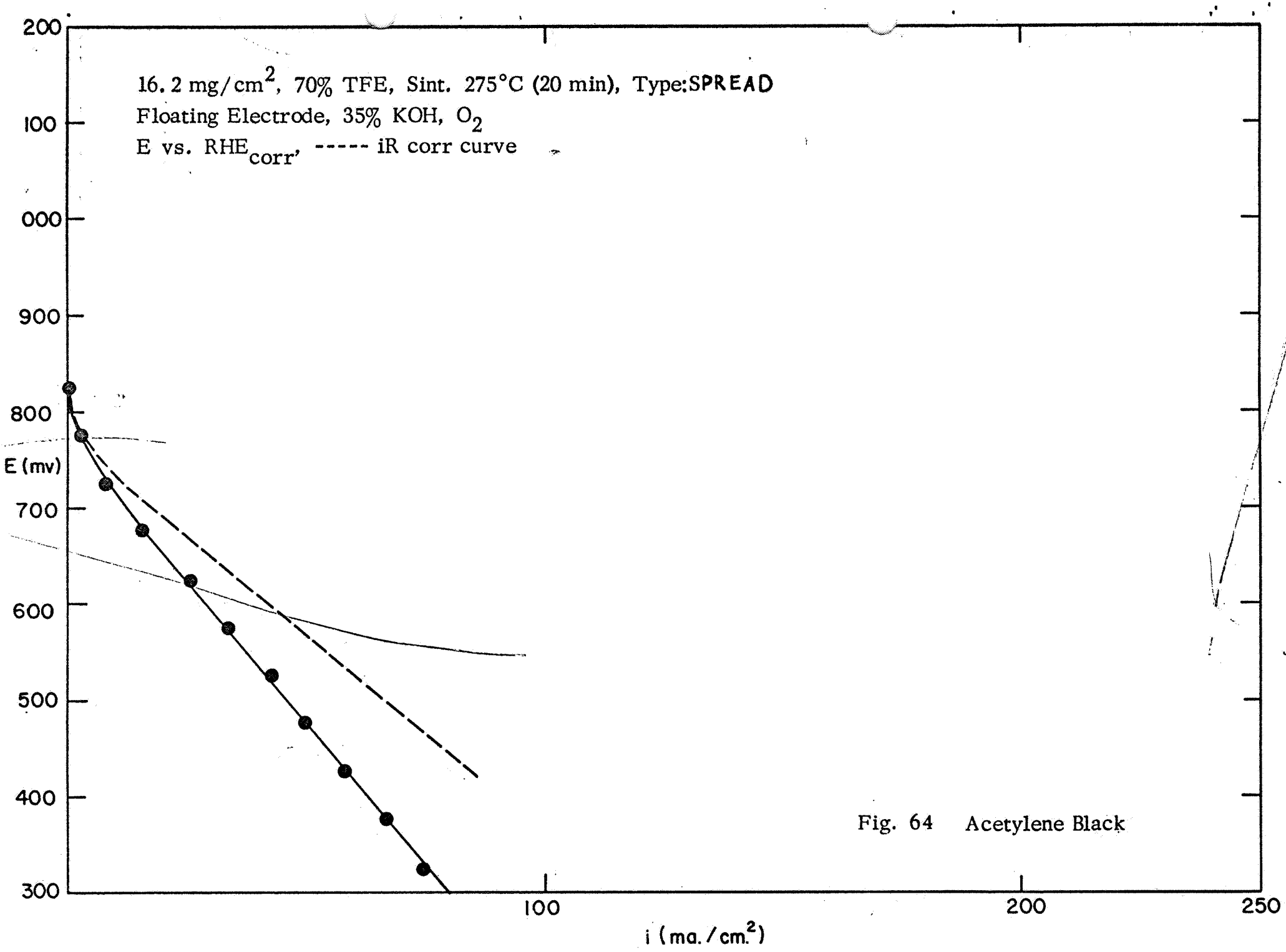

Fig. 64 Acetylene Black

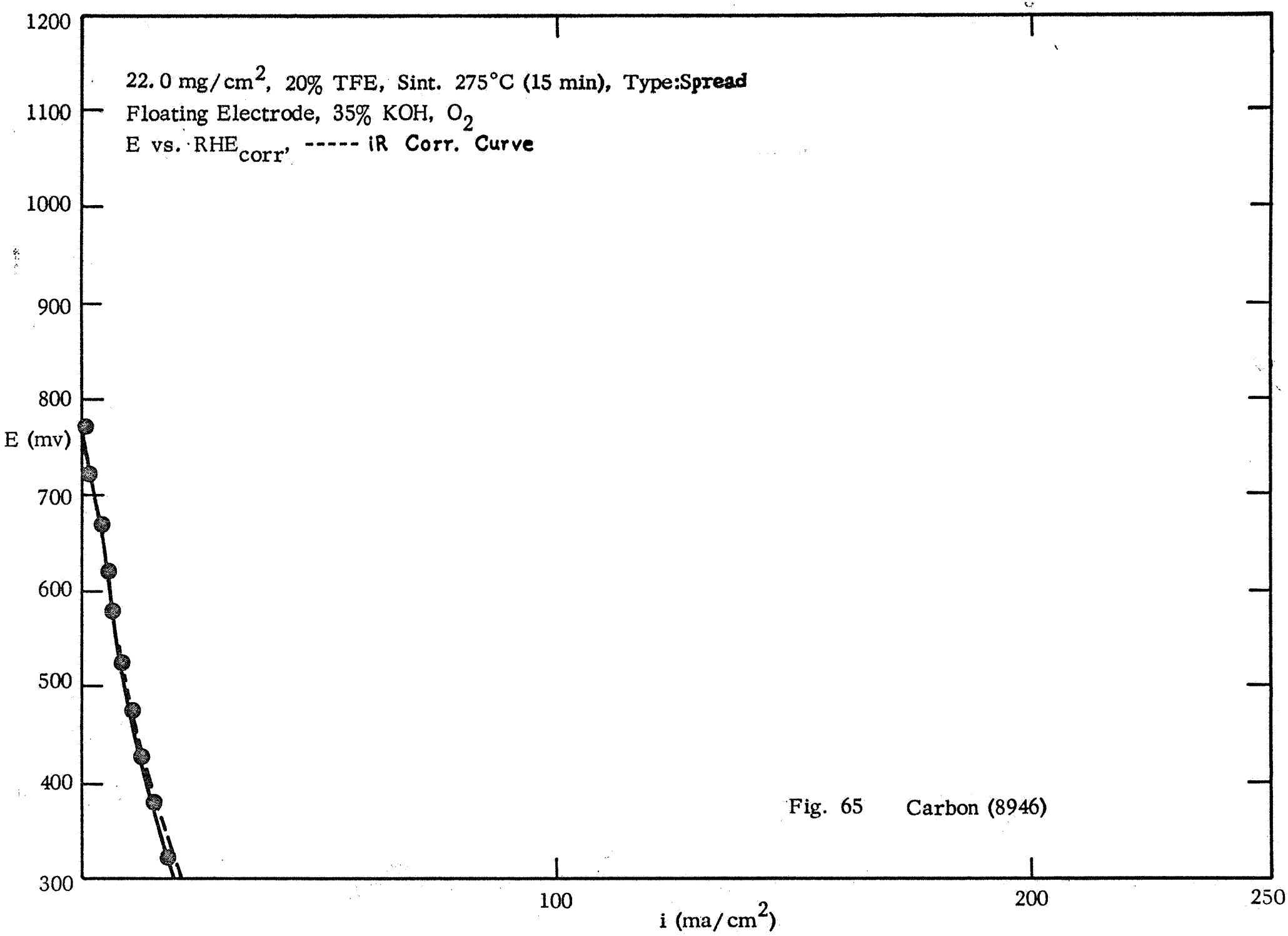

Fig. 65 Carbon (8946)

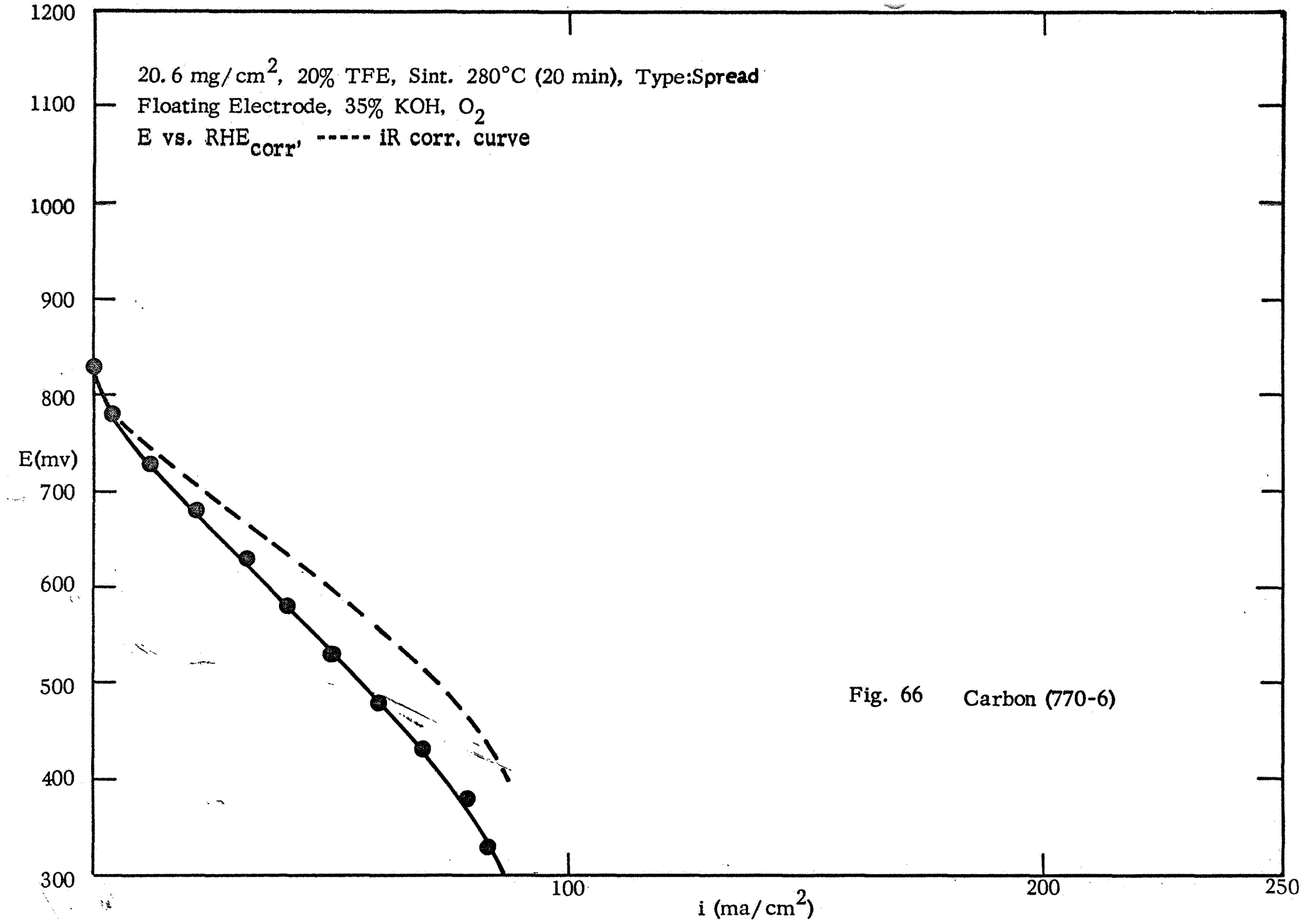

Fig. 66 Carbon (770-6)

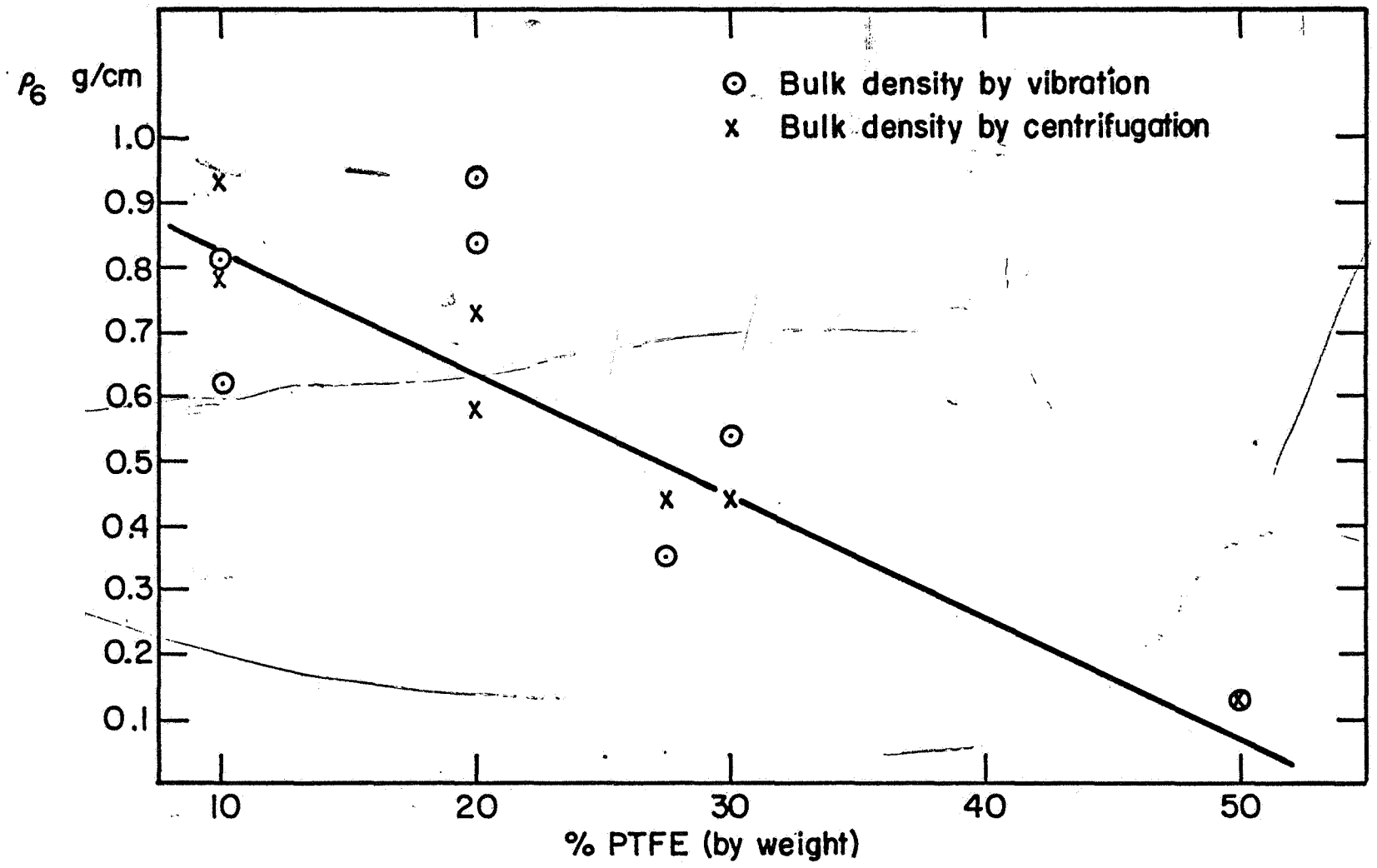

Fig. 67 Plot of Bulk Density vs. PTFE Content of Electrodes

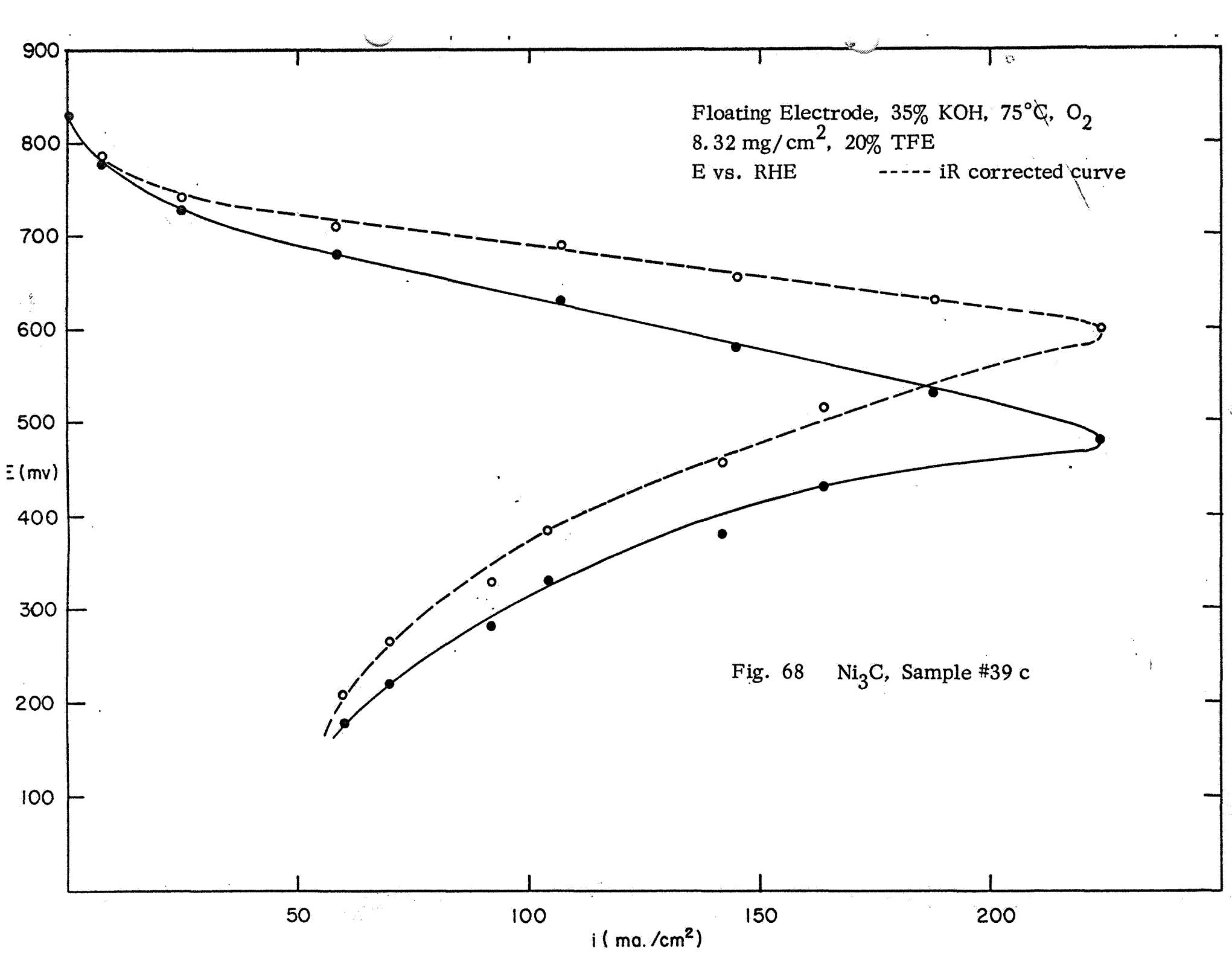

Fig. 68 Ni_3C, Sample #39 c

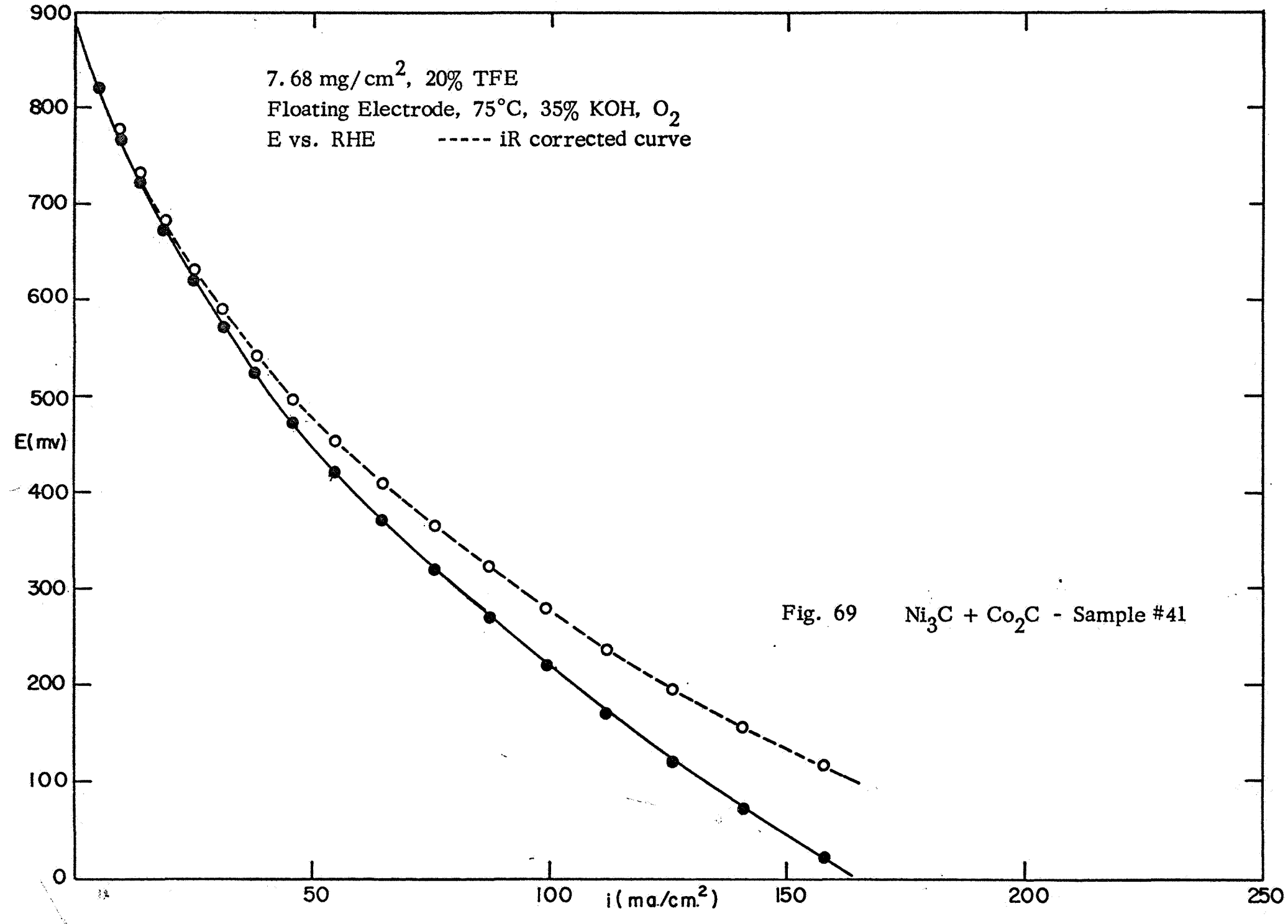

Fig. 69 $Ni_3C + Co_2C$ - Sample #41

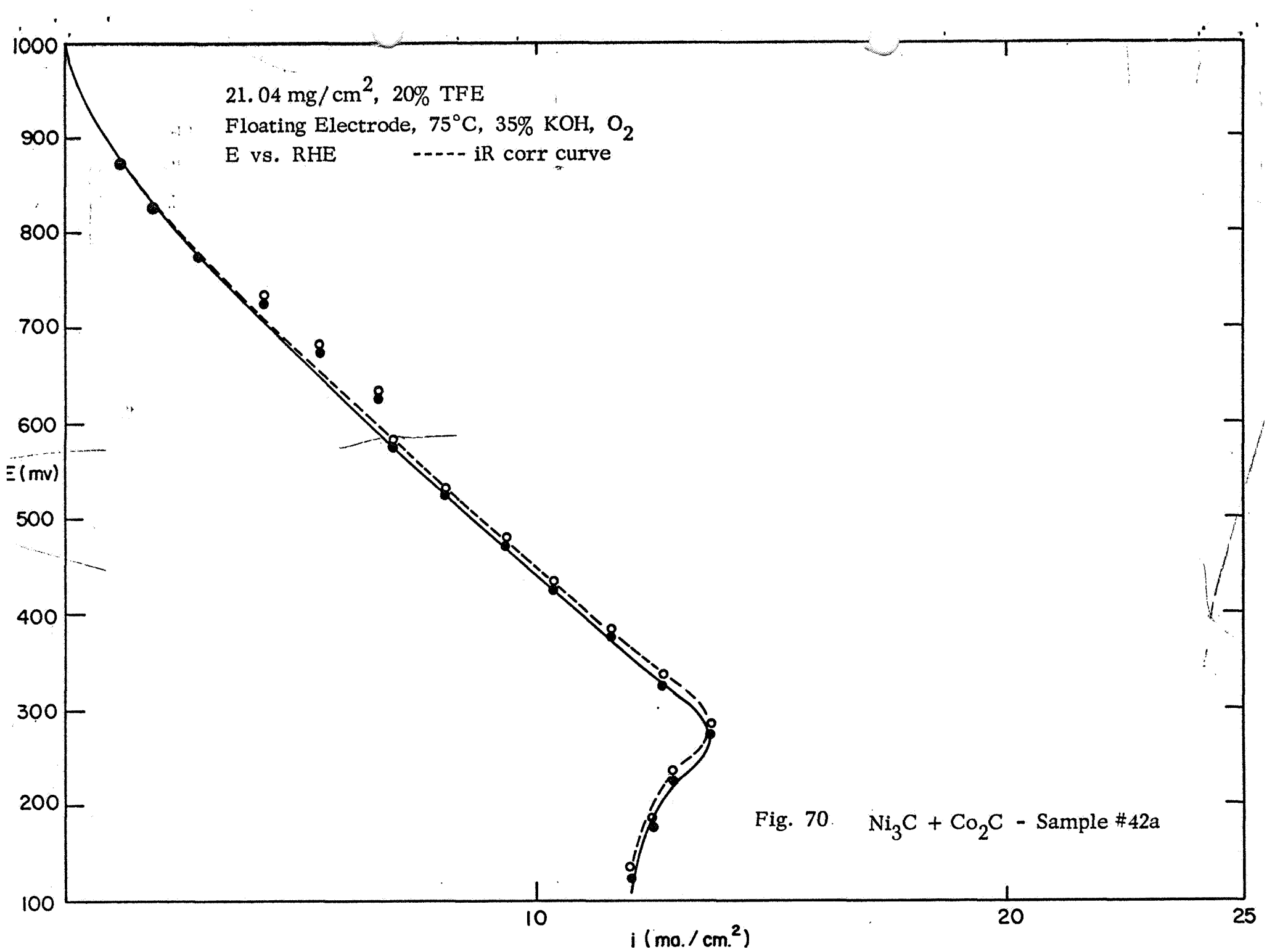

Fig. 70 $Ni_3C + Co_2C$ - Sample #42a

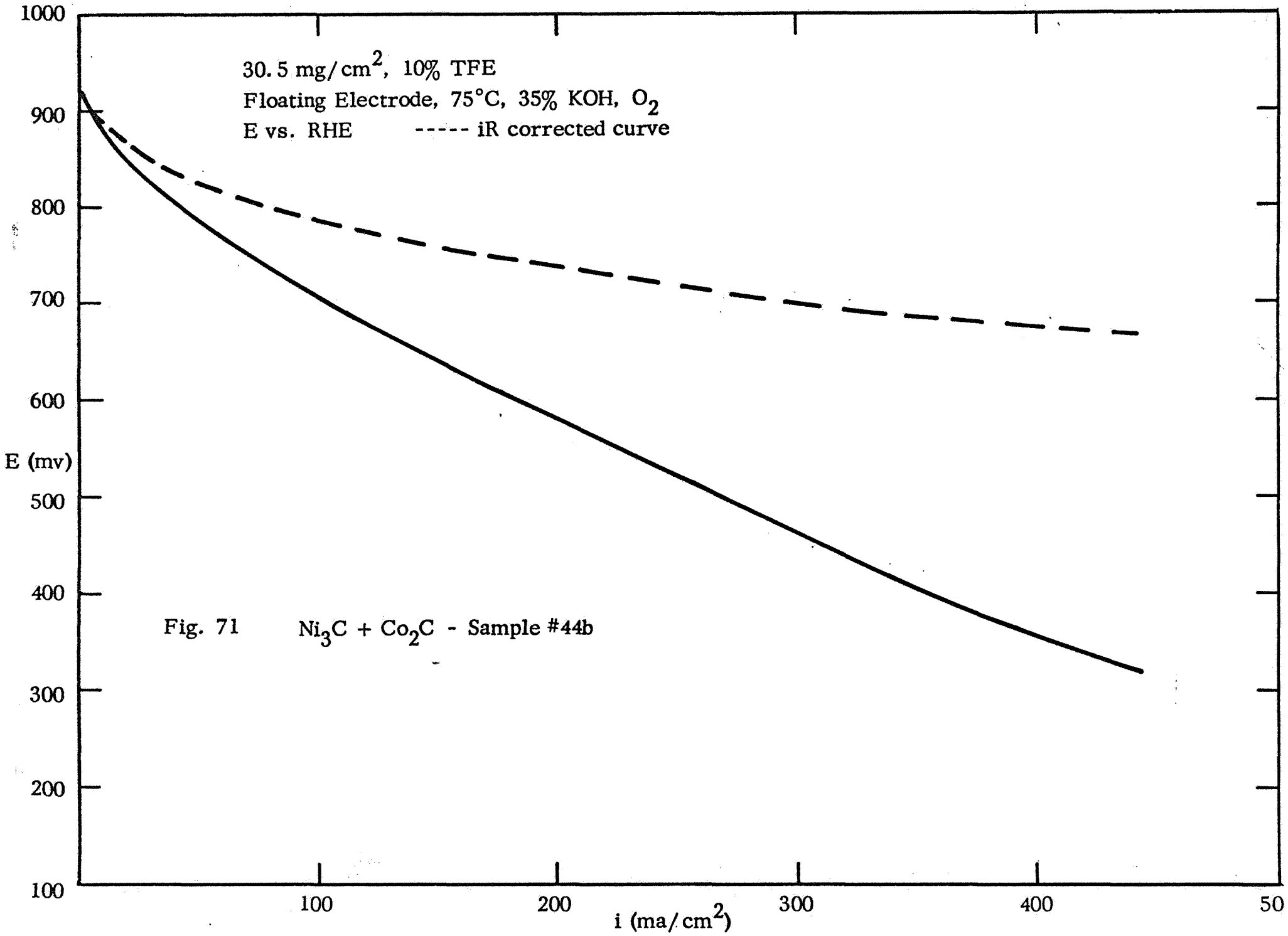

Fig. 71 $Ni_3C + Co_2C$ - Sample #44b

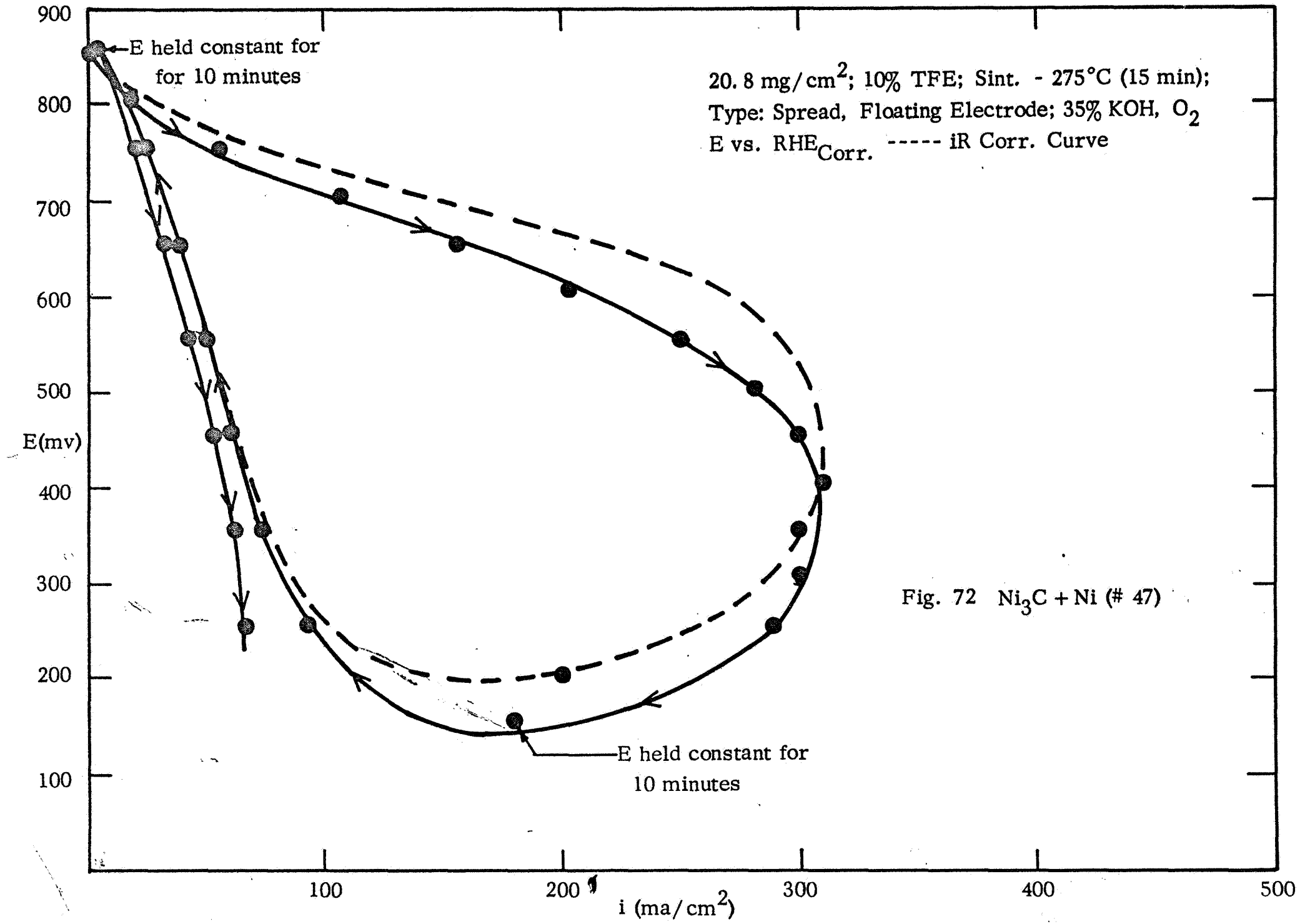

Fig. 72 $Ni_3C + Ni$ (# 47)

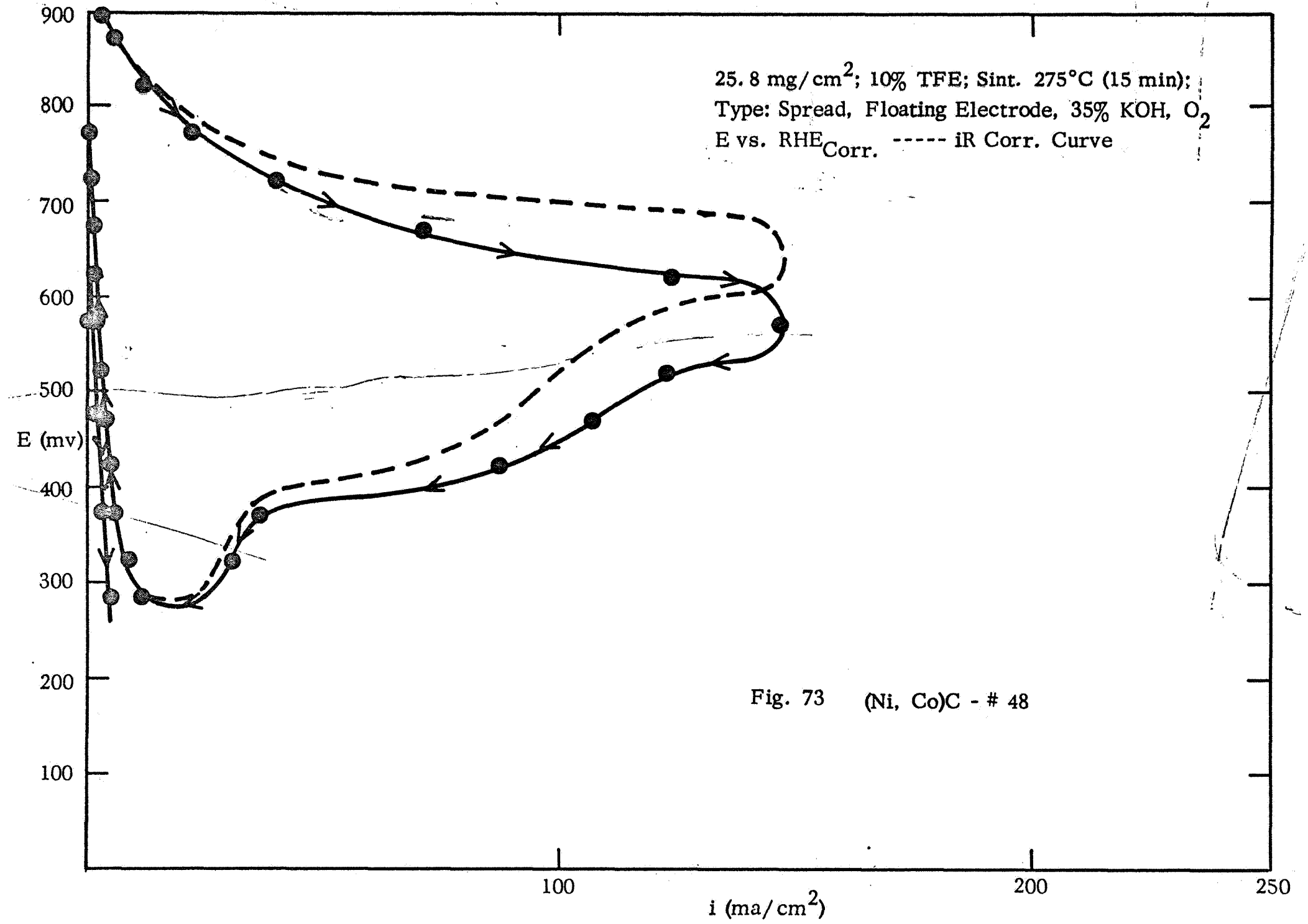

Fig. 73 (Ni, Co)C - # 48

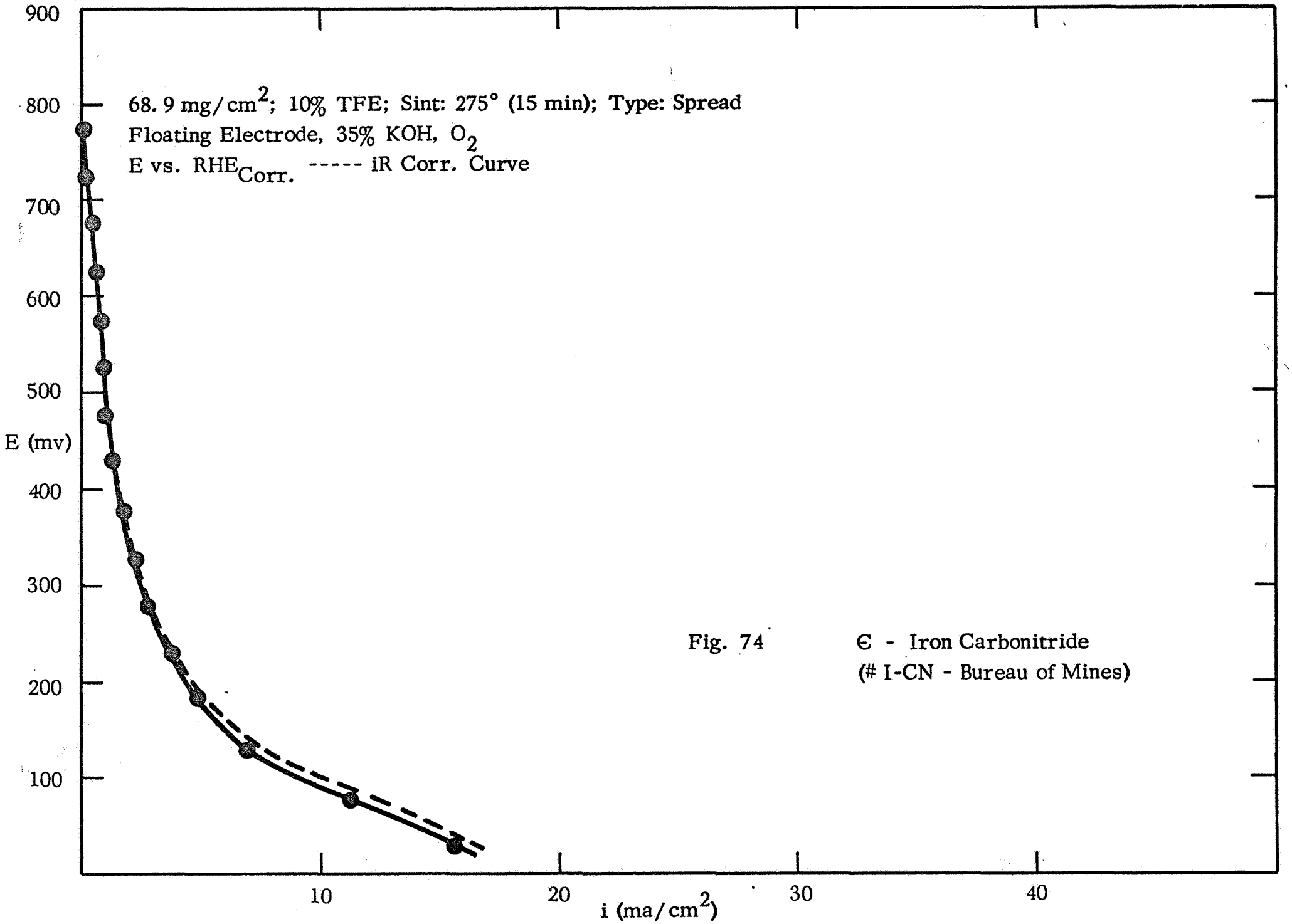

Fig. 74 Є - Iron Carbonitride
(# I-CN - Bureau of Mines)

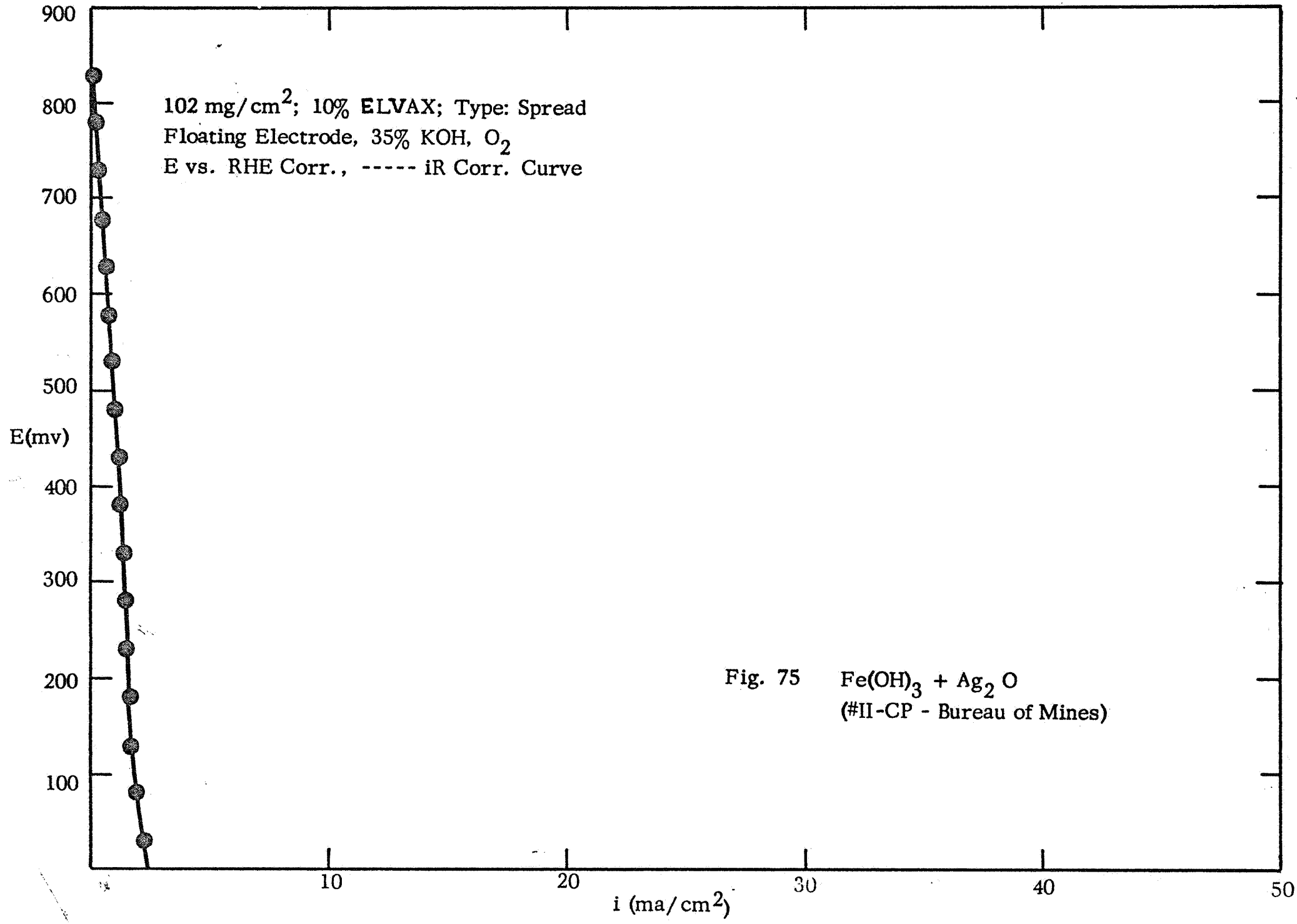

Fig. 75 $Fe(OH)_3 + Ag_2O$
(#II-CP - Bureau of Mines)

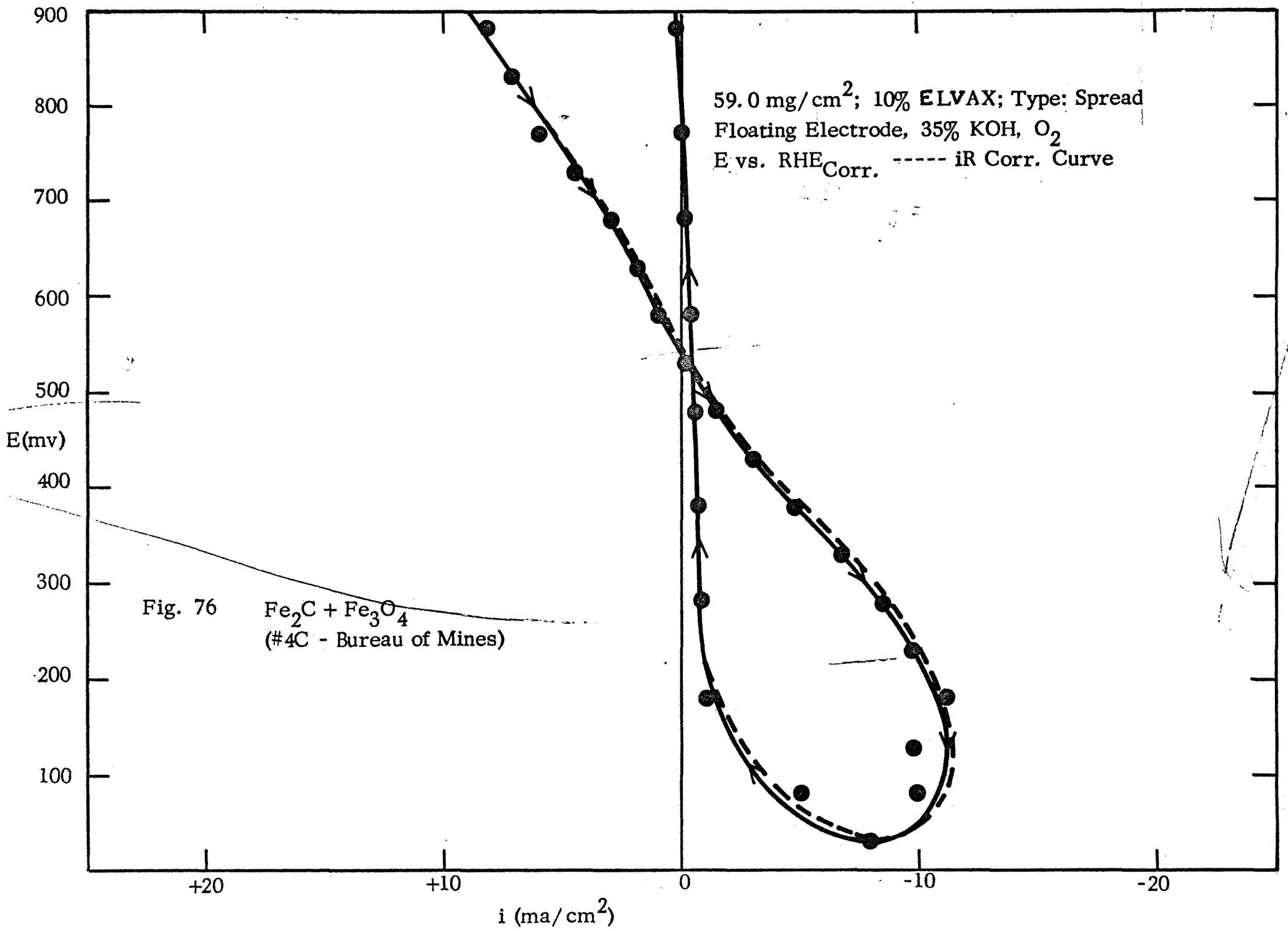

Fig. 76 $Fe_2C + Fe_3O_4$
(#4C - Bureau of Mines)

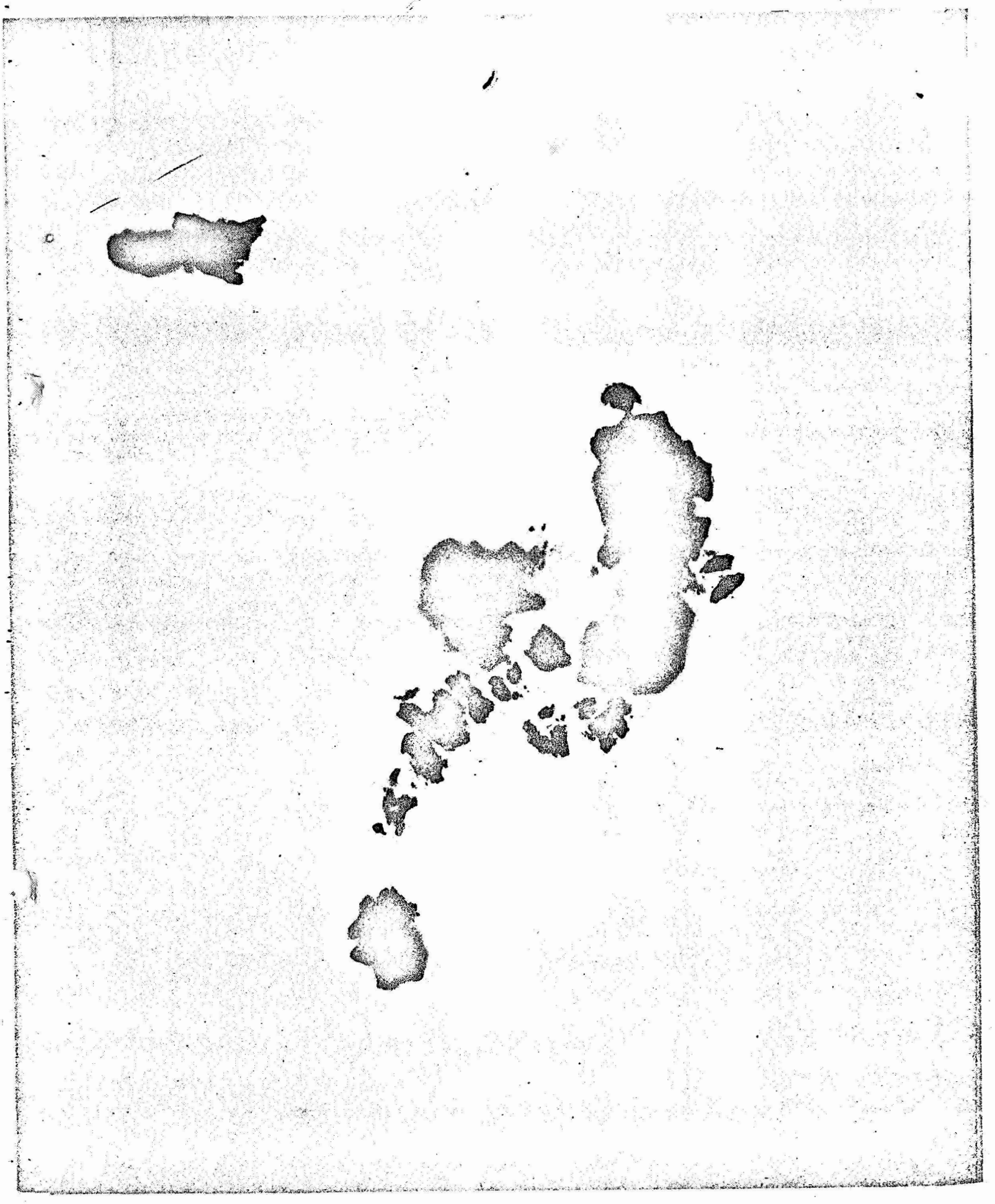

Fig. 77 1-CN ϵ - Iron Carbonitride X 40,000

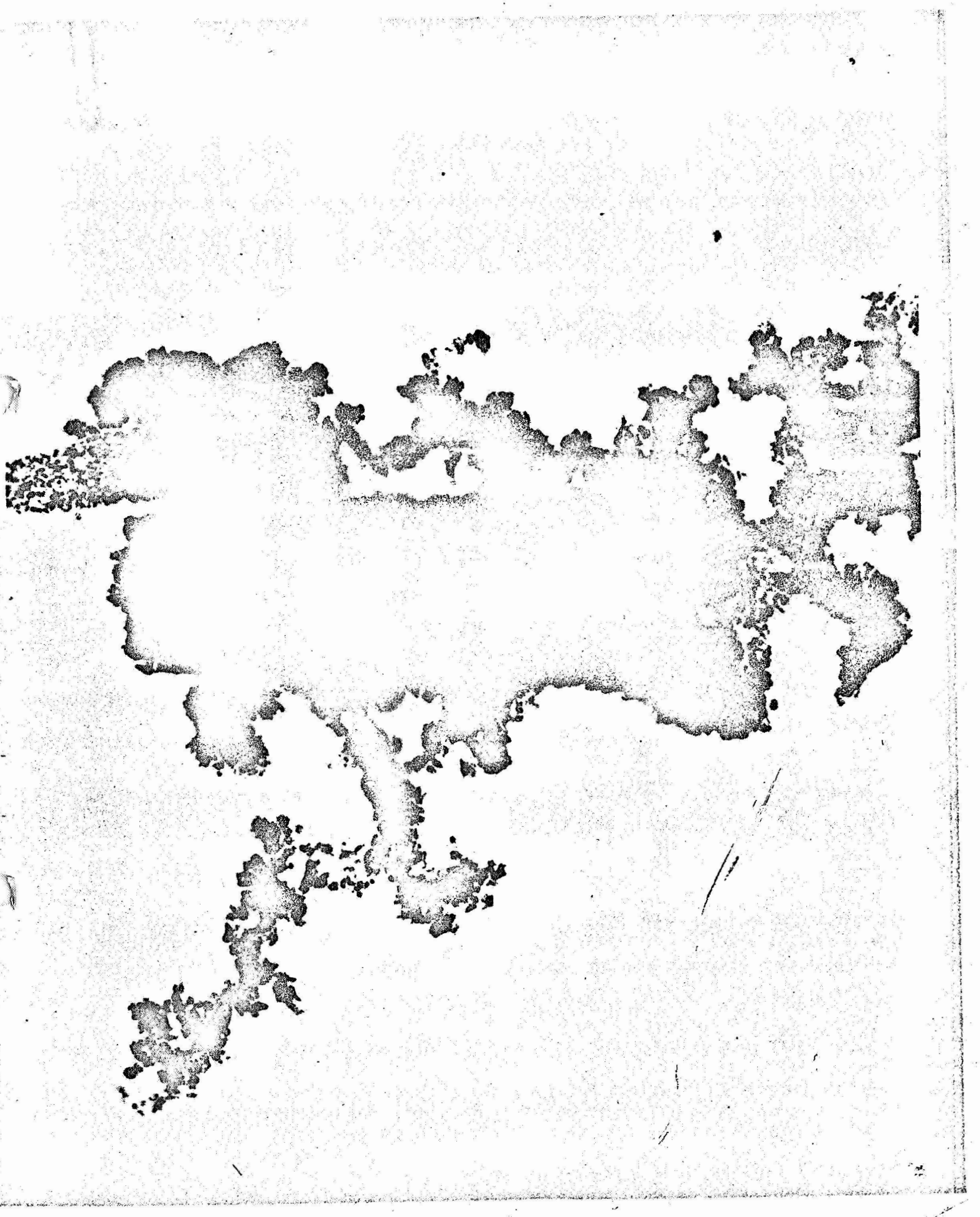

Fig. 78 4C χ-Fe_2C + Fe_3O_4 X 40,000

Fig. 79 II-CP $Fe(OH)_3 + Ag_2O$ X 40,000

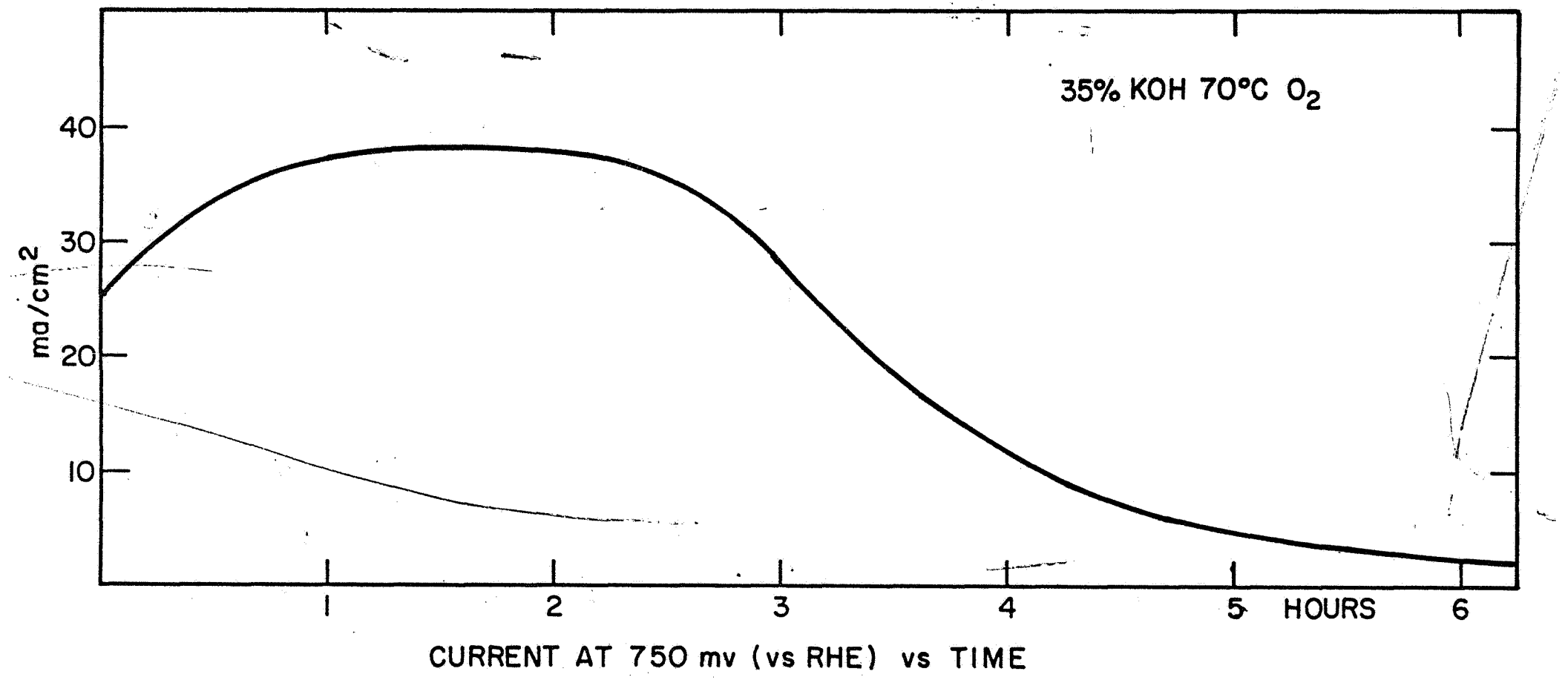

Fig. 80 #47 Ni_3C